PEOPLE'S DEMOCRATIC REPUBLIC OF ALGERIA
MINISTERY OF HIGHER EDUCATION AND SCIENTIFIC RESEARCH
UNIVERSITY YAHIA FARES OF MEDEA
FACULTY OF TECHNOLOGY
MECHANICAL ENGINEERING DEPARTMENT

THESIS

Presented to obtain the Doctorate degree in Sciences
in Mechanical Engineering

Contribution to the Study of Heat Transfers in Cavities Containing a Nanofluid and Subjected to an External Magnetic Field

Option: MECHANICAL ENGINEERING

By
ALILAT DJAMEL

Presented on 10 /04 /2021

JURY COMPOSED OF:

Dr Boumahdi Mouloud	Lecturer Class A	Médéa Univesity	President
Dr Hanini Salah	Professor	Médéa Univesity	Examiner
Dr Chikh Salah	Professor	USTHB Algiers	Examiner
Dr Ait Saada Mabrouk	Professor	USTHB Algiers	Examiner
Dr Alliche Mounir	Lecturer Class A	Médéa Univesity	Thesis Director
Dr Borjini Mohamed Naceur	Professor	ENIM, Monastir, Tunisia	Thesis Co-Director
Dr Rebhi Redha	Lecturer Class A	Médéa Univesity	Guest member

ABSTRACT

In this work, we present the study of natural convection heat transfer with nanofluid inside inclined two-dimensional porous medium enclosure influenced by external magnetic field. The Dupuit Darcy model has been used to describe the fluid flow inside the porous medium, for analysing the departure from the linear Darcy situation. The enclosure bounded by differentially heated vertical walls, and the horizontal ones kept adiabatic. The governing equations have been solved together with boundary conditions using the finite difference method with uniform grid size mesh by an implemented FORTRAN code.

Two applications have been performed, where the dependency of the fluid flow and the heat transfer rate on Raleigh number (R_T); nanoparticles volume fraction (ϕ); Hartman number (Ha); inertial effect parameter (G); porosity of the porous medium (ε), inclination angle of the cavity (γ) and inclination angle of the magnetic field (ξ) is analysed.

The first application performed for the Copper-Water (Cu-Water) nanofluid saturated Aluminium foam porous medium. The main findings are: the increasing of inertial effect parameter reduces the intensity of convection, and the conduction mode is dominated for the high value of inertial effect parameter. Furthermore, the increasing of nanoparticles volume fraction has a negative effect on convection intensity due to the increases of dynamic viscosity.

The second application performed for Single Wall Carbon Nanotube –Water (SWCNT-Water) and Aluminum oxide-Water (Al_2O_3- Water) saturated the porous medium under the effect of external magnetic field. The main findings are : the increasing of SWCNT concentration enhances significantly the convection intensity until a threshold value of Rayleigh number due to the increase of dynamic viscosity. The increase of inertial effect parameter and the Hartman number reduces the fluid flow and the convection strength, and the conduction mode is dominated for the high value for the both parameters. Furthermore, the heating of the cavity by the left vertical walls produces better fluid flow and convection strength for Hartman number more than 2. The inclination angle $\xi = 45°$ of the magnetic field represents the best for fluid flow strength and heat transfer rate regardless the Hartman and Rayleigh numbers.

Key words: Free convection, Nanofluid, Porous media, Magnetic field, Inertial effect parameter, Dupuit-Darcy model.

RÉSUMÉ

Dans ce travail, nous présentons l'étude du transfert de chaleur par convection naturelle avec des nanofluides à l'intérieur d'une enceinte de milieu poreux bidimensionnelle inclinée influencée par un champ magnétique externe. Le modèle Dupuit Darcy a été utilisé pour décrire l'écoulement de fluide à l'intérieur du milieu poreux, pour analyser l'écart par rapport à la situation linéaire de Darcy. L'enceinte délimitée par des parois verticales différentiellement chauffées, et les horizontales maintenues adiabatiques. Les équations gouvernantes ont été résolues ainsi que les conditions aux limites en utilisant la méthode des différences finies avec un maillage de taille de grille uniforme par un code FORTRAN implémenté.

Deux applications ont été réalisées, où la dépendance de l'écoulement du fluide et du taux de transfert de chaleur sur le nombre de Raleigh (R_T); fraction volumique de nanoparticules (ϕ); nombre de Hartman (Ha); paramètre d'effet inertiel (G); la porosité du milieu poreux (ε), l'angle d'inclinaison de la cavité (γ)et l'angle d'inclinaison du champ magnétique (ξ) sont analysés.

La première application a été réalisée pour le milieu poreux en mousse d'aluminium saturé avec le nanofluide Cuivre-Eau (Cu-Eau). Les principales conclusions sont les suivantes : l'augmentation du paramètre d'effet inertiel réduit l'intensité de la convection et le mode de conduction est dominé pour la valeur élevée du paramètre d'effet inertiel. De plus, l'augmentation de la fraction volumique des nanoparticules a un effet négatif sur l'intensité de convection en raison de l'augmentation de la viscosité dynamique.

La deuxième application a été réalisée pour les nanotubes de carbone à paroi unique - eau (SWCNT - eau) et L'oxyde d'aluminium-eau (Al_2O_3-eau) saturés le milieu poreux sous l'effet du champ magnétique externe. Les principales conclusions sont les suivantes : l'augmentation de la concentration en SWCNT améliore considérablement l'intensité de convection jusqu'à une valeur seuil du nombre de Rayleigh en raison de l'augmentation de la viscosité dynamique. L'augmentation du paramètre d'effet inertiel et du nombre de Hartman réduit l'intensité de l'écoulement et de la convection, et le mode de conduction est dominée pour les valeurs élevées pour les deux paramètres. En outre, le chauffage de la cavité par les parois verticales gauches produit une meilleure intensité d'écoulement de fluide et de la convection pour le nombre Hartman supérieur à 2. L'angle d'inclinaison du champ magnétique $\xi = 45°$

représente le meilleur pour l'intensité de l'écoulement du fluide et le taux de transfert de chaleur quels que soient les nombres de Hartman et Rayleigh.

Mots clés: Convection libre, Nanofluide, Milieux poreux, Champ magnétique, Paramètre d'effet inertiel, Modèle de Dupuit-Darcy.

ملخص

في هذا العمل ، نقدم دراسة نقل الحرارة بالحمل الطبيعي مع السائل النانوي داخل حاوية مسامية ثنائية الأبعاد مائلة تحت تأثير مجال مغناطيسي خارجي. تم استخدام نموذج دوبوي دارسي لوصف تدفق السوائل داخل الوسط المسامي، لتحليل التباعد من وضع دارسي الخطي. السطحين العموديين للحاوية ذواتي درجتين حراريتين مختلفتين و ثابتتين، والجدران الأفقية معزولة حراريا. تم حل المعادلات المتحصل عليهاجنبًا إلى جنب مع شروط الحدود باستخدام طريقة الفروق المحدودة مع شبكة حجم شبكة موحدة بواسطة كود فورترون الذي تم انجازه .

تم تنفيذ تطبيقين، حيث تمت دراسة اعتماد تدفق السائل ومعدل نقل الحرارة على عدد رايلي (R_T) ؛ نسبة الجسيمات النانوية (ϕ)، رقم هارتمان (Ha) Hartman ؛ معامل تأثير العطالة (G) ؛ مسامية الوسط المسامي (ε)؛ زاوية ميل الحاوية (γ) وزاوية الميل للمجال المغناطيسي (ξ).

تم عمل أول تطبيق للوسط المسامي رغوة الألومنيوم المشبعة بسائل نانوي نحاس-ماء (Cu-Water). الاستنتاجات الرئيسية هي كما يلي: زيادة معامل تأثير العطالة الذاتي يقلل من شدة الحمل الحراري ، ويهيمن وضع التوصيل الحراري على الحمل الحراري بالنسبة للقيم العالية لمعامل تأثير العطالة. بالإضافة إلى ذلك، فإن الزيادة في نسبة الجسيمات النانوية لها تأثير سلبي على كثافة الحمل الحراري بسبب زيادة اللزوجة الديناميكية.

تم عمل التطبيق الثاني على الأنابيب الكربونية النانوية أحادية الجدار - ماء (Water - SWCNT) وأكسيد الألومنيوم- ماء (Al2O3-Water) المشبعة للوسط المسامي تحت تأثير المجال المغناطيسي الخارجي. الاستنتاجات الرئيسية هي كما يلي: الزيادة في تركيز الأنابيب الكربونية النانوية أحادية الجدار يحسن بشكل كبير كثافة الحمل الحراري حتى قيمة أقصى لرقم رايلي Rayleigh بسبب الزيادة في اللزوجة الديناميكية. تؤدي زيادة معامل العطالة وعدد هارتمانHartman إلى تقليل شدة التدفق والحمل الحراري، ويهيمن وضع التوصيل الحراري على القيم العالية لكلاهما. بالإضافة إلى ذلك، فإن تسخين الحاوية عبر الجدار العمودي الأيسر ينتج تدفق أفضل للسائل والحمل الحراري بالنسبة لعدد هارتمان أكبر من 2. تمثل زاوية ميل المجال المغناطيسي $\xi = 45°$ الأفضل لشدة تدفق السائل ومعدل نقل الحرارة بغض النظر عن أرقام هارتمانHartman ورايلي Raleigh.

الكلمات المفتاحية: حمل حراري طبيعي، نانو فلويد ، وسائط مسامية ، مجال مغناطيسي ، معامل تأثير العطالة، نموذج دوبوي دارسي

ACKNOWLEDGEMENT

Praise be to God Creator of the universes, the All-Knower, Who gave me strength, courage and endurance until the completion of this work

With immense pleasure and deep sense of gratitude, I wish to express my sincere thanks to my supervisor Dr. **Alliche Mounir**, for the appreciable help, precious advice the trust he has placed in me, for his ideas which have served to enrich this thesis and the adequate supervision, without his motivation and continuous encouragement, this research would not have been successfully completed.

My thanks also go to my Co-supervisor Mr. **Borjini Mohamed Naceur** Professor at Engineers Natinal School, Monastir University in Tunisia for his encouragement and invaluable advice.

I am also very grateful to Mr. **Ali Chamkha** Professor at Kuwait College of Science and Technology for the many discussions which enlightened me on the problems treated on convection in porous media.

I express my sincere thanks to Dr **Rebhi Redha** Lecturer in the University of Medea for his appreciable help and his constant and unrelenting support throughout this period of doctoral study.

I would also like to address my thanks to Dr **Boumahdi Mouloud** for agreeing to chair the examination jury for this thesis. I also thank the professors **Hanini Salah**, **Chikh Salah, Ait Saada Mabrouk**, and the Dr **Rebhi Redha** for having accepted to examine this thesis and to participate in my jury and for the interest they have shown in our research work. , despite their multiple occupations.

I would like to extend a big thank you and express my extreme gratitude to all my family for their patience and encouragement throughout these years of study and research.

I thank my mother very much who has been present with me from the start as well as my wife Amriya , my children Amira Meriem and Hicham.

Alilat Djamel

DEDICATIONS

I dedicate this modest work:

*To my Mother **Hadda**,*
In memory of my father and grandparents,
*To my wife **Amriya**,*
*To my children **Amira Meriem** and **Hicham**.*

Table of contents

ABSTRACT vi
Acknowledgments ivi
Dedication v
Table of Contents vi
Abreviations and Nomenclatures viii
Liste of figures x
List of Tables xiv
General Introduction 1
1. Objectives of this study 2
2. Scope of this Study 3
CHAPTER I : GENERALITIES AND STATE OF THE ART REVIEW 4
1.1 Introduction 4
1.2. General information on porous media 4
1.2.1 Flow models in porous media 7
1.2.1.1. Darcy's law 8
1.2.1.2. Dupuit-Darcy's law 10
1.2.1.3. Darcy-Brinkaman's law 11
1.2.1.4. General model 12
1.3 General information on nanofluids 12
1.3.1 Suitable applications for nanofluids 16
1.3.2 Advantages and disadvantages of nanofluids 16
1.3.3 Transport equations for nanofluids 17
1.3.3.1 Single-phase approaches 17
1.3.3.2 Two-phase approaches 17
1.4 General information on magnetohydrodynamics (MHD) 18
1.4.1 Lorentz force 21
1.4.2 Faraday's law 21
1.4.3 Maxwell's equations 22
1.4.4 The Navier–Stokes equation 22
1.4.5 Ohm's law 23
1.5 State of the art review 23
1.6 Conclusion 31
CHAPTER II : PHYSICAL MODEL AND MATHEMATICAL FORMULATION 33
2.1 Problem description 33
2.2 Simplifying assumptions 34

2.3 Mathematical formulation **34**
2.3.1 Continuity equation **35**
2.3.2 Equation of motion: Dupuit-Darcy's law **35**
2.3.3 Energy equation **35**
2.4 Applications **38**
2.4.1 **First application:** Cu-Water nanofluid saturated Aluminium foam porous medium without magnetic field effect **38**
2.4.2 **Second application:** SWCNT - Water and Al_2O_3 - Water nanfluid saturated porous medium with external magnetic field effect **40**
2.5 Boundary conditions **42**
2.5.1 Hydrodynamic boundary conditions **42**
2.5.2 Thermal boundary conditions **42**
2.6 Heat transfer **42**
2.7 Conclusion **43**

CHAPTER III : NUMERICAL METHOD **44**

3.1 Thermal boundary conditions discretization **45**
3.2 Energy equation discretization **46**
3.3 Momentum equation discretization **48**
3.4 Velocity fields discretization **50**
3.5 Discretization of velocity boundary conditions **51**
3.6 Calculation algorithm **51**
3.7 Conclusion **53**

CHAPTER IV : RESULTS AND DISCUTION **54**

4.1 First application : Cu-Water nanofluid saturated Aluminium foam porous medium without magnetic field effect **54**
4.2 Second application : SWCNT-Water and Al_2O_3 - Water nanofluid saturated porous medium with magnetic field effect ... **72**
4.3 Conclusion **92**

CHAPTER V : CONCLUSION AND RECOMMENDATIONS **93**

5.1 Conclusion **93**
5.1.1 Cu - Water nanofluid saturated Aluminium foam porous medium **93**
5.1.2 WCNT-Water nanofluid saturated porous medium and influenced by external magnetic field **94**
5.2 Recommandations **95**

REFERENCES **96**

ABBREVIATIONS AND NOMENCLATURE

List of Symbols

$\vec{B}$	Applied magnetic field ($Wb.m^{-2}$)
C_p	Specific heat ($J{\cdot}kg^{-1}{\cdot}K^{-1}$)
d	Particle size (diameter) (m)
$\vec{D}$	Electric displacement ($C.m^{-2}$)
$\vec{E}$	Electric field ($V.m^{-1}$)
$\vec{F}$	Force (N)
g	Gravitational acceleration vector ($m{\cdot}s^{-2}$)
$\vec{H}$	Magnetic field strength ($A.m^{-1}$)
I	Electric current (A)
$\vec{J}$	Electric current density ($A.m^{-2}$)
k	Thermal conductivity ($W{\cdot}m^{-1}{\cdot}K^{-1}$)
K	Permeability of porous medium (m^2)
$\tilde{K}$	Material parameter (m)
L, H	Dimensions of cavity (m)
p	Pressure ($N{\cdot}m^{-2}$)
q	Charge of particle (C)
T	Temperature (K)
V	Velocity vector
u,v	Velocity components in x and y directions ($m.s^{-1}$)
x,y	Cartesian coordinates (m)

Greek Symbols

γ	Inclination angle of the cavity to the horizontal (°)
ξ	Inclination angle of the of applied magnetic field (°)
α	Thermal diffusivity ($m^2.s^{-1}$)
β	Thermal expansion coefficient (K^{-1})
ϕ	Nanoparticle volumetric fraction
μ	Dynamic viscosity ($kg{\cdot}m^{-1}{\cdot}s^{-1}$)
μ_e	Magnetic permeability (henries per metre (H/m) or $N{\cdot}A^{-2}$)
ν	Kinematic viscosity ($m^2.s^{-1}$)
ρ	Density ($kg{\cdot}m^{-3}$)
ρ_c	Electric charge density ($C.m^{-3}$)

τ	Time (s)
σ	Electrical conductivity ($\Omega^{-1}.m^{-1}$)
Φ	Electrical potential (V)
ε_e	Permittivity (or dielectric constant) (farad per meter ($F.m^{-1}$))
ε	Porosity

Subscript

0	Reference value
C	Cold
f	Fluid
h	Hot
max	Maximum value
nf	Nanofluid
p	Nanoparticle
x, y	Component of a vector quantity

Dimensionless Quantities

G	Parameter that measures the inertial effects
t	Time
U,V	Velocity components
X	Cartesian coordinate in x direction
V	Cartesian coordinate in y direction
Ψ	Stream function
θ	Temperature

Dimensionless Numbers

Ha	Hartmann number
Nu	Nusselt number
Nu_m	Average Nusselt number
$\overline{Nu}_L$	Average Nusselt number of the left wall
$\overline{Nu}_R$	Average Nusselt number of the right wall.
R_T	Darcy-Rayleigh number

Abbreviations

CNT	Carbon Nanotube
SWCNT	Single-Wall Carbon Nanotube

Liste of figures

Figure 1.1.	Examples of porous media.....	**5**
Figure 1.2.	Illustration of the intermediate size of the R.E.V between the size of the porous medium at the macroscopic scale L and pore scale d.....	**6**
Figure 1.3.	Device for measuring permeability on consolidated material,.....	**8**
Figure 1.4.	Thermal conductivity of some common liquids and solids, the high thermal conductivity of solids gives the idea to mix them with liquids to enhance the effective thermal conductivity.....	**13**
Figure 1.5.	Comparaison entre les tailles de nanotubes de carbone en tant que nanoparticule typique avec d'autres éléments.....	**14**
Figure 1.6.	The preparation of nanofluids does not only consist in mixing nanoparticles and a liquid, but special physical and chemical techniques are necessary to have a stable nanofluid,.....	**14**
Figure 1.7.	Parameters influencing the effective thermal conductivity of nanofluids	**15**
Figure 1.8.	Some applications of nanofluids.....	**16**
Figure 1.9.	Main approaches for modeling the flow of nanofluids	**18**
Figure 1.10.	Induced current in a conductive fluid in the presence of a magnetic field.....	**19**
Figure 1.11.	(a and b) Effect of the magnetic field on the flow of the conductive fluid; (c) Law of the right hand. (Blue line: magnetic field, purple line: current, green line: movement).....	**19**
Figure 1.12.	The Two-Key Physical Effects Occurring in Magnetohydrodynamic.....	**21**
Figure 1.13.	Relation Between the Lorentz Force and Faraday's Law	**21**
Figure 2.1.	Physical model and coordinate system.....	**33**
Figure 3.1.	Meshing of the computational domain in (i, j).....	**44**
Figure.4.1.	Comparison between the present results (a) and "Sheremet et al. (2015)," (b) at $\phi = 0.05$, $\varepsilon = 0.5$, $G = 0.5$, $R_T = 100$, $\gamma = 0°$ and the aluminium foam as the solid matrix of the porous medium.....	**55**
Figure 4.2.	Streamlines (upper) and isotherms (lower) for $R_T = 200$, $\phi = 0.05$, $\varepsilon = 0.5$, $\gamma = 0°$	**56**
Figure.4.3.	Variation of the maximum absolute stream function (a) and the average left Nusselt number (b) with the Rayleigh number for $\phi = 0.05$, $\varepsilon = 0.5$, $\gamma = 0°$ and different values of inertial effects parameter G	**57**

Figure.4.4. Streamlines (upper) and isotherms (lower) for $R_T = 200$, $G = 0.5$, $\varepsilon = 0.5$ and $\gamma = 0°$ **59**

Figure. 4.5. Variation of the maximum absolute stream function (a) and the average left Nusselt number (b) for $G = 0.5$, $\varepsilon = 0.5$, $\gamma = 0°$ with the Rayleigh number, R_T, and different values of nanoparticles volume fraction, ϕ **60**

Figure. 4.6. Streamlines (upper) and isotherms (lower) for $R_T = 200$, $G = 0.5$, $\phi = 0.05$ and $\gamma = 0°$ **61**

Figure. 4.7. Variation of the maximum absolute stream function (a) and the average left Nusselt number (b) with the Rayleigh number for $G = 0.5$, $\phi = 0.05$, $\gamma = 0°$ and different values of porosity ε **63**

Figure.4.8. Dependence of the maximum absolute stream function (a) and the average left Nusselt number (b) on inertial effect parameter for $R_T = 200$, $\phi = 0.05$ and $\gamma = 0°$ and different porosity, ε **64**

Figure.4.9. Streamlines (upper) and isotherms (lower) for $R_T = 200$, $G = 0.5$, $\phi = 0.05$, and $\varepsilon = 0.5$ **65**

Figure.4.10. Dependence of the maximum absolute stream function (a) and the average left Nusselt number (b) on inclination angle γ for $R_T = 200$, $\phi = 0.05$, $\varepsilon = 0.5$ and different inertial effect parameter G **66**

Figure.4.11. Dependence of the maximum absolute stream function (a) and the average left Nusselt number (b) on inclination angle γ for $R_T = 200$, $G = 0,5$, $\varepsilon = 0.5$ and different nanoparticles volume fraction ϕ ... **68**

Figure 4.12. Variation of the average left Nusselt number with Rayleigh number for different values of nanoparticles volume fraction ϕ (G =0.5, $\varepsilon = 0.5$, γ =90°)..... **69**

Figure.4.13. Dependence of the maximum absolute stream function (a) and the average left Nusselt number (b) on nanoparticles volume fraction for $R_T = 200$, $G = 0.5$, $\gamma = 0°$ and different porosity values ε **70**

Figure.4.14. Dependence of the maximum absolute stream function (a) and the average left Nusselt number (b) on nanoparticles volume fraction for $R_T = 200$, $\varepsilon = 0.5$, $\gamma = 0°$ for different inertial parameter G **71**

Figure. 4.15. Comparison between the present results (a) and Mahmud et al. [6] (b) at $\phi = 0$, $G = 0$, $\gamma = 0°$, $\xi = -90°$ **74**

Figure. 4.16. Streamlines (upper) and isotherms (lower) for SWCNT at $R_T = 200$, $G = 0.5$, $Ha = 0.5$. $\gamma = 0°$. $\xi = 0°$ **76**

Figure. 4.17. Variation of the maximum absolute stream function (a) and the average left Nusselt number (b) with the Rayleigh number, R_T, and different values of nanoparticles volume fraction, ϕ at $G=0$, $Ha=0$, $\gamma=0°$, $\xi=0°$ 77

Figure. 4.18. Variation of average Nusselt number ration with Rayleigh number for different nanoparticles volume fraction at $G=0$, $Ha=0.5$, $\gamma=0°$, $\xi=0°$ 78

Figure.4.19. Streamlines for different values of G and Ha for SWCNT at $R_T=200$. $\phi=0.05$. $\gamma=0°$ $\xi=0°$ 79

Figure. 4.20. Isotherms for different values of G and Ha for SWCNT at $R_T=200$. $\phi=0.05$. $\gamma=0°$. $\xi=0°$ 80

Figure. 4.21. Dependence of the maximum absolute stream function (a) and the average left Nusselt number (b) on nanoparticles volume fraction for SWCNT at $R_T=200$, $G=0.5$, $\gamma=0°$, $\xi=0°$ for different Hartmann number Ha 82

Figure. 4.22. Dependence of the maximum absolute stream function (a) and the average left Nusselt number (b) on nanoparticles volume fraction for SWCNT at $R_T=200$, $Ha=0.5$, $\gamma=0°$, $\xi=0°$ for different inertial effect parameter G 83

Figure. 4.23. Dependence of the maximum absolute stream function (a) and the average Nusselt number (b) on inertial effect parameter G for SWCNT at $R_T=200$, $\phi=0.05$, $\gamma=0°$ and $\xi=0°$ for different Hartmann number..... 84

Figure.4.24. Variation of the average Nusselt number ration with SWCNT loading (a) for different Harman number for SWCNT at $R_T=200$, $G=0.5$, $\gamma=0°$, $\xi=0°$, (b) for different inertial effect parameter at $R_T=200$, $Ha=0.5$, $\gamma=0°$, $\xi=0°$ 85

Figure.4.25. Variation of the average Nusselt number ration with inertial effect parameter for different Harman number for SWCNT at $R_T=200$, $\phi=0.05$, $\gamma=0°$, $\xi=0°$ 87

Figure. 4.26. Dependence of the maximum absolute stream function (a) and the average Nusselt number (b) on magnetic field inclination angle for SWCNT at $R_T=200$, $G=0.5$ $Ha=0.5$ and $\gamma=0°$ for different nanoparticles volume fraction..... 88

Figure. 4.27. Dependence of the maximum absolute stream function (a) and the average Nusselt number (b) on Hartmann number for SWCNT at

$R_T = 200, G = 0.5$ $\phi = 0.05$ and $\xi = 45°$ for different inclination angles of the cavity..... 89

Figure.4.28. Variation of the maximum absolute stream function (a) and the average Nusselt number (b) with the inclination of the cavity γ for different Hartmann numbers Ha and magnetic field inclination angle ξ for SWCNT at $R_T = 200, G = 0.5, \phi = 0.05$ 90

Figure. 4.29. Variation of the maximum absolute stream function (a) and the average Nusselt number (b) with the Rayleigh number R_T for different Hartmann numbers Ha and magnetic field inclination angle ξ for SWCNT at $G = 0.5$ $\phi = 0.05, \gamma = 0°$ 91

List of Tables

Table 2.1. Thermophysical properties of fluid (water), Copper (Cu),Aluminium Oxide (Al_2O_3) and Single-Wall Carbon Nanotube (SWCNT) **38**

Table 4.1. Variations of the average Nusselt number of hot wall , cold wall and the maximum absolute value of stream function with different grid sizes (Cu water nanofluid-Aluminium foam as solid matrix of porous medium $R_T = 1000$, $\phi = 0.05$, $\varepsilon = 0.8$, $\gamma = 0°$, $G = 0$)..... **55**

Table 4.2. Effect of the inertial effects parameter G on the average Nusselt number and the maximum absolute value of stream function for $R_T = 1000$, $\phi = 0$ and $\gamma = 0°$ **56**

Table 4.3. Variations of the average Nusselt number of hot wall and the maximum absolute value of stream function with different grid sizes ($R_T = 200$, $G = 0.5$, $\gamma = 0$, $\xi = 0$, $Ha = 0.5$, $\phi = 0.05$)..... **72**

Table 4.4. Comparison of the average Nusselt number with previous numerical results for $G = 0$, $Ha = 0$, $\phi = 0$ and $\gamma = 0$ **73**

Table 4.5. Effect of the inertial effects parameter G on the average Nusselt number and the maximum absolute value of stream function for $R_T = 1000$, $\phi = 0$, $Ha = 0$ and $\gamma = 0$ **73**

Table 4.6. Comparison of average Nusselt number with the results of Mahmud et al. $\phi = 0$, $G = 0$, $\gamma = 180°$, $\xi = 90°$ **74**

GENERAL INTRODUCTION

General Introduction

The reduction of energy consumption, as well as the control of energies, constituting one of the major challenges of our society. The main sources of energy today are fossil fuels (oil and coal for example) with an increasingly limited stock therefore more and more expensive. Our energy consumption is such that the induced pollution is high, with in particular a very large amount of greenhouse gases released into the atmosphere. It is therefore necessary to control energy consumption and develop other sources of energy, in particular so-called renewable energies, which in recent years, have developed considerably (at least in rich countries). However, today, the power supplied by such sources is too far to ensure sufficient energy consumption. For example, it is still very expensive to ensure the energy independence of a building with solar panels.

Therefore, in order to optimize these systems, it becomes important to know the convection flows (natural or mixed) induced by heating or air conditioning. Natural convection refers to the process of heat transfer resulting from the movement of elementary particles of a fluid between areas with different temperatures. This movement causes the fluid particles to mix, which exchange energy and the amount of movement between them. Unlike forced convection, the movement of the fluid of which is due to an external energy supply, natural convection originates from variations in the density within the fluid itself, linked to variations in its temperature. The structure and intensity of natural convection are directly related to the external thermal stresses that trigger it, the nature of the fluid and the geometry of the space where the process takes place. The technological importance of natural convection is confirmed by the exploitation of this phenomenon in fields as numerous as different such as metallurgy, building, cooling of nuclear reactors, cooling of electronic circuits and transformers. Furthermore, researchers have become increasingly interested in the problems of heat transfer induced by natural convection within a confined medium (fluid medium or porous medium saturated by a fluid).

Finding out the more suitable heat transfer fluid in industrial applications is an important concern for researchers and engineers. Since the Maxwell's theories in 1873, they attempted to break the limitation against enhancing the conventional fluids thermal conductivity by dispersing millimetre or micrometre sized particles in liquid, but the major problem recorded

by this technique is the rapid sedimentation of those particles in the fluid and the erosion of equipment working with those type of fluids. During the last two decades, nanotehnology has made a considerable progress. It represents the fifth technology revolution in history after the steam engine in the late 1700s; steel, electricity and railway in the late 1800s; cars, chemicals and mass production in the early 1900s and computers in the mid-1900s. With the implementation of nanotechnology, the dispersion of nanosized solid particules of size below 100nm in traditional base fluid such as water, oil and ethylene glycol and the so called nanofluid can be realized. The nanofluid thermo physical properties as specific gravity, density, viscosity, convective heat transfer coefficient and electrical conductivity can be significantly improved compared to the base fluid to subsequently improve the overall thermal and hydrodynamic behaviour of working fluid. The notable improvement in heat transfer properties of nanofluids increases their use in various engineering applications such as the cooling of electronic devices, automotive nuclear reactors, solar thermal energy, thermal energy storage, refrigeration and air conditioning systems and so on.

1. Objectives of this study

The present work concerns the numerical study of the effect of the addition of nanoparticles on the behavior of natural convection of a fluid saturating a porous matrix and subjected to an external magnetic field. The study concerns an inclined square geometric configuration subjected to two diffferent temperatures T_h and T_f . Three nanoparticles are used in this study: Copper (Cu), Aluminum oxide (Al_2O_3) and Single-Wall Carbon Nanotube (SWCNT), while the water is used as abase fluid.

An implemented FORTRAN code based on the finite difference method is used for solving governing equations.

The Dupuit-Darcy model, which includes the effect of inertia for low or large Reynolds flows, and the Boussinesq approximation were used to model natural convection inside the porous medium.

Also the Tiwari and Das model for calculating the thermophysical properties of the nanofluids was used for the nanofluides.

For SWCNT, the Xue model is used to determine the thermal conductivity of SWCNT-Water nanofluid. The influence of controling parameters such as ; the Rayleigh number R_T , the inertial effect parameter G , the Hartman number Ha , the volumetric fraction of the nanoparticles ϕ , the porosity of the porous medium ε , the inclination angle of the cavity (γ) and the inclination angle of of the magnetic field (ξ) on the intensity of the flow and heat transfer rate will be discussed for a wide range of basic parameters.

2. Scope of this Study

This thesis consists of five chapters. The first chapter is an introduction to the present work and a bibliographic search of the previous works found in the literature in this area of investigation. The second chapter of the thesis is devoted to the definition of the studied geometry, and the mathematical formulation of the problem, where the basic equations governing the system and the associated boundary conditions will be presented. All the stages of the numerical approach (finite difference method) as well as the calculation algorithm used in this work are presented in the third chapter. The fourth chapter deals with the different results obtained in this work and their discussions. Finally in the fifth chapter, we showed the main results found along this study with a general conclusion and future perspectives.

CHAPTER I
GENERALITIES AND STATE OF THE ART REVIEW

CHAPTER I

GENERALITIES ANS STATE OF THE ART REVIEW

1.1 Introduction

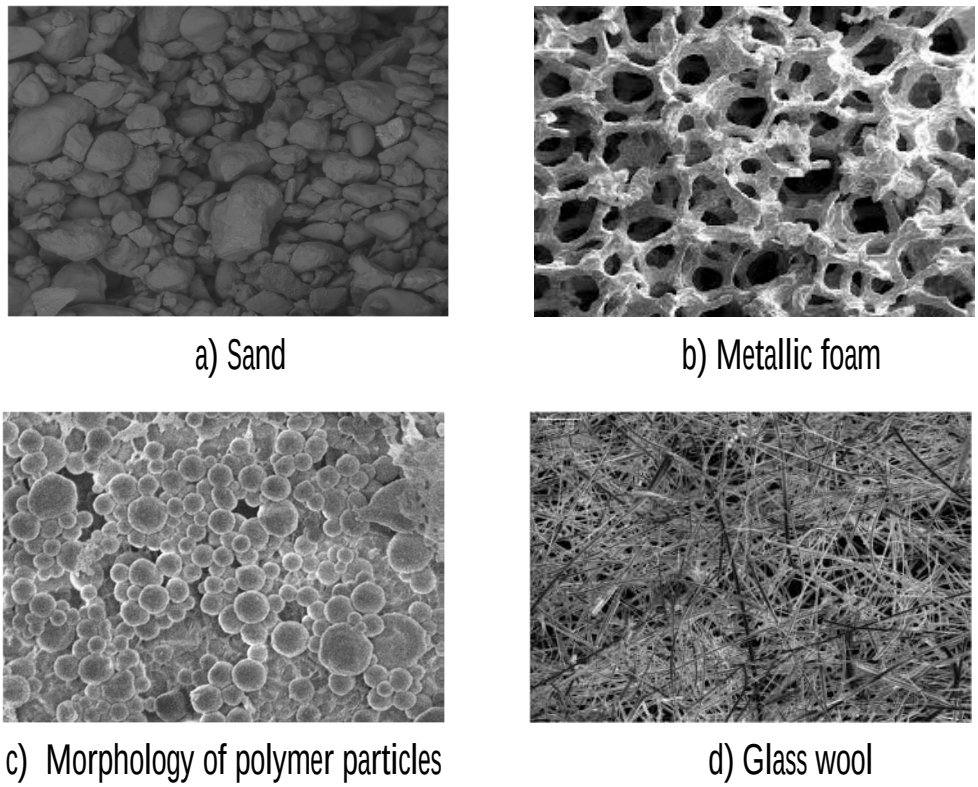
In recent years, researchers have become increasingly interested in the problems of heat transfer induced by natural convection within a confined medium (fluid medium or porous medium saturated by a fluid). A saturated porous medium is a continuous medium, cohesive or not, which internally has a fraction of volume accessible to a fluid. This fraction of non-solid volume, composed of caves, crevices, pores, etc., constitutes what is called the porosity of the porous medium (Figure 1.1). Porosity is obviously an essential descriptive element of the medium, however two porous media having the same porosity can have very different properties. Pores that do not open (blind pores) or occluded can be found in a porous medium; a porous medium containing both blind pores and more or less interconnected open pores, may, through these open pores, the fluid can flow. In the complex reality of a porous medium, parameters such as capillary diameter or porosity are only average global values, it is unable to translate the complex topology of the actual flow through the medium accurately. In the case where the empty spaces are filled with the same phase (liquid or gaseous), the porous medium is said to be saturated with the fluid. Porous media play an important role in many industrial sectors such as petroleum engineering, chemical engineering, civil engineering, medicine, etc. Some examples of porous media are illustrated in Figure 1.1.

1.2. General information on porous media

When studying flows in porous media, two scales are essential for the description of phenomena **(Bories 1985)**. The pore scale, or microscopic scale, is associated with the average pore diameter *d*. Within this scale, the local quantities can vary widely. On the porous medium scale, or macroscopic scale, the variation of physical quantities is defined on average vaues over a certain volume of porous medium, called representative elementary volume and denoted R.E.V (Figure 1.2).

This macroscopic scale is associated with a geometric dimension of the environment. L_a . Let *L* the characteristic dimension of the R.E.V. This dimension *L* must satisfy the following double inequality:

$$d \leq L \leq L_a \tag{1.1}$$



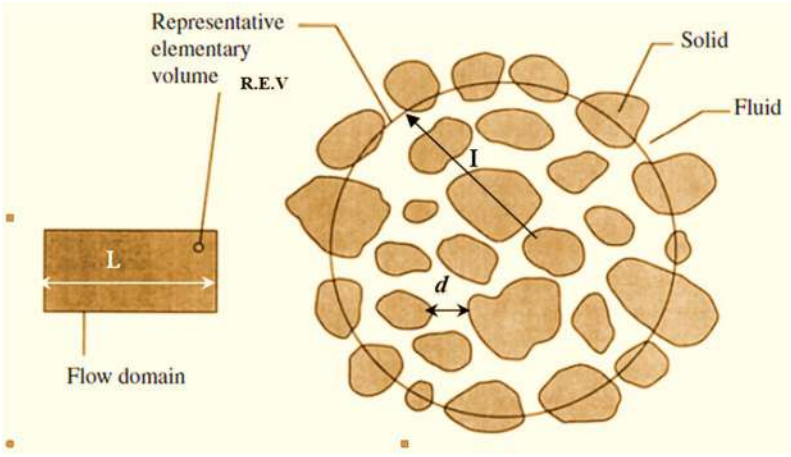
a) Sand b) Metallic foam

c) Morphology of polymer particles d) Glass wool

Figure 1.1: Examples of porous media

The parameters characterizing the porous medium are therefore obtained by taking an average on the R.E.V. However, in what follows we present a macroscopic definition of these parameters, which appear in these different empirical models.

The developing phenomena in a porous medium depend on the properties of the fluid and the geometry of the solid matrix. This is characterized by a certain number of mean, geometric or statistical quantities. In what follows, we define the different characteristics that appear at the level of the different empirical models for macroscopic description of flows in porous media.



Macroscopic scale porous medium *L* Porous medium at pore scale *d*

Figure 1.2: Illustration of the intermediate size of the R.E.V between the size of the porous medium at the macroscopic scale *L* and at the pore scale *d*.

- **Porosity**

The porosity of a porous medium, denoted ε, is the ratio of the volume of the pores to the total volume of the porous matrix.

$$\varepsilon = \frac{\text{Pore volume}}{\text{Total volume of the porous medium}} \tag{1.2}$$

- **Permeability**

The permeability is the property of a material to transmit a fluid under pressure, the permeability *K* depends only on the porosity and the geometry of the solid matrix. Several evaluations of the permeability K as a function of ε and of a characteristic dimension of the porous matrix at the pore scale have been proposed. The different expressions giving the permeability depend on the geometry of the porous medium. The value of the permeability is generally determined experimentally. Several empirical models have been proposed. In particular, we recall :

Kozeny-Carman's (1927) relation for an unconsolidated porous medium made up of identical elements of simple geometry:

$$K = \frac{d^2\varepsilon^2}{36C_0\left(1-\varepsilon\right)^2} \tag{1.3}$$

where d is the characteristic length of the pores or the diameter of the particles and C_0 is a constant which depends on the shapes of the grains. It is between 3.6 and 5.

Ergun's (1952) relation, similar to the above equation when considering the unidirectional flow of an incompressible fluid within a porous column made up of spherical particles of diameter *d* and the column is subjected to a pressure gradient.

$$K = \frac{d^2 \varepsilon^3}{150(1-\varepsilon)^2} \tag{1.4}$$

This relation is similar to that of Kozeny-Carman for the value of C_0=4.16. When we model the porous matrix as a bundle of parallel capillary tubes leads to the following expression of permeability:

$$K = \varepsilon^2 \frac{d^2}{32} \tag{1.5}$$

where $\varepsilon = n\pi d^2/4$ and *n* is the number of capillaries per unit area perpendicular to the direction of flow.

- **Tortuosity**

The description of the pore geometry involves the notion of connectivity, corresponding to the complexity of a continuous path through the pore space. It is also necessary to take into account the "dead arms" which are numerous in low porous and very heterogeneous environments. To describe these different aspects, we introduce the parameter τ designating the tortuosity, which we define as follows :

$$\tau = \left(\frac{L_e}{L}\right)^2 \tag{1.6}$$

where L_e is the real length of the fluid contour lines crossing a sample of length *L* from a porous medium, modeled as a network of parallel or wavy capillaries. This report plays an important role in diffusion issues.

1.2.1. Flow models in porous media

Due to the geometrical complexity of the pore space, the approach of the mechanics of continuous media to establish the models of conservation of momentum, energy and mass, can only be applied after passing to a macroscopic scale which allows to establish an equivalence

between the real dispersed medium and a fictitious continuous medium. The establishment of macroscopic conservation equations is formally obtained from microscopic equations. The first model was proposed by **Darcy (1856)**.

1.2.1.1. Darcy's law

The theory of flows in porous media is based on the results of experiments carried out by **Darcy (1856)**. Darcy's experiment consists in measuring a flow rate and a load gradient which make it possible to calculate a permeability with the formula (1.10). This experience was initially developed for sands or inconsistent materials. The sample is in a tube of radius R, and subjected to a load gradient due to the difference in water height, for the two upstream and downstream reservoirs, the levels of which are kept constant. The flow direction is opposite to the load gradient. This load gradient can also be determined by measuring the difference in water height (Δh) in two piezometric tubes distant from L (Figure 1.3).

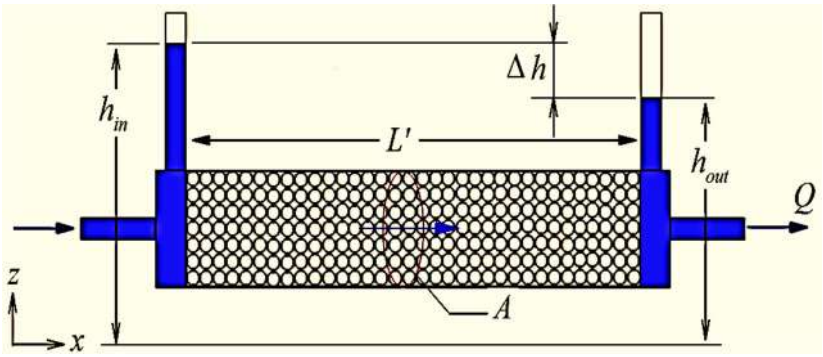


Figure 1.3: Device for measuring permeability on consolidated material.

The filter fluid flows from the upper level to the base of the column through the porous layer and rises in the pressure tubes at decreasing levels in the direction of flow. The piezometric height decreases linearly as a function of the vertical traveled distance; the slope of the piezometric line measures the linear pressure drop:

$$J = \frac{\bar{h}_2 - \bar{h}_1}{L} \tag{1.7}$$

If the porous medium is fine enough, experience shows that the flow rate of the device is proportional to the slope of this straight line as long as it is not too steep; with the usual sign convention, we have the equation:

$$Q = -KA\frac{\Delta h}{L} \tag{1.8}$$

where *K* is a constant which depends on both the fluid and the porous medium.

If, instead of reasoning in manometric height, we write the previous law in terms of pressure we obtain;

$$q = \frac{Q}{A} = -k\left(\frac{P_2 - P_1 + \rho g h}{h}\right) \tag{1.9}$$

The permeability can be considered as significant of the surface usable for the flow; it depends on the geometry of the porous medium. Darcy's law, and therefore permeability is defined for laminar flow conditions in a homogeneous, isotropic and continuous medium; the fluid does not interact with the medium. We define the hydraulic conductivity *k*; or coefficient of permeability, such as:

$$k = \frac{K}{\mu} \tag{1.10}$$

where k is the hydraulic conductivity which is a characteristic of the flow conditions in a given material for a given fluid.

The previous scalar expression is then replaced by a following vector relation:

$$\vec{V} = -\frac{K}{\nu}\left(\vec{\nabla}P - \vec{g}\right) \tag{1.11}$$

where *K* is the permeability and υ the kinematic viscosity of the fluid.

This law is only valid for flows at low speeds and for media with relatively small porosity. If the imposed temperature differences are not too great, the fluid velocities are low enough for the flows to be considered Darcyens. The value of the Reynolds number is used as a criterion to characterize the transition from a laminar flow regime of the Darcy type to a laminar regime of the Dupuit type. For this we defined a Reynolds number of pores for the flows in porous medium. By defining *d* as the characteristic length, which represents the characteristic dimension of the pores, the Reynolds number is written:

$$Re = V\frac{d}{\nu} \tag{1.12}$$

In order to determine characteristic length *d*, **Collins (1961)** proposed the expression $d = \sqrt{K/\varepsilon}$ whereas **Ward (1964)** rather suggested that $d = \sqrt{K}$ whatever is the porosity.

Depending on the value of the pore Reynolds number, **Bear (1972)** distinguishes three flow regimes. **Dybbs and Edwards (1984)**, using velocity measurements, distinguish several flow regimes which can be classified as follows :

For pore Reynolds numbers less than 1, the flow regime is laminar, the viscous forces are predominant and Darcy's law is applicable.

When Re is between 1 and 10, the boundary layers at the level of the solid walls of the pores develop. Outside these boundary layers, an inertial flow regime appears. The inertia forces then become significant and there is no longer any proportionality between the pressure gradient and the filtration speed: Darcy's law is no longer applicable. This steady laminar flow regime persists up to a Reynolds number of around 150.

For pore Reynolds numbers between 150 and 300, an unsteady laminar flow regime develops. This regime is first of all oscillatory resulting from the superposition of several distinct period and amplitude modes.

Beyond Re in the order of 300, the flow regime becomes chaotic, and has the characteristics of a turbulent flow.

1.2.1.2. Dupuit-Darcy's law

The **Dupuit-Darcy formulation (1863)** has been verified for flows of the Reynolds number (Re> 1). This formulation introduces a term of drag of shape of the porous matrix, which is a quadratic term of the speed considered falsely recognized as a term of inertia in the previous studies; the term is very answered among the scientific community under the name of **Forchheimer (1901)** or term of inertia.

The general compact form of Dupuit-Darcy's law, including the body force for flows in isotropic porous media, is given by:

$$\nabla P' = -\frac{\mu}{K} V' - \frac{\rho C_{DF}}{K^{1/2}} |V'| V' - \rho g \qquad (1.13)$$

where P' is the pressue, V' the infiltration velocity vector, μ the dynamic viscosity of the fluid, ρ fluid density K permeability of the porous matrix, g is the acceleration of gravity and C_{DF} is a coefficient independent of the flow and properties of fluids, but it depends on the regime and behavior of the flow through the geometry of the porous matrix, as well as on the

shape and the size of the grains of the porous medium. In other words, the coefficient of C_{DF} is directly linked to the coefficient of the form drag (pressure) of a grain or of the elementary porous solid which delimits the pores within the solid porous matrix. From the hydrodynamic and aerodynamic point of view, a viscous flow around a submerged grain induces a drag force, called profile drag whose coefficient, $C_D = C_{DV} + C_{DF}$, is the sum of the coefficient of the viscous drag C_{DV} (related to Darcy) and the drag coefficient C_{DF} (related to Dupuit). For any Reynolds number the viscous drag is always present, but the shape drag or the pressure drag depends on the behavior of the flow around the grain if it is attached or separated. If the flow is attached, at a very low Reynolds number, the recovery of the pressure gradient around the grain occurs and the shape drag is close to zero and the viscous drag is dominant. However, for a relatively high Reynolds number and due to the non-kernel shape of the grain, the flow separates and the shape drag becomes significant and overcomes the viscous drag. In a porous matrix, one grain is surrounded by others and the "individual grain" form drag takes into account the mutual hydrodynamic / aerodynamic interference between the grains. Then a grain is subjected to a very complex upstream flow and the coefficient of the force of the form drag C_{DF} strongly depends on the shape of the grain and the Reynolds number which influences the behavior of the flow. Thus, it cannot be considered as a universal constant, susceptible for a solid sphere where the coefficient of the form drag (beyond Stokes flow regime) is a function of the Reynolds number. Overall, the coefficient of drag C_{DF} depends on the size and shape of the grains of the porous matrix as well as the behavior of the flow.

1.2.1.3.Darcy-Brinkaman's law

Brinkman (1947) further generalized Darcy's law by introducing a term equivalent to the term viscous dissipation in the stokes law.

$$\Delta P' = -\frac{\mu}{K} V' + \mu_e \nabla^2 V' + \rho g \qquad (1.14)$$

This empirical law is known as the Darcy-Brinkman formulation, which is highly useful in the case of high porosity. The first term to the right of the above equation containing the viscosity μ is the Darcy term and the second containing the effective viscosity is called the Brinkman term. The difficulty in using this model lies in the evaluation of the equivalent viscosity of the medium μ_e. Indeed, this quantity is a function not only of the porosity of the medium but also

of its geometry (tortuosity). Brinkman has equated the equivalent viscosity of the medium with that of the fluid $(\mu_e = \mu)$. This approximation has been experimentally proven and is in agreement with the work of **Neal and Nader (1974)** and **Beckerman and Viskanta (1988)**. Brinkman's model thus allows the non-slip condition to be imposed on the filtration speed field, at the level of the impermeable walls.

1.2.1.4 .General model

We generalize the last three equations by introducing a transitory term and the convective term $(V'\nabla V')$, which leads to the following equation:

$$\frac{\rho}{\varepsilon}\frac{\partial V'}{\partial t}+\frac{\rho}{\varepsilon^2}(V'\nabla V')=-\nabla P'+\rho g-\frac{\mu}{K}V'+\mu_e\nabla^2 V'-\frac{\rho C_{DF}}{K^{1/2}}|V'|V' \qquad (1.15)$$

This equation is equivalent to the Navier-Stokes equation from the momentum balance in a fluid medium. It should also be noted that the complexity of a flow in a porous medium can be the result of the effects of drag and viscosity, and of a significant variation of the porosity at the level of the walls.

1.3 General information on nanofluids

In the case of heat transfer fluids, one of the first parameters to take into account in order to assess the heat exchange potential is the thermal conductivity. However, the most widely used fluids such as water, oil or ethylene glycol (EG) have only a low thermal conductivity compared to that of crystalline solids.

Finding the most suitable heat transfer fluid in industrial applications is an important concern for researchers and engineers. Since **Maxwell's theories in 1873**, they have tried to break the limitation against improving the thermal conductivity of conventional fluids by dispersing particles of millimeter or micrometric size in liquid. But the major problem recorded by this technique is the fast sedimentation of these particles in the fluid and the erosion of equipment operating with those types of fluids, **Haddad et al. (2012)**. Nanotehnology has made considerable progress in the past two decades. It represents the fifth technological revolution in history after the steam engine in the late 1700s; steel, electricity and railways in the late 1800s; cars, chemicals and mass production in the early 1900s; and computers in the mid-1900s **Khan et al. (2018)**. With the implementation of nanotechnology, the dispersion of nanometric

solid particles smaller than 100 nm in a traditional base fluid such as water, oil and ethylene glycol and the so-called nanofluid can be achieved . The thermo-physical properties of nanofluids such as density, viscosity, thermal conductivity and electrical conductivity can be considerably improved compared to the basic fluid to further improve the overall thermal and hydrodynamic behavior of the fluid. Figure 1.4 shows the difference between the thermal conductivity of liquids, including water and oil, with certain solids such as ceramic, metals and graphene (known as semi-metal), **Mahian et al. (2018)** . Some solids like graphene have very high thermal conductivity (thousands of times higher than liquids), making it a suitable option for use in thermal systems. The significant improvement in the heat transfer properties of nanofluids increases their use in various engineering applications such as the cooling of electronic devices, automotive nuclear reactors, solar thermal energy, thermal energy storage, systems refrigeration and air conditioning, etc.

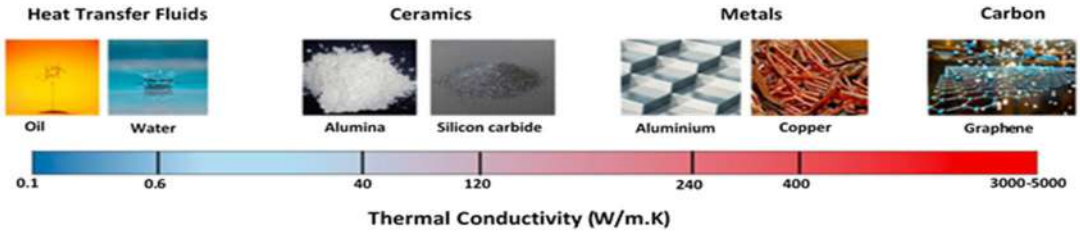


Figure 1.4: Thermal conductivity of some common liquids and solids, the high thermal conductivity of solids gives the idea to mix them with liquids to enhance the effective thermal conductivity Mahian et al. (2018)

In **1993, Masuda et al**. have measured the thermal conductivity and the viscosity of three water-based suspensions with different containing nanoparticles of Al2O3, TiO2 and SiO2 (particles of size between 1 and 100 nm). They reported that the thermal conductivity and viscosity of water become higher than before by adding nanoparticles. Then, "**Choi (1995)"** is the first to use the term nanofluid to designate the fluid with nanoparticles in suspension. In addition, **Choi et al. (2001)**, have shown that the thermal conductivity of conventional heat transfer fluid can be increased approximately twice by adding a small amount of nanoparticles (less than 1% by volume).

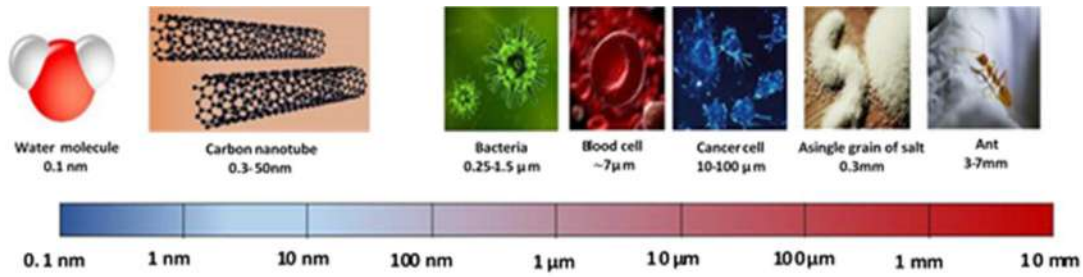


Figure 1.5. Comparison between sizes of carbon nanotubes as a typical nanoparticle with other elements, Mahian et al. (2018)

Figure 1.5 compares the diameter of typical carbon nanotubes to the size of some well-known things such as an ant and a single grain of salt to better visualize the size of a nanoparticle. As we can see, the diameter of a carbon nanotube can be 1 million times smaller than that of a single grain of salt.

It should be mentioned that nanofluids are not prepared simply by adding nanoparticles to water or oil and stirring the mixture, as for mixing sugar and tea, but the formation of a nanofluid rather requires special physical and chemical processes to produce a uniform and efficient dispersion of particles for long-term applications.

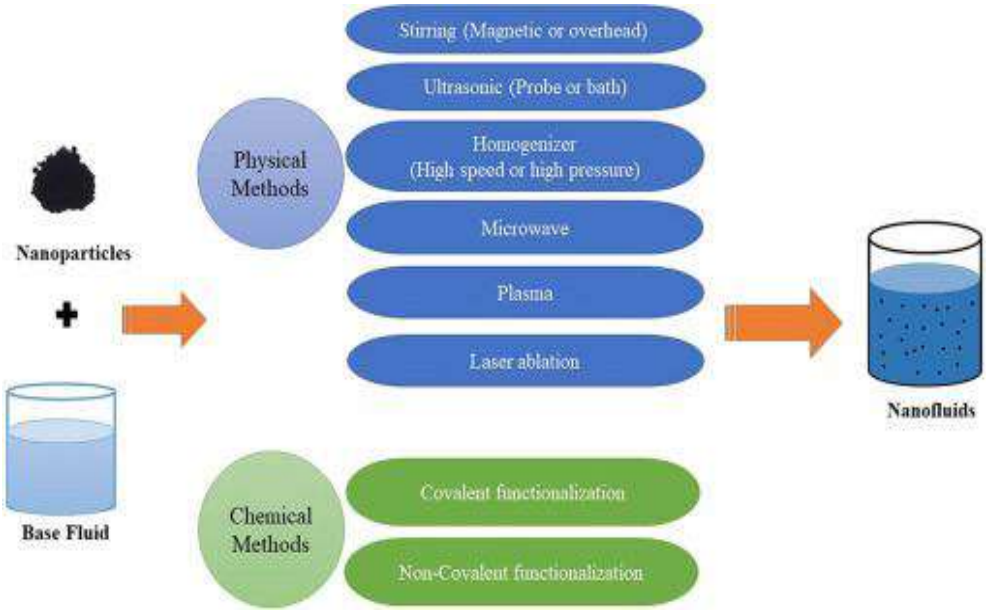


Figure 1.6. The preparation of nanofluids does not only consist in mixing nanoparticles and a liquid, but special physical and chemical techniques are necessary to have a stable nanofluid, Mahian et al. (2018)

The use of surfactant (non-covalent functionalization), the functionalization of nanoparticles, pH control and sonication are some of the main approaches to increase the stability of nanofluids, **Ghadimi (2011)**.

Figure 1.6 shows the main physical and chemical approaches that could be used to prepare stable nanofluids. The most suitable method for preparing stable nanofluids is determined according to the type of nanoparticles and the choice of base liquid.

Factors to consider when selecting nanomaterials when preparing nanofluids for heat transfer applications are: chemical stability, thermophysical properties, toxicity, availability, compatibility with base fluid and cost. The most used nanoparticles used for the formulation of nanofluids are aluminum (Al), copper (Cu), silver (Ag), iron (Fe), titanium (Ti), silicon (Si), zinc (Zn), magnesium (Mg), carbon nanotubes (CNT), graphene, graphene oxide and diamond. The basic fluids used for the formulation of nanofluids are water, ethylene glycol (EG), EG - H2O mixtures and oils, **ALI et al. (2018).**



Figure 1.7. Parameters influencing the effective thermal conductivity of nanofluids Ali et al. (2018).

The term "effective" was introduced to describe the thermophysical property of nanofluids and to differentiate between the thermophysical properties of the base fluid itself and the newly formed fluid which consists of the base fluid and its dispersed nanoparticles [13]. Figure 1.7 shows the main parameters that influence the effective thermal conductivity of any nanofluid, **ALI et al. (2018)**.

1.3.1 Suitable applications for nanofluids

In most applications in which conventional fluids are used such as for cooling or heating, nanofluids can be used to replace single-phase fluids. Nanofluids can be used in solar collectors and photovoltaic systems, car radiators, refrigerators, boilers, drug delivery, cooling of electronic equipment, lubrication of components, heating and cooling of buildings, desalination, CO2 absorption, porous media, aerospace, oil recovery and all types liquid-based heat exchanger. Figure 1.8 provides an overview of the primary applications of nanofluids.

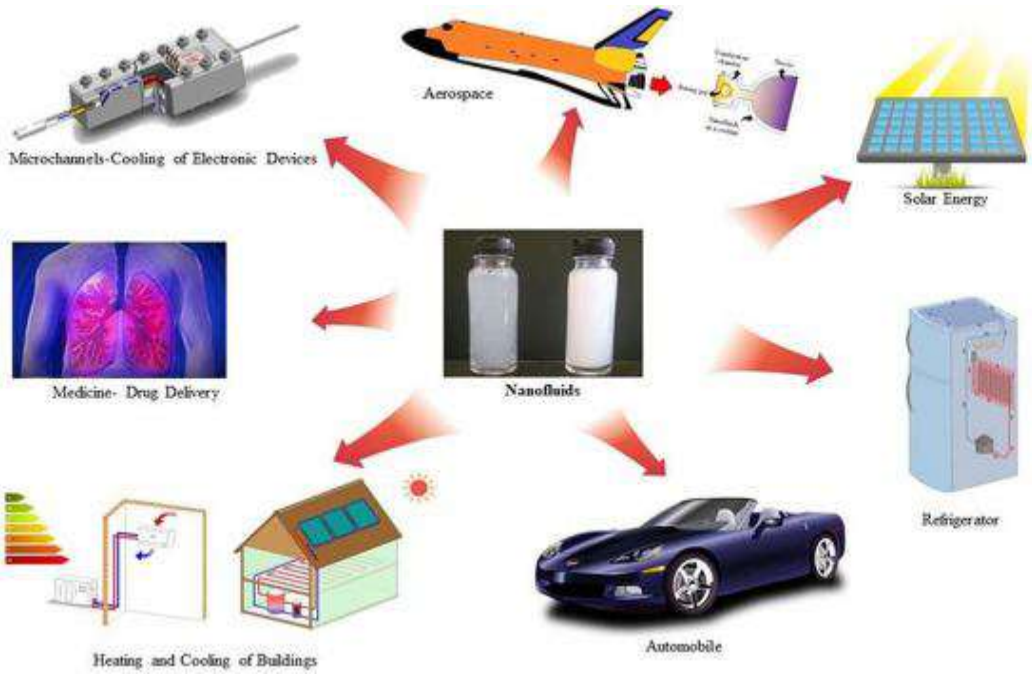


Figure 1.8. Some applications of nanofluids Mahian et al. (2018)

1.3.2 Advantages and disadvantages of nanofluids

Generally, by using a nanofluid, the heat exchange rate in thermal systems is improved due to the higher thermal conductivity of the nanofluids compared to the base fluid. Therefore, to transfer a specified heat value, the size of a thermal system can be reduced by using nanofluids

to improve the rate of heat transfer, which implies a more compact system and a saving in weight and expense. In comparison with microfluids, nanofluids have higher stability and a better ability to improve thermal conduction. On the other hand, nanofluids have certain disadvantages, which can be listed as follows **Mahian et al. (2018)**.

• Nanofluids have a relatively high production cost.

• Preserving nanofluids for long-term use without aggregation and sedimentation of nanoparticles is a challenge.

• The higher viscosity of nanofluids compared to base fluids, which leads to an increase in the pumping power required and increases the rate of heating by friction.

• The use of nanofluids can increase the corrosion and erosion rates of components that come into contact with nanofluids.

1.3.3 Transport equations for nanofluids

Taking into account the transport equations mentioned for conventional liquids, the main approaches for modeling the flow of nanofluids, can be classified as single-phase or two-phase approaches.

1.3.3.1 Single-phase approaches

A nanofluid is intrinsically a two-phase fluid (solid-liquid); however, for numerical simulations under certain conditions, certain appropriate assumptions can be made to model nanofluids as single-phase fluids.

In single-phase models, the governing equations are only solved for an efficient liquid phase. Single-phase models can be divided into three main approaches, including homogeneous, thermal dispersion and Buongiorno models.

1.3.3.2 Two-phase approaches

Nanofluids act as two-phase fluids. In two-phase approaches, the base liquid and the nanoparticles are modeled in two individual phases with different velocities and different temperatures, so that the particles can move relative to the base fluid (the relative velocity of the particles through a fluid is called the sliding velocity particle, although it is not related to the boundary condition without sliding). Although two-phase approaches can obtain more realistic results by considering the movement between the fluid and the nanoparticles, they

require longer simulation times for simulation and the models are more complex. Figure 1.9 presents the main approaches for modelling the flow of nanofluids, which can be classified as single-phase or two-phase approaches.

1.4. General information on magnetohydrodynamics (MHD)

Magnetohydrodynamic (MHD) (magnetofluid dynamics or hydromagnetics) is the study of the dynamics of electrically conducting fluids. Such as, fluids include liquid metals, plasmas, and salt electrolytes or water. Magnetohydrodynamic word is derived from the words magneto (meaning magnetic field), hydro (meaning liquid), and -dynamic (meaning movement). The field of MHD was initiated by **Hannes Alfven (1942)**, for which he received the Nobel Prize in physics in 1970.

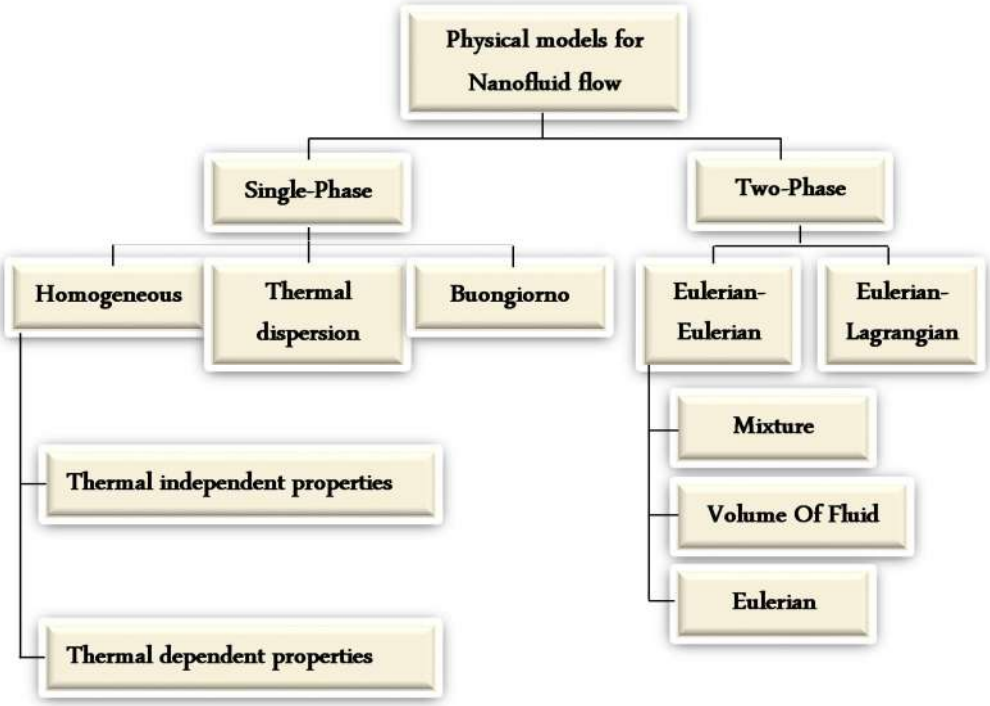


Figure 1.9. Main approaches for modeling the flow of nanofluids Mahian et al. (2018)

The fundamental concept behind MHD is that magnetic fields can induce currents in a moving conductive fluid, which in turn creates forces on the fluid and changes the magnetic field itself (Figure. 1.10).

Equations that describe MHD are a combination of the Navier–Stokes equations (fluid dynamics) and Maxwell's equations (electromagnetism), which have to be solved all together, analytically or numerically. An MHD flow can differ significantly from an equivalent ordinary hydrodynamic flow. The movement of the metal particles through magnetic field lines produces an electric current which interacts with the magnetic field to produce an electromagnetic driving force (Lorentz force), which opposes the movement of the liquid.

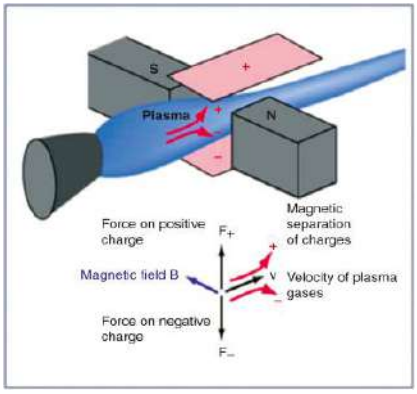


Figure 1.10. Induced current in a conductive fluid in the presence of a magnetic field, Sheikholeslami and Rokni (2017).

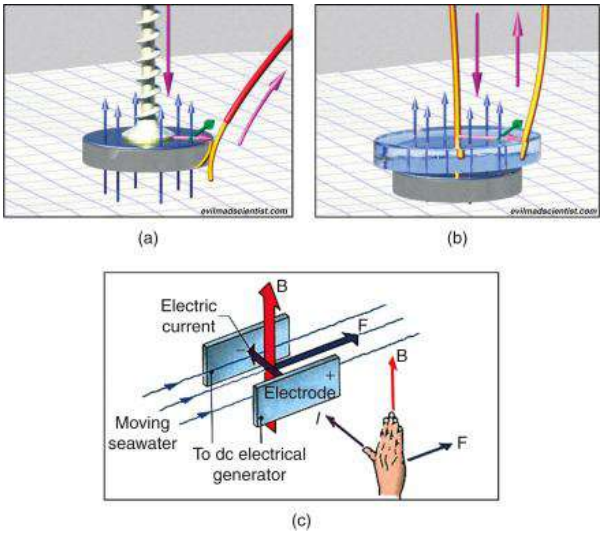


Figure 1.11. (a and b) Effect of the magnetic field on the flow of the conductive fluid; (c) Law of the right hand. (Blue line: magnetic field, purple line: current, green line: movement.), Sheikholeslami and Rokni (2017).

Even a weak magnetic field provides enough EM damping force to eliminate turbulence and instability in most of the movement involved, thereby eliminating many micro-defects in the

crystal. The damping rate will depend on the strength of the applied magnetic field as well as its orientation with respect to the convective circulation **(Bessaïh et al., 2003).**

Figure 1.11 shows the effect of a magnetic field on the conductive fluid flow. In Figure. 1.11a, we have a current that flows down the screw and into the magnetic field, moving at an angle of 90° through the magnet and out from the wire.

This current and magnetic field produce a force that is orthogonal to both forces, causing the magnet to rotate while it is magnetically attached to the screw. The similar thing occurs in Figure. 1.11b; however, instead of the force exerted on the magnet, the salt water in which the magnet is immersed turns because of the resulting force (called Lorentz force) that is applied to the water and is not applied on the magnet. Fig. 1.11c shows the right-hand side law for finding out the Lorentz forces direction.

Ther are two basic physical effects happen in MHD (Figure. 1.12), and understanding them well is the key to develop physical intuition in MHD subject. The first one is the effect that appears when a good conductor moves into a magnetic field, which induces an electric current in the conductor iteself, and creating its own magnetic field follwing Lenz's law. This induced magnetic field tends to cancel out the original, externally supported field, thus, effectively excluding the conductor's magnetic field lines. Inversely, when the magnetic field infiltrates the conductor and the conductor is taken out of the field, the Induced field reinforces the applied one. The result is that the lines of force "go with the flow", they appear to be pulled along with the conductor. Naturally, the magnetic field distribution is quite complex if a fluid with complex motions is the conductor and the current will increase until get balanced by Ohmic dissipation

The second basic effect is dynamical. If a conducting fluid motion induces currents through a magnetic field, a Lorentz force (or $j \times B$) will affect the fluid and change its motion. In Magnetohydrodynamic, the motion modifies the magnetic field, and the magnetic field in turn reacts back and modifies the motion, which makes the theory highly nonlinear.

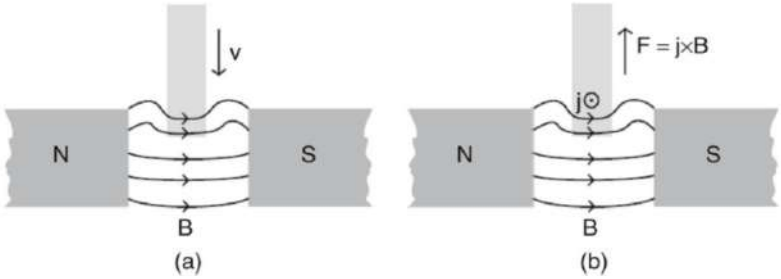


Figure 1.12. The Two-Key Physical Effects Occurring in Magnetohydrodynamic Sheikholeslami and Rokni (2017).

1.4.1 Lorentz force

The MHD is based on the the Lorentz force law, which states that while a charged particle is moving in the electromagnetic field, will experience a force that can be explained as

$$\vec{F} = q\left(\vec{u} \times \vec{B}\right) \tag{1.16}$$

Where $\vec{F}$ is the force acting on charged particle, q is the charge of the particle, $\vec{u}$ is the velocity of particle, and $\vec{B}$ is the magnetic induction.

1.4.2 Faraday's law

Faraday's law states that when a charged particle moves through the electromagnetic field, it experiences a retarding force along with producing voltage (Figure. 1.13).

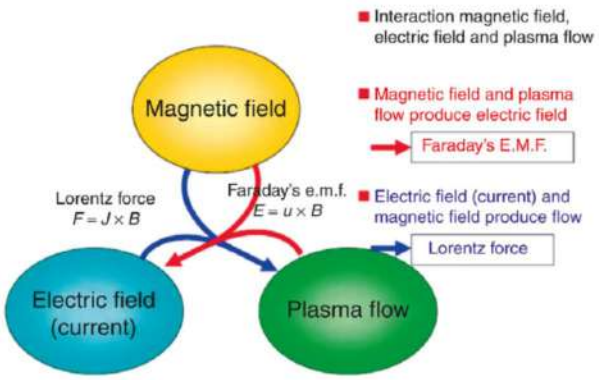


Figure 1.13. Relation between the Lorentz Force and Faraday's Law, Sheikholeslami and Rokni (2017).

1.4.3 Maxwell's equations

The electromagnetic field is described through Maxwell's equations which govern the evolution of electric and magnetic fields:

$$\vec{\nabla}\times\vec{D}=\rho_e \;\; \vec{\nabla}\times\vec{E}=-\frac{\partial\vec{B}}{\partial\tau},\;\vec{\nabla}.\vec{B}=0\;\;,\vec{\nabla}\times\vec{H}=\vec{j}+\frac{\partial\vec{D}}{\partial\tau} \tag{1.17}$$

where

$\vec{B}$: formally the magnetic flux density, but we shall refer to it as the magnetic field

$\vec{H}$: the magnetic field strength

$\vec{E}$: the electric field

$\vec{D}$: the electric displacement

$\vec{J}$: the electric current density

ρ_c : the electric charge density

In an isotropic medium (which we shall assume)

$$\vec{D}=\varepsilon_e\vec{E}\,,\vec{B}=\mu_e\vec{E} \tag{1.18}$$

Where where ε_e is the permittivity (or dielectric constant) and μ_e is the magnetic permeability of the medium. ε_e and μ_e can be approximated by their values in a vacuum.

1.4.4. The Navier–Stokes equation

The equation governing the flow of a fluid is the Navier–Stokes (or momentum) equation:

$$\rho\left(\frac{\partial u}{\partial\tau}+(u.\nabla)u\right)=-\nabla p+\rho\upsilon\nabla^2u+other\;\;forces \tag{1.19}$$

where ρ is the fluid density, u is its velocity, p is the pressure, and υ υ is the kinematic viscosity.

When the fluid contains electrical charge ρ_c per unit volume, then there is a force per unit volume of $\rho_c\vec{E}$

When an electric current density $\vec{j}$ flows through the fluid, there is a force per unit volume of $\vec{j}\times\vec{B}$ then the Navier-Stokes equation becomes

$$\rho\left(\frac{\partial u}{\partial \tau}+(u.\nabla)u\right)=-\nabla p+\rho\upsilon\nabla^2 u+\rho_c\vec{E}+\vec{j}\times\vec{B}+other\ \ forces \tag{1.20}$$

1.4.5 Ohm's law

Ohm's law states that the total electric current flowing in a conductor is related to the total electric field. Besides to the field $\vec{E}$ acting on a fluid at rest, a moving fluid with velocity u through a magnetic field $\vec{B}$ is subject to an additional electric field $u\times\vec{B}$. Ohm's law then gives

$$\vec{j}=\sigma\left(\vec{E}+\vec{u}\times\vec{B}\right) \tag{1.21}$$

where the constant of proportionality σ is called the electrical conductivity

1.5. State of the art review

Reducing energy consumption has become the main interest for engineers and researchers from all the globe for a future energy security and diversity by securing energy sources and in order to provide answers for the environmental concerns. So as to minimize energy consumption, efficient and compacted thermal products with improved design need to be developed. The thermal control, material and energy saving in such a process can be achieved by enhancing the heat transfer rate using one of the two main techniques, passive or active technology **"Khan et al. (2018)," "Ganji and Malvandi (2016)," "Alam and Kim (2018)."** The enhancement of heat transfer by natural convection has received continuous increase in interest as an important heat transfer phenomenon because of its numerous advantages such the absence of need for external power for inducing the convective heat transfer, plus the fact that no electronic regulation and supply is required and the exclusion of mechanical repair for the powering systems which reduces the cost and time **"M. Ghalambaz (2015)."** Researchers are always looking toward the development of new numerical methods to study and solve the natural convection in order to design efficient equipment's **"Alkasassbeh et al. (2019)."**

Currently, the studies of heat transfer with porous media is gaining growing interest due to their large use in many engineering applications like heat exchangers, ground water and oil flow. The convective heat transfer and fluid flow in porous medium have been the subject of many research papers and have received important consideration. The published papers reached the rate of one a day due to their wide variety of applications like heat exchangers, solar technology, cooling electronic devices, chemical catalytic reactors, heat pipe technology, drying processes and nuclear reactors "**Rashidi et al. (2017)," "Nield and Bejan (2017)," "Hoseinzadeh et al. (2019)," "Buonomo et al. (2019)."** The convective flow in porous media literature is plentiful and typical studies can be found in the following books **"Vafai (2015 "Vadasz (2008)."** Ten to thirty trillion Btu of energy per year are saved in the USA since 2008, when nanofluid started being used as a cooling agent in electric power industry. This resulted in reducing 21000 metric tons of SiO_2, 5.6 million metric tons of CO_2 and 8600 metric tons of NO_x. The thermal conductivity of the particle material, metallic or nonmetalic, such as Al_2O_3, CuO, SiO and TiO are typically an order of magnitude higher than the base fluids, even at low concentration reset in significant increases in the heat transfer coefficient **"Khan et al. (2018)," "Haddad et al. (2014)," "Asharafizadeh and Tan (2018)," "Roubort (2008)."**

"Choi (1995)," is the first who used the term nanofluid to refer to the fluid with suspended nanoparticules. In addition, **"Choi et al. (2001),"** showed that the thermal conductivity of conventional heat transfer fluid can be increased approximately to two times by the addition of small amount of nanoparticules (less than 1% by volume).

The literature on the use of nanofluid in heat transfer enhancement, influence of parameters like particles concentrations, material, size and shape on the thermophysical properties of nanofluids and on free convection is widespread.

"Sakar (2011)," presented a summary on the correlations developed for heat transfer and nanofluids characteristics in both forced and free convection flows. He reported that a large deviation of predicted results for proposed correlations were observed due to strong influence of particles proportion and nanofluid composition on flow and heat transfer characteristics. **"Raja et al. (2016),"** provided an overview of most numerical and experimental research papers on nanofluids in the literature by considering various parameters which govern nanofluids characteristics, heat transfer performance and its applications. **"Gupta et al. (2017),"** summarized the main results recorded for the improvement in thermophysical properties of

nanofluids. They considered the influence of important parameters like particuls material, particuls loading, particuls size, particuls shape, base fluid type, additives and PH values. **"Jabbari et al. (2017),"** reviewed and discussed the molecular dynamics studies performed on the nanofluids thermophysical properties, taking into account the two important factors for industrial applications: thermal conductivity and shear viscosity. A comprehensive review on heat transfer characteristics of TiO_2 nanofluids presented by **"Yang and Du (2017)."** They have focused on heat transfer characteristics of TiO_2 nanofluid and its comprehensive properties such as sensational dispersity, chemical stability and non-toxicity. **"Mikkola et al. (2018),"** conducted an experimental work to examine the nanoparticules properties (size and thermal conductivity) of three types of nanoparticules, polysterene, SiO_2 and Al_2O_3 on the convection heat transfer of nanofluids using water as a base fluid. It was found that moderate enhancement in the thermal conductivity was obtained and small particle sizes is preferable for convective heat transfer applications. Another experimental work conducted by **"Alawi et al. (2018),"** where the thermal conductivity and viscosity of various types of metallic Oxides (Al_2O_3, CuO, SiO_2, ZnO) were determined for various nanoparticles shapes (blades platelets, cylindrical, bricks and spherical). They found that the effective thermal conductivity and thermal conductivity ratio of those nanofluids increase with temperature and concentration, in addition to the increase of effective viscosity and viscosity ratio with the increase of nanoparticles concentrations**. "Vanaki et al. (2016),"** reviewed numerical studies about the convective heat transfer of nanofluids. A detailed summary presented on the influence of base fluid, nanoparticles types, volume concentration, size, shape, Brownian diffusion and thermophories effect on hydrodynamic and thermal characteristics on convective heat transfer using nanofluids. **"Mahdi et al. (2015),"** summarized the published papers on the thermophysical properties of nanofluids and the studies on convective heat transfer in porous media with nanofluids. They concluded that porous media with nanofluid is highly suited for practical heat transfer process, and it represents an opportunity for engineers to develop highly compact and effective heat transfer equipments. Another comprehensive review of **"Kasaeian et al. (2017),"** looked at the simultaneous application of nanofluids and porous media for heat transfer enhancement purposes in thermal systems with different structures, flow regimes and boundary conditions. **"Shermet and Pop (2015),"** studied numerically the natural convection flow in a porous concentric horizontal annulus saturated with water based nanofluid. Their results indicate that the inclusion of

nanoparticles into pure water changes the flow structure at low values of Rayleigh number. **"Emami et al. (2018),"** published a paper about a numerical study on the natural convective heat transfer inside an inclined square porous cavity filled with Cu-Water nanofluid using the two phase mixture and Darcy-Brinkman-Forchheimer models. The main result is that the simultaneous use of nanofluid with porous media in weak convection flow is beneficial, but in case of strong natural convection fields, it would be unfavourable and decrease the heat transfer rate. The porous matrix material and porosity were taken into consideration in the studies of **"Sheremet et al. (2015)," "Sheremet et al. (2015)," "Sheremet et al. (2015),"** where the free convection in a square and parallelogrammic cavities filled with nanofluid was analysed. The reported results as a function of the volume fraction of nanoparticles, porosity, types of the porous matrix, inclination angle, aspect ratio and different Rayleigh numbers showed that the presence of the nanoparticles inside the enclosure deteriorates the heat transfer rate due to the increase of dynamic viscosity because of the presence of nanoparticles. **"Raza et al, (2019),"** published a paper where a three-stage Lobatto III-A formula is used to investigate the effect of MoS2 nanoparticles shape suspended in water on MHD flow inside a channel that has expanding walls. They found that the spherical nanoparticles have strong effect on local Nusselt number compared to the other nanoparticles shapes, in addition to the increase of nanoparticles volume fraction, which enhances the heat transfer. The natural convection of Cu-water nanofluid filled a cylindrical annulus heated by two discrete heat sources was presented in the paper of **"Mebarek-Oudina et al. (2019),"** the obtained equations resolved by the finite volume method, they found the that heat transfer increases with the increase of the nanoparticles volume fraction. **"Ghalambaz (2019),"** published a paper about the free convection nano-encapsulated phase change materials (NEPCMs) in a square enclosure which undergoes phase change from solid to liquid phase. They concluded that globally the use of a NEPCM particles enhance the heat transfer. They also recorded an increase of dynamic viscosity and a decrease of both sensible heat capacity and buoyancy forces. **"Alsabery et al. (2019),"** published a numerical work about the mixed convection of Al_2O_3/water nanofluid and entropy generation inside a square cavity that resulted from the rotation of cylinder using the Galerkin weighted residual method. Thy found that the average Nusselt number increases with the increase of Rayleigh number and volume fraction of nanoparticle. Furthermore, the global entropy generation increases with the increase of nanoparticles volume fraction the angular rotational

velocity for the bigger radius of the rotating cylinder used in the study. **"Ishak et al. (2019),"** presented a numerical work about the natural convection of Al_2O_3–water nanofluid filled a square enclosure heated with heat source from the bottom. They focused on the effect of wall thickness on the convective heat transfer and the entropy generation using the finite difference method. They revealed that the wall thickness and thermal conductivity have an important effect on the heat transfer strength. **"Alsabery et al. (2020),"** investigated numerically the transient natural convection of non-Darcy porous annulus saturated with alumina-water nanofluid between a square cavity confined a solid conductive bulk. The Buongiorno model was used for taking the slipping of nanoparticles in the base fluid into consideration and the porous medium was described using the Brinkman-Forchheimer-extended Darcy model. The finite difference method was used to resolve the obtained equations. They found that the increase of Darcy number increases the Nusselt number. Also the Nusselt number increases with the increase of porosity for high Darcy values while no change recorded for low Darcy number. Furthermore, the Nusselt number reaches its maximum for a given porosity at a critical value of nanoparticles volume fraction.

During the last years, researchers started working toward the development of a new generation of nanofluids called hybrid nanofluids, where they working by dispersing dissimilar nanoparticls as individual constituents or by dispersing nanocomposite particles in the base fluid instead of using single kind of nanoparticles. **"Babu et al. (2017),"** reported a state of art review on those hybrid nanofluids. Also, **"Ghalambaz (2019),"** investigated the conjugate free convection in a square cavity saturated with hybrid nanofluid (Ag–MgO) using the local thermal non-equilibrium (LTNE) and Darcy models, the obtained equations resolved by the finite element method. They found that the use of hybrid nanoparticles decreases the flow strength and the heat transfer rate. **"Mehryan et al. (2019),"** studied the mixed convection in a square enclosure produced by a hot oscillating cylinder using the nanofluid Al_2O_3/water and the hybrid Cu–Al_2O_3/water nanofluid. They found that for low Rayleigh number, both types of nanofluides show an increase of average Nusselt number, while for high Rayleigh number, the heat transfer enhancement recorded only the Al_2O_3, the average Nusselt number decreases with using the Cu–Al_2O_3 nanoparticles. In addition, an increase of heat transfer at low Rayleigh number recorded for both types of nanoparticles for a period of oscillation increases. In other

paper of **"Mehrayn et al. (2019),"** the free convection of MWCN–Fe3O4/water saturated square porous medium under the influence of magnetic field was numerically studied. The effect of Rayleigh and Hartman numbers, magnetic field inclination angle, Darcy number, magnetic number and the porosity on the heat transfer and the fluid flow was presented and discussed.
A new type of hybrid nanofluid (Ag-MgO/water) ws used in the study of **"Ghalambaz et al. (2019),"** where a square enclosure saturated with Ag–MgO/water was used for analysing the conjugate natural convection using the finite element method. They concluded that for small Rayleigh number, the increase of hybrid nanoparticles volume fraction increases the local and average Nusselt numbers. However, for high Rayleigh number they decrease. A numerical study of MHD natural convection of porous enclosure divided into two equal parts via a vertical flexible partition and saturated with hybrid nanofluid (Cu–Al2O3 water) under the influence of magnetic field by using the Galerkin finite element method was presented by **"Ghalambaz et al. (2019)."** They showed that the increase of Rayleigh number increases the convective heat transfer and the pure fluid imposed a high stress on the flexible partition compared to the nanofluid and the hybrid nanofluid.
Recently, the literature concerning convective flow with nanofluids has become available, and representative studies may be found in the recent books by **"Bianco et al. (2015)," "Minea (2017)," "Sheikholslami and Ganj (2017)," "Chand (2017)," "Sheikholslami (2019)."**
In the process of designing a fusion reactor, the natural convection heat transfer, electrically-conducting fluids and liquid metals are essential problems because of the strong magnetic field and high temperature difference. The magnetic field is used for the technologies of drying and lubrication, food cleaning, float glass, hydrodynamic behaviour control during the processes of float glass production, solidification and crystal growth. Moreover, magnetic field applications on nanofluid flows are gaining a growing interest due to their large use in many technological applications such as in nuclear reactors coolers, plasma, molten metals purification, metal working process, where the convection is controlled by an external magnetic field (Magneto hydrodynamics), **Minea (2017)**.
The modelling approaches of fluid flow and heat transfer in porous media have received a continuous increase in interest for researchers and engineers in order to develop efficient and compacted thermal products **(Wang et al. (2017) et Sivaraj et al. (2017))**. Recently, researchers and engineers started working toward the study and the use of nanofluids as heat transfer fluids

due to their enhanced thermal conductivity in combination with a magnetic field in order to design efficient equipment.

The studies of heat transfer by convection in a porous medium have been the subject of many research papers. **Wang et al. (2017)** published a work on 3D liquid metal free convection in a rectangular cavity under the effect of a magnetic field. They revealed that according to the magnetic field strength, two modes are found such that for a low magnetic field strength, the flow is described as three-dimensional while for a high magnetic field strength, the flow is quasi-two-dimensional.

Sivaraj et al. (2017) presented a work about MHD free convection of a fluid flow in a tilted saturated porous enclosure containing a heat conducting solid in its center. They found that the heat transfer rate decreases with the effect of the magnetic field. **Shankar et al. (2017)** provided a study for the free convection stability of magnohydrodynamic fluid in a saturated porous channel; they concluded that the magnetic field has a stabilizing effect on the stabilities of both the stationary and the oscillatory modes. **Javaherdeh et al. (2018)** examined MHD free convection in an enclosure with a sinusoidal temperature distribution using the Lattice Boltzmann method. They found that the heat transfer rate declines with the increase of Hartmann number. **Mahmud et al. (2004)** published a paper about the MHD free convection and entropy generation of a pure fluid in a square saturated porous enclosure. They found that the increase of Hartmann number inhibits the fluid motion and decreases the Nusselt number. **Mansour et al. (2010)** presented a numerical work about the MHD free convection in an inclined square cavity with a heat source. They revealed that the Nusselt number takes a large value with the presence of magnetic field. **Nkurikiyimfura et al. (2013)** presented a review about the heat transfer enhancement by magnetic nanofluids. They emphasized on the thermal conductivity enhancement and the thermomagnetic convection in devices using magnetic nanofluids. A numerical study about the description of liquid metal flows in a capillary porous system under the influence of external uniform magnetic field is published by **Bühler et al. (2015)**. They concluded that the liquid metal MHD flows in porous media depended on the electric properties of the porous material and on the orientation and strength of the magnetic field. **Chamkha al. (2015)** reviewed some research works done on MHD convection of nanofluids in various geometries and applications. Another review published by **M'hamed et al. (2016)** about the application of external magnetic field on nanofluids was published in order to

answer the question of why researchers apply external magnetic field on nanofluids. They concluded that the applied external magnetic field has an effect on controlling the nanofluid flow characteristics rather than the thermal conductivity enhancement.

The effect of inclination angle and magnetic field of free convection of a porous cavity saturated by a nanofluid was studied by **Nithyadevi et al. (2016)**. They recorded a decrease on the heat transfer strength with the increase of Hartmann number. **Sheikholeslami et al. (2017)** presented the impact of magnetic field on nanofluid free convection in the presence of melting heat transfer. Their results indicated that the conduction mechanism is dominated in high Hartmann numbers. Another paper was published by **Sheikholeslami (2018)** about the MHD CuO-H2O nanofluid flow in a porous channel using mesoscopic method, and he found that the increase of Hartmann number enhances the heat transfer strength, but reduces the flow velocity. The influence of Lorentz forces on natural convection in a square cavity heated from below and saturated with a nanofluid was analyzed by **Sheikholeslami et al. (2017)**. They found that the increase of Lorentz forces decreases the heat transfer rate.

A study of free convection of MWCN-Fe3O4/water hybrid nanofluid saturating a square porous medium under the influence of a magnetic field was conducted by **Mehryan et al. (2019)**. They concluded that an enhancement on heat transfer is recorded by dispersing nanoparticles for a low Rayleigh number, while it decreases for the high values, also an enhancement on the average Nusselt number is recorded for magnetic field inclination between 135° and 180°. Ghalambaz et al. (2019) studied the free convection of a hybrid nanofluid saturating a square enclosure divided by a flexible partition and under a magnetic field effect. They revealed that the heat transfer rate decreases with the increase of the magnetic field strength. The MoS2 nanoparticles shape effect on MHD flow in a channel was studied by **Raza et al. (2019)**. The outcomes confirm that the use of spherical nanoparticles enhances the local heat transfer compared to other shapes.

Zahmatkesh et al. (2019) published a numerical study using Taguchi experimental design method for natural and mixed convection in porous medium saturated with an MHD nanofluid. Several couples of nanoparticles and fluids used in the study in addition to porous matrix materials under the effect of a magnetic field. They concluded that in the case of natural convection with the absence of magnetic field, the heat transfer rate is affected by the

nanoparticles type, while for a high magnetic field strength, the controlling parameter is the solid matrix material. The influence of nanoparticles shape and radiation on free convection of nanofluid-saturated porous medium under the effect of a magnetic field was examined by **Shah et al. (2019)**. They indicated that the Lorentz force reduces the convection rate. The impact of inclined magnetic field and internal heat generation on convection and entropy generation of nanofluid-saturated porous medium was presented in the work of **Armaghani et al. (2020)**. They concluded that the application of an inclined magnetic field enhances the heat transfer rate. **Sureshkumar et al. (2020)** surveyed the free convection of MHD nanofluid saturating a 2D enclosure taking into account the aspect ratio. They reported that the increase of the enclosure aspect ratio increases the heat transfer rate under the magnetic field effect.

1.6. Conclusion

Most of published papers on the heat convection in porous media using nanofluids relied on Darcy's law, which is valid only when the pore-diameter-related Reynolds number is less than unity. For high porous medium permeability or at higher flow rates, the inertial effects become important, and the drag effect due to the solid matrix and the viscous stresses near the solid walls may become significant and the flow becomes non-Darcien. There is a departure from the linear law, which is physically believed to be owing to the flow separation in the porous medium, while mathematically is represented as a nonlinear term in the velocity-pressure-gradient relationship **"Riley and Rees (1985), Nawaf and Pop (2005)**. It was found out by Dupuit in 1863 and Forchheimer in 1901 that for high velocities, the drag is quadratic of the velocity **Nield and Kuznetsov (2013)**, It was pointed out by **Lage (1998)**, **Lage and Antohe (2000)**, that what is nowadays named Forchhaimer equation, should actually named Dupuit-Darcy equation, **Nield and Kuznetsov (2013)**. The Dupuit-Darcy model has been used in the studies of free convection in porous media of **Poulikakos and Bejan (1985), Riley and Rees (1985), Hossain and Rees (1997), Rees and Hossain (1999), Nawaf and Pop (2005), Rebhi et al. (2014), Rebhi et al. (2016), Alloui et al. (2017), Rebhi et al. (2017), Rebhi et al. (2020) and Rebhi et al. (2021).**

The main purpose of this study is to examine the effect of a magnetic field and inertial effect parameter on free convection in a tilted rectangular porous enclosure saturated with a nanofluid using the Dupuit-Darcy model for describing the fluid flow inside the porous medium. The

sidewalls are subjected to a temperature difference, while the horizontal walls are insulated. The aluminium foam is selected as the solid matrix of porous medium in the first application in this study, where in the seconde application, the effect of external magnetic filed is presented. With the presence of inertia and magneyic field, the dependency of the fluid flow and the heat transfer rate on Raleigh number (R_T); nanotubes volume fraction (ϕ); Hartmann number (Ha); inertial effect parameter (G);inclination angle of the cavity $(\gamma)$and inclination angle of the magnetic field (ξ) is investigated.

CHAPTER II
PHYSICAL MODEL AND MATHEMATICAL FORMULATION

CHAPTER II

PHYSICAL MODEL AND MATHEMATICAL FORMULATION

2.1 Problem description

We propose in this section the study of natural convection of naofluid saturated inclined porous medium. Two applications will be performed, the first application is the study of free convection of Copper-Water nanofluid (Cu-Water) saturated Aluminium foam porous medium where the porosity and the matrix material have been taken into consideration without the effect of magnetic field. The second application is the study of natural convection of Oxide Aluminium -Water (Al_2O_3-Water) and Single Wall Carbon Nanotube –Water (SWCNT-Water) nanofluids saturated an inclined porous enclosure under the effect of external magnetic field and taking into account the inertial effect on fluid flow and heat transfer rate.
The schematic geometry of the problem under investigation is shown in Figure 2.1, where x and y are the Cartesian coordinates. The length, height and width of the cavity are designated by L, H and W, respectively.

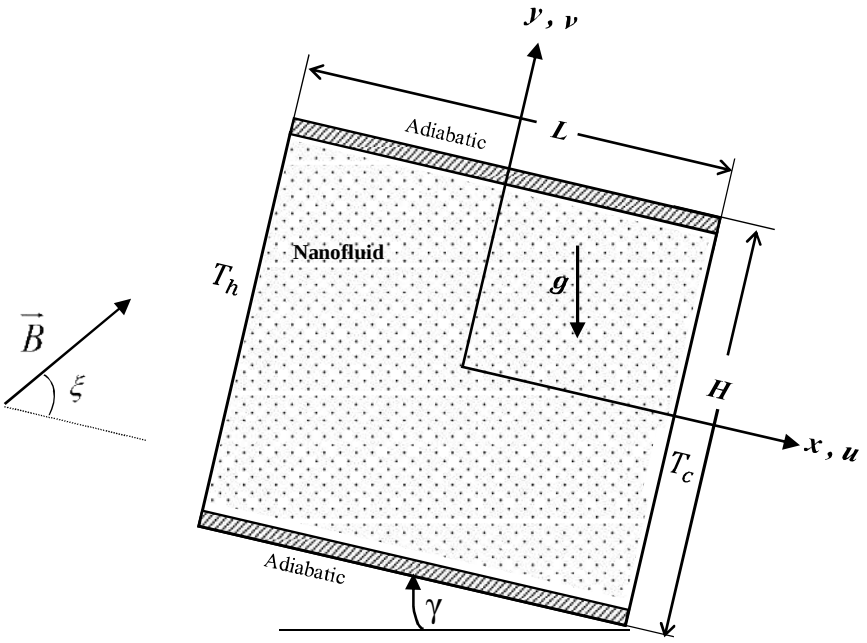


Figure 2.1: Physical model and coordinate system.

It is assumed that the left vertical wall is heated and maintained at the constant temperature T_h, while the right vertical wall is cooled and has the constant temperature T_c. The horizontal walls are adiabatic and γ is the angle of inclination with respect to the horizontal plane.

2.2 Simplifying assumptions

Several approximations are adopted in order to simplify the formulation of the mathematical model, **Rashad et al. (2017)**:

- The cavity is located in a constant uniform gravity field
- The width of the enclosure, W, is assumed to be sufficiently large compared to the other dimensions (W/L and W/H >> 1) so that the three-dimensional effects become negligible.
- The solution is a Newtonian and incompressible fluid.
- The flow generated is assumed to be laminar.
- The porous matrix is isotropic, permeable and homogeneous.
- There is no chemical reaction or source of heat or mass and the heat transfer by radiation is negligible
- The work, induced by viscous and pressure forces, is negligible.
- The nanoparticles have a spherical shape
- A thermal equilibrium between the base fluid and the solid nanoparticles
- A homogeneity and local thermal equilibrium in the porous medium.
- The nanofluid, is simulated as a single-phase fluid
- The thermophysical properties of the nanofluid are constant and are evaluated at the reference temperature, except for density variation in the buoyancy force which has been evaluated according to the Boussinesq approximation
- The induced magnetic field is negligible because the Reynolds Magnetic number Rm << 1

2.3 Mathematical formulation

Under the previous cited assumptions, the conservation equations describing the problem are the continuity equation, the momentum conservation equation and energy equation.
The Dupuit-Darcy model or extended Darcy law is adopted to describe the nanofluid flow inside the porous medium, which include the nonlinear term of inertial effect on fluid flow.

It is assumed that the porous matrix is solid, permeable, homogeneous, isotropic and saturated by the nanofluid. The equations relating to heat and matter flows in the presence of thermal gradient and magnetic field, **Poulikakos and Bejan, (1985), Riley and Rees (1985), Nawaf and Pop (2005), Rebhi et al. (2014), Rebhi et al. (2016), Alloui et al. (2017), Rebhi et al. (2017), Sheikholeslami and Rokni . (2017), Armaghani et al. (2020),** are given by :

2.3.1 Continuity equation

The continuity equation expressing the principle of conservation of the mass of a moving fluid is given by:

$$\nabla \cdot V = 0 \tag{2.1}$$

2.3.2 Equation of motion: Dupuit-Darcy's law

The local formulation of the momentum conservation equation is written as follows:

$$-\frac{K}{\mu_{nf}}\left(\nabla p - \rho_{nf} g - I \times B\right) = \left(1 + \frac{\tilde{K}}{\mu_{nf}} \rho_{nf} \left|\vec{V}\right|\right) \cdot V \tag{2.2}$$

2.3.3 Energy equation

The first law of thermodynamics makes it possible to establish relations between the different forms of energy take place in porous media. The energy equation, in which the terms of viscous dissipation are neglected, is written as follows:

$$\frac{\partial T}{\partial \tau} + (V \cdot \nabla) T = \alpha_{mnf} \nabla^2 T \tag{2.3}$$

where, $V(u,v)$ is the velocity vector, $B\left(B_x, B_y\right)$ is the magnetic induction, I is the electric current p is the pressure, g is the gravitational acceleration vector, α_{mnf} is the thermal diffusivity of the nanofluid saturated porous medium, μ_{nf} is the nanofluid dynamic viscosity and τ is the time. K and $\tilde{K}$ are the permeability of porous medium and the material parameter which measure the inertial impedance of the matrix **"Rees and Hossain (1999),"** respectively. It is clear from the Eq. (2.2) that with $\tilde{K} = 0$, the Darcy law recovered.

Note that from the equation (2.2), to illustrate how the additional nonlinear term effect appear when the porosity ε is high, we can cite **Ergun's (1952)** for the relations K and $\tilde{K}$.

$$K=\frac{d^2\varepsilon^2}{150(1-\varepsilon)^2},\quad \tilde{K}=\frac{1.75d}{150(1-\varepsilon)}$$

(2.4)

where d , is the characteristic pore or particle diameter.

We have that the electric current density is related to the fluid velocity V by Ohm's law (Moreau 1990):

$$I=\sigma\left(-\nabla\Phi+V\times B\right) \tag{2.5}$$

and $$\nabla\cdot I=0 \tag{2.6}$$

According to **Garandet et al. (1992)**, Eqs. (4.5) and (4.6) reduce to $\nabla^2\Phi=0$ which has a unique solution $\nabla\Phi=0$ since the cavity is electrically insulated.

The equations system through x and y axis becomes:

$$\frac{\partial u}{\partial x}+\frac{\partial v}{\partial y}=0 \tag{2.7}$$

$$\frac{\mu_{nf}}{K}\left(1+\frac{\tilde{K}}{\mu_{nf}}\rho_{nf}\left|\vec{V}\right|\right)\cdot u=-\frac{\partial p}{\partial x}-\rho_{nf}g\sin\gamma+\sigma_{nf}\left(vB^2\sin\xi\cos\xi-uB^2\sin^2\xi\right) \tag{2.8}$$

$$\frac{\mu_{nf}}{K}\left(1+\frac{\tilde{K}}{\mu_{nf}}\rho_{nf}\left|\vec{V}\right|\right)\cdot v=-\frac{\partial p}{\partial y}-\rho_{nf}g\cos\gamma+\sigma_{nf}\left(uB^2\sin\xi\cos\xi-vB^2\cos^2\xi\right) \tag{2.9}$$

$$\frac{\partial T}{\partial\tau}+u\frac{\partial T}{\partial x}+v\frac{\partial T}{\partial y}=\alpha_{mnf}\left(\frac{\partial^2T}{\partial x^2}+\frac{\partial^2T}{\partial y^2}\right) \tag{2.10}$$

We eliminate the pressure from the momentum equation by the usual way and we apply the Boussinesq approximation for describing the density variation in the buoyancy force.

The governing equations become:

$$\frac{\partial u}{\partial y}-\frac{\partial v}{\partial x}+\frac{\tilde{K}}{\mu_{nf}}\rho_{nf}\left[\frac{\partial}{\partial y}\left(\left|\vec{V}\right|\cdot u\right)-\frac{\partial}{\partial x}\left(\left|\vec{V}\right|\cdot v\right)\right]=$$

$$-\frac{gK\rho_{nf}}{\mu_{nf}}\beta_{Tnf}\left(\frac{\partial T}{\partial x}\cos\gamma-\frac{\partial T}{\partial y}\sin\gamma\right)+\frac{\sigma_{nf}KB_0^2}{\mu_{nf}}\left(\frac{\partial u}{\partial y}\sin^2\xi+2\frac{\partial v}{\partial y}\sin\xi\cos\xi+\frac{\partial v}{\partial x}\cos^2\xi\right) \tag{2.11}$$

$$\frac{\partial T}{\partial\tau}+u\frac{\partial T}{\partial x}+v\frac{\partial T}{\partial y}=\alpha_{mnf}\left(\frac{\partial^2T}{\partial x^2}+\frac{\partial^2T}{\partial y^2}\right) \tag{2.12}$$

The thermophysical properties of nanofluid are calculated using **Tiwari and Das model (2007), Bourantas et al. (2014), Mahian et al. (2018).**

The physical properties of the nanofluid: density ρ_{nf}, viscosity μ_{nf}, heat capacitance $(\rho C_p)_{nf}$, thermal conductivity K_{nf} and the buoyancy coefficient $(\rho\beta_T)_{nf}$ are given by

$$\rho_{nf} = (1-\phi)\rho_f + \phi\rho_p \quad , \quad \mu_{nf} = \mu_f / (1-\phi)^{2.5} \quad , \quad (\rho C_p)_{nf} = (1-\phi)(\rho C_p)_f + \phi(\rho C_p)_p$$

$$K_{nf} = K_f \left[\frac{(K_p + 2K_f) - 2\phi(K_f - K_p)}{(K_p + 2K_f) + \phi(K_f - K_p)} \right] \quad , \quad (\rho\beta_T)_{nf} = (1-\phi)(\rho\beta_T)_f + \phi(\rho\beta_T)_p \qquad (2.13)$$

where ϕ is the volume fraction of nanoparticules, f and p refer to fluid and (nano) particle, respectively. The thermophysical properties of fluid (water) and nanoparticles (Cu) and sloid structure of porous medium (Aluminium foam) are reported by the Table 2.1.

It is known that the thermal conductivity given by this Model is only valid for spherical particles, which has been used in this study for calculating the thermal conductivity of the Cu –Water and Al_2O_3 –Water nanofluid. For the Single Wall Carbon nanotube- Water nanofluid, the thermal conductivity has been evaluated by Xue model, **Xue (2005), Khan et al.(2013),** where the effect of space distribution and axial ratio of the Carbon nanotubes have been taken into consideration(Eq.2.14).

$$K_{nf} = K_f \left[\frac{1-\phi + 2\phi \dfrac{K_{CNT}}{K_{CNT} - K_f} \ln\left(\dfrac{K_{CNT} + K_f}{2K_f} \right)}{1-\phi + 2\phi \dfrac{K_f}{K_{CNT} - K_f} \ln\left(\dfrac{K_{CNT} + K_f}{2K_f} \right)} \right] \qquad (2.14)$$

Where ϕ is the volume fraction of nanoparticles, f, and *CNT* refer to fluid and Carbon nanotube respectively.

The thermophysical properties of Water, Cu, Al_2O_3, SWCNT and porous matrix material (Aluminium foam) are given in the Table 2.1.

The electrical conductivity of nanofluid is presented by taking into account both electrical conductivities of the base fluid and the nanoparticles as given by to **Maxwell (1904)** formula:

$$\frac{\sigma_{nf}}{\sigma_f} = 1 + \frac{3(\chi - 1)\phi}{(\chi + 2) - (\chi - 1)\phi} \qquad (2.15)$$

where σ the electrical conductivity, σ_p is the electrical conductivity of nanoparticles, σ_f the electrical conductivity of base fluid and $\chi = \sigma_p / \sigma_f$.

In our study, we assume that the cavity has a square shape ($L = H$).

Physical properties	Base fluid (water)	Cu	Aluminium foam	Al_2O_3	SWCNT
$C_p\left(J.kg^{-1}.K^{-1}\right)$	4179	385	897	765	425
$\rho\left(kg.m^{-3}\right)$	997.1	8933	2700	3970	2600
$k\left(W.m^{-1}.K^{-1}\right)$	0.613	400	205	40	6600
$\beta\times10^{-5}\left(K^{-1}\right)$	22.5	1.67	2.22	0.85	1.6
$\sigma\left(\Omega m^{-1}\right)$	0.05	5.96×10^{7}	--	35×10^{6}	4.8×10^{-7}

Table 2.1. Thermophysical properties of fluid (water), Copper (Cu),Aluminium Oxide (Al_2O_3) and Single-Wall Carbon Nanotube (SWCNT), see **Zahmatkesh et al. (2019), Hayat et al (2017).**

2.4 Applications

2.4.1 First application: Cu-Water nanofluid saturated Aluminium foam porous medium without magnetic field effect

In this application, the magnetic field effect has not been taken into consideration, which means there is no Lorentz force applied and that the parameter $I\times B=0$ in the momentum equation (eq 2.2)

In order to explore the effect the thermal conductivity and the porosity of the solid matrix porous medium, we have the overall heat capacity per unit volume $(\rho C_p)_m$ and the overall thermal conductivity k_m for parallel heat conduction mode in the solid and fluid phases, which are given by **Nield and Bejan (2017), Xu at al. (2019)**:

$$(\rho Cp)_m=\varepsilon(\rho Cp)_f+(1-\varepsilon)(\rho Cp)_S \quad \text{and} \quad k_m=\varepsilon k_f+(1-\varepsilon)k_S \tag{2.16}$$

where s and f refer to the solid matrix of porous medium and fluid phases.

The thermal conductivity and thermal diffusivity of the nanofluid saturated porous medium can be evaluated by using the thermophysical properties of nanofluid (Eqt 2.13) as follows:

$$(\rho Cp)_{mnf}=\varepsilon(\rho Cp)_{nf}+(1-\varepsilon)(\rho Cp)_S=(\rho Cp)_m\left[1-\varepsilon\varphi\frac{(\rho Cp)_f-(\rho Cp)_p}{(\rho Cp)_m}\right] \tag{2.17}$$

$$k_{mnf} = \varepsilon k_{nf} + (1-\varepsilon) k_S = k_m \left[1 - \frac{3\varepsilon\phi k_f \left(k_f - k_p \right)}{k_m \left[k_p + 2k_f + \phi \left(k_f - k_p \right) \right]} \right] \tag{2.18}$$

$$\alpha_{mnf} = \frac{k_{mnf}}{(\rho Cp)_{nf}}, \qquad \alpha_m = \frac{k_m}{(\rho Cp)_f} \tag{2.19}$$

where α is the thermal diffusivity, ε is the porosity of porous medium and the subscripts, m , *mnf* and s are related to clear fluid saturated porous medium, nanofluid saturated porous medium and solid matrix of the porous medium, respectively.

By assuming the cavity has a square shape ($L = H$), and taking the velocity is dimensionless in relation to the thermal diffusivity. Furthermore, the temperature is dimensionless relative to the difference in temperature between the two horizontal walls of the cavity.

The dimensionless variables are given by, **Sheremet et al (2015)** :

$$X = \frac{x}{L}, \quad Y = \frac{y}{L}, \quad U = \frac{uL}{\alpha_{mnf}}, \quad V = \frac{vL}{\alpha_{mnf}}, \quad \theta = \frac{T - T_C}{\Delta T}, \quad t = \frac{\tau \alpha_{mnf}}{HL} \tag{2.20}$$

In addition, the dimensionless stream function Ψ is defined as

$$U = \frac{\partial \Psi}{\partial Y}, \qquad V = -\frac{\partial \Psi}{\partial X} \tag{2.21}$$

By introducing the nanofluid thermophysical properties equations (2.13), the thermal conductivity and diffusivity of the nanofluid saturated porous medium equations (2.18) and (2.19) and the dimensionless variables (2.20) and (2.21) into equations (2.11) - (2.12), we obtain the following dimensionless governing equations describing, respectively, the conservation of motion and energy.

$$\left[1 + V_a \times G \times F(\phi) \right] \nabla^2 \Psi + \frac{G \times F(\phi)}{V_a} S_\Omega = -R_T \cdot H(\phi) \left(\frac{\partial \theta}{\partial X} \cos\gamma - \frac{\partial \theta}{\partial Y} \sin\gamma \right) \tag{2.22}$$

$$\frac{\partial \theta}{\partial t} + \frac{\partial \psi}{\partial Y}\frac{\partial \theta}{\partial X} + \frac{\partial \psi}{\partial X}\frac{\partial \theta}{\partial Y} = \frac{\partial^2 \theta}{\partial X^2} + \frac{\partial^2 \theta}{\partial Y^2} \tag{2.23}$$

where the parameters $S_\Omega, G, R_T, V_a, F(\phi)$ and $H(\phi)$ in the momentum equation are given by:

$$S_\Omega = \left[\left(\frac{\partial \Psi}{\partial X} \right)^2 \frac{\partial^2 \Psi}{\partial X^2} + \left(\frac{\partial \Psi}{\partial Y} \right)^2 \frac{\partial^2 \Psi}{\partial Y^2} + 2 \frac{\partial \Psi}{\partial X} \frac{\partial \Psi}{\partial Y} \frac{\partial^2 \Psi}{\partial X \partial Y} \right] \tag{2.24}$$

$$V_a = \left[\left(\partial \Psi / \partial X \right)^2 + \left(\partial \Psi / \partial Y \right)^2 \right]^{1/2} \tag{2.25}$$

$G = \dfrac{\tilde{K} \alpha_m}{\nu_f L}$ is the inertial effect parameter (2.26)

$R_T = \dfrac{gKL\Delta T\left(\rho\beta_T\right)_f}{\mu_f \alpha_m}$ is the Darcy-Rayleigh number (2.27)

$$F(\phi) = \left(1-\phi\right)^{2.5}\left(1-\phi+\phi\frac{\rho_p}{\rho_f}\right)\times\frac{\left[1-\dfrac{3\varepsilon\phi k_f\left(k_f-k_p\right)}{k_m\left[k_p+2k_f+\phi\left(k_f-k_p\right)\right]}\right]}{\left[1-\phi+\phi\dfrac{\left(\rho Cp\right)_p}{\left(\rho Cp\right)_f}\right]} \quad (2.28)$$

$$H(\phi) = \left(1-\phi\right)^{2.5}\left(1-\phi+\phi\frac{\left(\rho\beta\right)_p}{\left(\rho\beta\right)_f}\right)\times\frac{\left[1-\phi+\phi\dfrac{\left(\rho Cp\right)_p}{\left(\rho Cp\right)_f}\right]}{\left[1-\dfrac{3\varepsilon\phi k_f\left(k_f-k_p\right)}{k_m\left[k_p+2k_f+\phi\left(k_f-k_p\right)\right]}\right]} \quad (2.29)$$

The functions $F(\phi)$ and $H(\phi)$ depend on the solid structure of the porous medium, the thermophysical properties of nanofluid (fluid and nanoparticles) and the nanoparticles concentration ϕ.

The parameter G measures the inertial effects and its value represents the departure from the linear Darcy situation. For high porosity ε and for hight particle or pore diameter d, the material parameter $\tilde{K}$ will have high value, and the inertial effect non linear parameter G become significant.

As it can be seen for $\phi = 0$; $F(\phi) = H(\phi) = 1$ (clear fluid) and for $G = 0$ into the momentum equation Eq. (2.22) the Darcy law retrieved.

2.4.2 Second application: SWCNT-Water and Al_2O_3-Water nanofluid saturated porous medium with external magnetic field effect

In this application, the magnetic field effect is taken into consideration. In addition, we take the thermal diffusivity in the energy equation (Eq 2.3):

$$\alpha_{mnf} = \alpha_{nf} = K_{nf}/\left(\rho Cp\right)_{nf} \quad (2.30)$$

And the dimensionless variables are the same used in the first applications, equations (2.20) and (2.21).

By introducing the following parameters into the momentum and energy equations (eqs (2.11) and (2,12)):

- The nanofluid thermophysical properties given by Tiwari and Das model used for calculating the properties of Al_2O_3-Water nanofluid.

- The SWCNT-Water nanofluid properties given by the Tiwari and Das model has been used, except for the thermal conductivity on SWCNT which has been calculated by the equations (2.14).

The momentum and energy equations become:

$$\left[1+V_a\times G\times F_1(\phi)\right]\nabla^2\Psi+\frac{G\times F_1(\phi)}{V_a}\left[\left(\frac{\partial\Psi}{\partial X}\right)^2\frac{\partial^2\Psi}{\partial X^2}+\left(\frac{\partial\Psi}{\partial Y}\right)^2\frac{\partial^2\Psi}{\partial Y^2}+2\frac{\partial\Psi}{\partial X}\frac{\partial\Psi}{\partial Y}\frac{\partial^2\Psi}{\partial X\partial Y}\right]=$$

$$-R_T\cdot H_1(\phi)\left(\frac{\partial\theta}{\partial X}\cos\gamma-\frac{\partial\theta}{\partial Y}\sin\gamma\right)-Ha^2C_1(\phi)\left(\frac{\partial^2\Psi}{\partial Y^2}\sin^2\xi+2\frac{\partial^2\Psi}{\partial X\partial Y}\sin\xi\cos\xi+\frac{\partial^2\Psi}{\partial X^2}\cos^2\xi\right) \quad (2.31)$$

$$\frac{\partial\theta}{\partial t}+\frac{\partial\psi}{\partial Y}\frac{\partial\theta}{\partial X}+\frac{\partial\psi}{\partial X}\frac{\partial\theta}{\partial Y}=E_1(\phi)\left(\frac{\partial^2\theta}{\partial X^2}+\frac{\partial^2\theta}{\partial Y^2}\right) \quad (2.32)$$

where the parameters, G , R_T , Ha , V_a, C_1 $F_1(\phi)$, $H_1(\phi)$ and $E_1(\phi)$ in the momentum and energy equations are given by:

$G=\dfrac{\tilde{K}\alpha_f}{\nu_f L}$ is the inertial effect parameter (2.33)

$R_T=\dfrac{gKL\Delta T\left(\rho\beta_T\right)_f}{\mu_f\alpha_f}$ is the Darcy-Rayleigh number (2.34)

$Ha=B_0\sqrt{\dfrac{\sigma K}{\mu}}$ is the Hartmann number (2.35)

$$V_a=\left[\left(\partial\Psi/\partial X\right)^2+\left(\partial\Psi/\partial Y\right)^2\right]^{1/2} \quad (2.36)$$

$$C_1(\phi)=(1-\phi)^{2.5}\left[1+\frac{3(\chi-1)\phi}{(\chi+2)-(\chi-1)\phi}\right] \quad (2.37)$$

$$F_1(\phi)=(1-\phi)^{2.5}\left(1-\phi+\phi\frac{\rho_p}{\rho_f}\right) \quad (2.38)$$

$$H_1(\phi)=(1-\phi)^{2.5}\left(1-\phi+\phi\frac{(\rho\beta)_p}{(\rho\beta)_f}\right) \quad (2.39)$$

$$E_1(\phi)=\frac{k_{nf}}{k_f}\frac{(\rho Cp)_f}{(1-\phi)(\rho Cp)_f+\phi(\rho Cp)_p} \quad (2.40)$$

The functions $F_1(\phi)$, $H_1(\phi)$ and $E_1(\phi)$ depend on the thermophysical properties of nanofluid (fluid and nanoparticles) and the nanoparticles concentration ϕ.

As it can be noticed for $\phi = 0$; $F_1(\phi) = H_1(\phi) = E_1(\phi) = 1$ (clear fluid), and the Darcy law can be retrieved for $G = 0$ into the momentum equation Eq. (2.31).

2.5 Boundary conditions

2.5.1 Hydrodynamic boundary conditions

These conditions express the impermeability of the walls of the cavity, they are given by:

$$\left.\begin{array}{l} \Psi = 0 \quad at \quad X = \pm\dfrac{1}{2} \\ \Psi = 0 \quad at \quad Y = \pm\dfrac{1}{2} \end{array}\right\} \tag{2.41}$$

2.5.2 Thermal boundary conditions

The boundary conditions on the adiabatic and impermeable walls of the cavity are expressed by:

$$\left.\begin{array}{l} \theta = 0.5 \quad at \quad X = -\dfrac{1}{2} \\ \theta = -0.5 \quad at \quad X = +\dfrac{1}{2} \\ \dfrac{\partial \theta}{\partial Y} = 0 \quad at \quad Y = \pm\dfrac{1}{2} \end{array}\right\} \tag{2.42}$$

2.6 Heat transfer

In the present study, we are particularly interested in the calculations of the rate of heat transfer rate at a given position; the physical quantities of interest are the local Nusselt number Nu and the average Nusselt number Nu_m at the vertical walls, which are defined as:

For the first application **Sheremet et al (2015)**:

$$Nu = -\frac{k_{mnf}}{k_f}\left(\frac{\partial \theta}{\partial X}\right)_{X=\pm 0.5} \tag{2.43}$$

$$Nu_m = \int_{-1/2}^{+1/2} Nu \, dY \tag{2.44}$$

For the second application **Rashad et al (2017):**

$$Nu = -\frac{k_{nf}}{k_f}\left(\frac{\partial \theta}{\partial X}\right)_{X=\pm 0.5} \tag{2.45}$$

$$Nu_m = \int_{-1/2}^{+1/2} Nu\, dY \tag{2.46}$$

We denote by $\overline{Nu}_L$ the average Nusselt number of the left wall and $\overline{Nu}_R$ the average Nusselt number of the right wall.

2.7 Conclusion

Through this chapter, we have presented a detailed study of two different configurations with the corresponding hypotheses. the first configuration is about Copper-Water nanofluid (Cu-Water) saturated Aluminium foam porous medium where the porosity and the matrix material have been taken into consideration without the effect of magnetic field. The second one is for the Oxide Aluminium - Water (Al2O3-Water) and Single Wall Carbon Nanotube –Water (SWCNT-Water) nanofluids saturated an inclined porous enclosure under the effect of external magnetic field

Our objective is to clarify the established mathematical formulation, the appropriate mesh and the method of the numerical resolution employed.

CHAPTER III
NUMERICAL METHOD

CHAPTER III

NUMERICAL METHOD

In this chapter, we use a numerical method for solving the of non-linear differential equations system.

The proposed method is based on the finite difference technique. This method is the oldest of the numerical methods. It was introduced in the 18th century by Euler, it turns out to be the most suitable and the easiest to use for problems with simple geometry. This method consists in discretizing the continuous equations at the nodes of a predefined mesh (see Figure. 3.1).

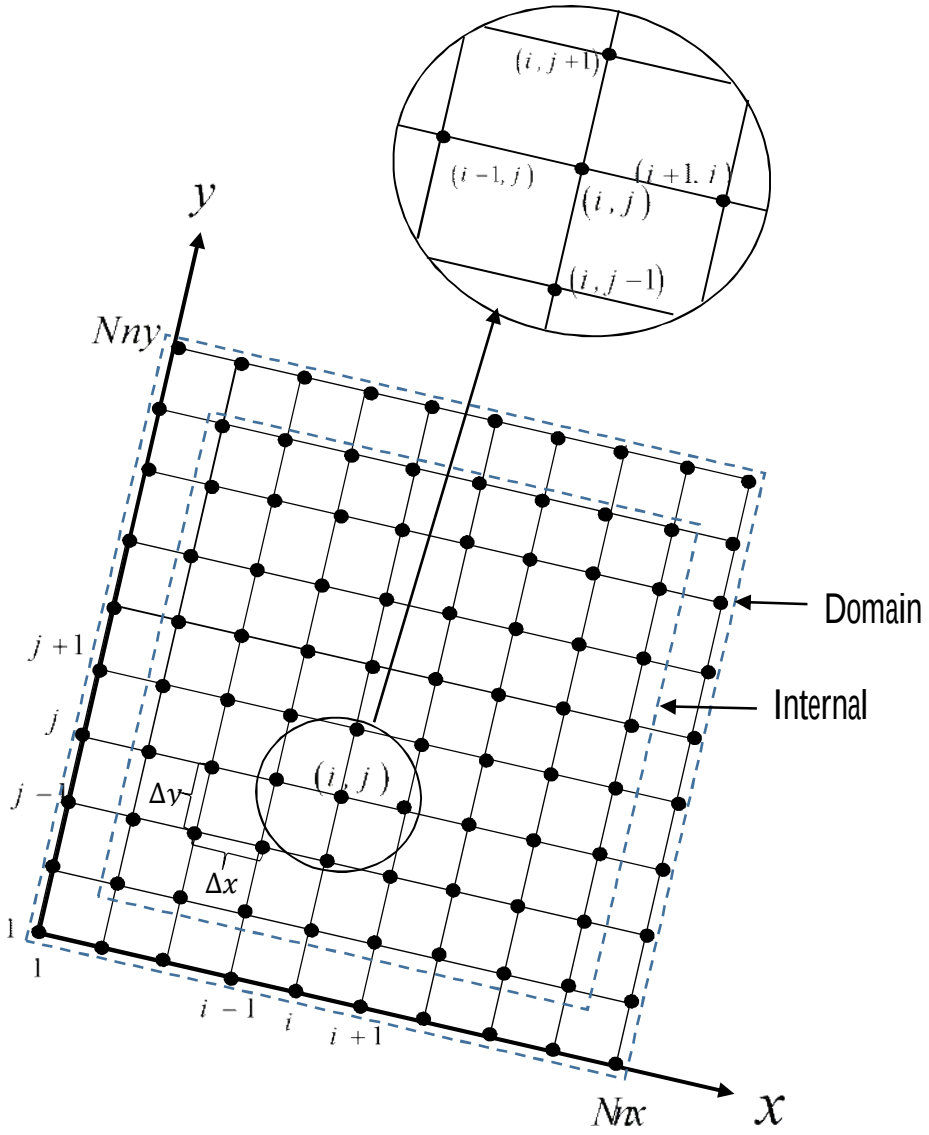


Figure 3.1: Meshing of the computational domain in (i, j).

In a Cartesian coordinate system, each node is designated by the pair of indices designating the intersection lines of the mesh. Neighboring nodes are implicitly defined by increasing or decreasing one of the indices by a unit increment.

The energy equation is discretized with a centered second order scheme and using the conservative form for the convective terms. For each time step the method implicit in alternate directions (ADI) gives rise to two tri-diagonal matrix systems to be resolved, one resulting from the implicit discretization in x and the other from the implicit discretization in y. The method (ADI) divides the time step into two equal parts, in the first half time step, the system is implicitly in x but explicitly in y and in the second half time step, and the system is implicitly in y and explicitly in x. For each time step, the solution is obtained by scanning the domain of calculation in the direction of x then in that of y. Knowing the temperature field at a time (n+1) Δt, the next step is the current function field calculation from the momentum equation, once discretized with a classic centered scheme and resolved with the successive point over-relaxation (SOR) method. This method proposed by **Frankel (1950)**, which is an explicit method giving directly the value of Ψ at the instant (n+1) Δt, to the considered node, with a sufficient number of iterations for the desired convergence criterion to be satisfied.

3.1 Thermal boundary conditions discretization

The boundary conditions (2.41) and (2.42) are discretized according to a scheme with finite differences decentered to the right and to the left of the second order according to the wall considered:

For the adiabatic and impermeable walls:

$$\theta_{i,1} = \frac{4\theta_{i,2} - \theta_{i,3}}{3} \quad \text{at} \quad Y = -\frac{1}{2} \tag{3.1}$$

$$\theta_{I,Nny} = \frac{4\theta_{i,Nny-1} - \theta_{i,Nny-2}}{3} \quad \text{at} \quad Y = +\frac{1}{2} \tag{3.2}$$

For active walls:

$$\theta_{1,j} = \frac{4\theta_{2,j} - \theta_{3,j} + 2\Delta X}{3} \quad \text{at} \quad X = -\frac{1}{2} \tag{3.3}$$

$$\theta_{Nnx,j} = \frac{4\theta_{Nnx-1,j} - \theta_{Nnx-2,j} - 2\Delta X}{3} \quad \text{at} \quad X = \frac{1}{2} \tag{3.4}$$

3.2 Energy equation discretization

The energy equation being parabolic with respect to time and elliptical with respect to spatial coordinates, the Alternating direction implicit method (ADI) is chosen as a resolution tool. Given the equation of energy (2.23) the latter is rewritten as follows:

$$\frac{\partial\theta}{\partial t}+\frac{\partial(U\theta)}{\partial X}+\frac{\partial(V\theta)}{\partial Y}=\frac{\partial^2\theta}{\partial X^2}+\frac{\partial^2\theta}{\partial Y^2} \tag{3.5}$$

Implicit scheme in x and explicit in y

It is a schema with differences centered at time (*n*+1/2) for the derivatives in x and at time *n* for the derivatives in *y*, each term of equation (3.5) is discretized as follows:

$$\left.\frac{\partial^2\theta}{\partial X^2}\right|_{i,j}=\frac{\theta_{i+1,j}^{n+1/2}-2\theta_{i,j}^{n+1/2}+\theta_{i-1,j}^{n+1/2}}{\Delta X^2}, \qquad \left.\frac{\partial^2\theta}{\partial X^2}\right|_{i,j}=\frac{\theta_{i,j+1}^{n}-2\theta_{i,j}^{n}+\theta_{i,j-1}^{n}}{\Delta Y^2} \tag{3.6}$$

$$\left.\frac{\partial(U\theta)}{\partial X}\right|_{i,j}=\frac{U_{i+1,j}^{n}\theta_{i+1,j}^{n+1/2}-U_{i-1,j}^{n}\theta_{i-1,j}^{n+1/2}}{2\Delta X}, \qquad \left.\frac{\partial(V\theta)}{\partial Y}\right|_{i,j}=\frac{V_{i,j+1}^{n}\theta_{i,j+1}^{n}-V_{i,j-1}^{n}\theta_{i,j-1}^{n}}{2\Delta Y} \tag{3.7}$$

$$\left.\frac{\partial\theta}{\partial t}\right|_{i,j}=2\frac{\theta_{i,j}^{n+1/2}-\theta_{i,j}^{n}}{\Delta t} \tag{3.8}$$

By substituting equations (3.6), (3.8) in equation (3.5), we obtain a three-dimensional matrix system of the form:

$$A_i\theta_{i+1,j}^{n+1/2}+B_i\theta_{i,j}^{n+1/2}+C_i\theta_{i-1,j}^{n+1/2}=D_i \tag{3.9}$$

with :

$$A_i=\left[\frac{U_{i+1,j}^{n}}{2\Delta X}+\frac{1}{\Delta X^2}\right], \quad B_i=2\left[\frac{1}{\Delta t}+\frac{1}{\Delta X^2}\right], \quad C_i=\left[\frac{U_{i-1,j}^{n}}{2\Delta X}+\frac{1}{\Delta X^2}\right]$$

$$D_i=\left[-\frac{V_{i,j+1}^{n}}{2\Delta Y}+\frac{1}{\Delta Y^2}\right]\theta_{i,j+1}^{n}+2\left[\frac{1}{\Delta t}-\frac{1}{\Delta Y^2}\right]\theta_{i,j}^{n}+\left[\frac{V_{j,j-1}^{n}}{2\Delta Y}+\frac{1}{\Delta Y^2}\right]\theta_{i,j-1}^{n}$$

By replacing the boundary conditions (3.1) - (3.4) in equation (3.9) we obtain the implicit discrete form in x in the following form:

For : $i=2$

$$\left[A_2-\frac{1}{3}C_2\right]\theta_{3,j}^{n+1/2}+\left[B_2+\frac{4}{3}C_2\right]\theta_{2,j}^{n+1/2}=D_2-\frac{2}{3}C_2\Delta X \tag{3.10a}$$

For : $i = N_{nx-1}$

$$\left[\frac{4}{3}A_{Nnx-1} + B_{Nnx-1}\right]\theta^{n+1/2}_{Nnx-1,\,j} + \left[C_{Nnx-1} - \frac{1}{3}A_{Nnx-1}\right]\theta^{n+1/2}_{Nnx-2,\,j} = D_{Nnx-1} + \frac{2}{3}A_{Nnx-1}\Delta X \quad (3.10b)$$

With the same approache, we obtain a three-dimensional matrix system for the energy equation (eq. 2.32) for the seconde case of the form:

$$A_i\theta^{n+1/2}_{i+1,\,j} + B_i\theta^{n+1/2}_{i,\,j} + C_i\theta^{n+1/2}_{i-1,\,j} = D_i \quad (3.11)$$

with :

$$A_i = \left[\frac{U^n_{i+1,\,j}}{2\Delta X} + \frac{E_1(\phi)}{\Delta X^2}\right], \quad B_i = 2\left[\frac{1}{\Delta t} + \frac{E_1(\phi)}{\Delta X^2}\right], \quad C_i = \left[\frac{U^n_{i-1,\,j}}{2\Delta X} + \frac{E_1(\phi)}{\Delta X^2}\right]$$

$$D_i = \left[-\frac{V^n_{i,\,j+1}}{2\Delta Y} + \frac{E_1(\phi)}{\Delta Y^2}\right]\theta^n_{i,\,j+1} + 2\left[\frac{1}{\Delta t} - \frac{E_1(\phi)}{\Delta Y^2}\right]\theta^n_{i,\,j} + \left[\frac{V^n_{j,\,j-1}}{2\Delta Y} + \frac{E_1(\phi)}{\Delta Y^2}\right]\theta^n_{i,\,j-1}$$

Implicit scheme in y and explicit in x

It is a diagram with differences centered at time (*n*+1/2) for derivatives in *x* and at time (*n*+1) for derivatives in *y*. The discretization of the partial derivatives is given by:

$$\left.\frac{\partial^2\theta}{\partial X^2}\right|_{i,\,j} = \frac{\theta^{n+\frac{1}{2}}_{i+1,\,j} - 2\theta^{n+\frac{1}{2}}_{i,\,j} + \theta^{n+\frac{1}{2}}_{i-1,\,j}}{\Delta X^2}, \qquad \left.\frac{\partial^2\theta}{\partial Y^2}\right|_{i,\,j} = \frac{\theta^{n+1}_{i,\,j+1} - 2\theta^{n+1}_{i,\,j} + \theta^{n+1}_{i,\,j-1}}{\Delta Y^2} \quad (3.12)$$

$$\left.\frac{\partial(U\theta)}{\partial X}\right|_{i,\,j} = \frac{U^n_{i+1,\,j}\theta^{n+\frac{1}{2}}_{i+1,\,j} - U^n_{i-1,\,j}\theta^{n+\frac{1}{2}}_{i-1,\,j}}{2\Delta X}, \qquad \left.\frac{\partial(V\theta)}{\partial Y}\right|_{i,\,j} = \frac{V^n_{i,\,j+1}\theta^{n+1}_{i,\,j+1} - V^n_{i,\,j-1}\theta^{n+1}_{i,\,j-1}}{2\Delta Y} \quad (3.13)$$

$$\left.\frac{\partial\theta}{\partial t}\right|_{i,\,j} = 2\frac{\theta^{n+1}_{i,\,j} - \theta^{n+\frac{1}{2}}_{i,\,j}}{\Delta t} \quad (3.14)$$

By substituting equations (3.12) - (3.14) in equation (3.5), we obtain a tridiagonal matrix system of the form:

$$A'_j\theta^{n+1}_{i,\,j+1} + B'_j\theta^{n+1}_{i,\,j} + C'_j\theta^{n+1}_{i,\,j-1} = D'_j \quad (3.15)$$

$$A_j^{'}=\left[\frac{V_{i,j+1}^{n}}{2\Delta Y}+\frac{1}{\Delta Y^2}\right],\quad B_j^{'}=2\left[\frac{1}{\Delta t}+\frac{1}{\Delta Y^2}\right],\quad C_j^{'}=\left[\frac{V_{i,j-1}^{n}}{2\Delta Y}+\frac{1}{\Delta Y^2}\right]$$

$$D_j^{'}=\left[-\frac{U_{i+1,j}^{n}}{2\Delta X}+\frac{1}{\Delta X^2}\right]\theta_{i+1,j}^{n+1/2}+2\left[\frac{1}{\Delta t}-\frac{1}{\Delta X^2}\right]\theta_{i,j}^{n+1/2}+\left[\frac{U_{i-1,j}^{n}}{2\Delta X}+\frac{1}{\Delta X^2}\right]\theta_{i-1,j}^{n+1/2}$$

By replacing the boundary conditions (3.1) - (3.4) in equation (3.15) we obtain the implicit discrete form in y in the following form:

For : $j=2$ $$\left[A_2^{'}-\frac{1}{3}C_2^{'}\right]\theta_{i,3}^{n+1}+\left[B_2^{'}+\frac{4}{3}C_2^{'}\right]\theta_{i,2}^{n+1}=D_2^{'} \tag{3.16a}$$

For: $j=N_y$ $$\left[\frac{4}{3}A_{Nny-1}^{'}+B_{Nny-1}^{'}\right]\theta_{i,Nny-1}^{n+1}+\left[C_{Nny-1}^{'}-\frac{1}{3}A_{Nny-1}^{'}\right]\theta_{i,Nny-2}^{n+1}=D_{Nny-1}^{'} \tag{3.16b}$$

With the same approache, we obtain a three-dimensional matrix system for the energy equation (eq. 2.32) for the seconde case of the form:

$$A_j^{'}\theta_{i,j+1}^{n+1}+\theta_j^{'}T_{i,j}^{n+1}+C_j^{'}\theta_{i,j-1}^{n+1}=D_j^{'} \tag{3.17}$$

$$A_j^{'}=\left[\frac{V_{i,j+1}^{n}}{2\Delta Y}+\frac{E_1(\phi)}{\Delta Y^2}\right],\quad B_j^{'}=2\left[\frac{1}{\Delta t}+\frac{E_1(\phi)}{\Delta Y^2}\right],\quad C_j^{'}=\left[\frac{V_{i,j-1}^{n}}{2\Delta Y}+\frac{E_1(\phi)}{\Delta Y^2}\right]$$

$$D_j^{'}=\left[-\frac{U_{i+1,j}^{n}}{2\Delta X}+\frac{E_1(\phi)}{\Delta X^2}\right]\theta_{i+1,j}^{n+1/2}+2\left[\frac{1}{\Delta t}-\frac{E_1(\phi)}{\Delta X^2}\right]\theta_{i,j}^{n+1/2}+\left[\frac{U_{i-1,j}^{n}}{2\Delta X}+\frac{E_1(\phi)}{\Delta X^2}\right]\theta_{i-1,j}^{n+1/2}$$

3.3 Momentum equation discretization

The momentum equation motion in the general case is written in the following form:

$$\left[1+V_a\times G\times F(\phi)\right]\nabla^2\Psi+\frac{G\times F(\phi)}{V_a}\left[U^2\frac{\partial^2\Psi}{\partial X^2}+V^2\frac{\partial^2\Psi}{\partial Y^2}-2UV\frac{\partial^2\Psi}{\partial X\partial Y}\right]=-R_T\cdot H(\phi)\left(\frac{\partial\theta}{\partial X}\cos\gamma-\frac{\partial\theta}{\partial Y}\sin\gamma\right) \tag{3.18}$$

where : $V_a=\left[\left(\partial\Psi/\partial X\right)^2+\left(\partial\Psi/\partial Y\right)^2\right]^{1/2}$

Before the discretization of the equation (3.16), we assume that the variables, V_a, U and V are already known.

Each term of the equation is discretized according to a classical centered scheme.

$$\left.\frac{\partial^2\Psi}{\partial X^2}\right|_{i,j} = \frac{\Psi_{i+1,j}^{n+1} - 2\Psi_{i,j}^{n+1} + \Psi_{i-1,j}^{n+1}}{\Delta X^2}, \qquad \left.\frac{\partial^2\Psi}{\partial Y^2}\right|_{i,j} = \frac{\Psi_{i,j+1}^{n+1} - 2\Psi_{i,j}^{n+1} + \Psi_{i,j-1}^{n+1}}{\Delta Y^2} \tag{3.19}$$

$$\left.\frac{\partial\theta}{\partial X}\right|_{i,j} = \frac{\theta_{i+1,j}^{n+1} - \theta_{i-1,j}^{n+1}}{2\Delta X} \tag{3.20}$$

and we apply a cross discretization for the following term:

$$\left.\frac{\partial^2\Psi}{\partial X\partial Y}\right|_{i,j} = \frac{1}{4\Delta x\Delta y}\left[\Psi_{i+1,j+1}^{n+1} - \Psi_{i-1,j+1}^{n+1} + \Psi_{i-1,j-1}^{n+1} - \Psi_{i+1,j-1}^{n+1}\right] \tag{3.21}$$

By replacing the expressions (3.19), (3.20) and (3.21) in equation (3.18) we obtain the general expression of the following function

$$\begin{aligned}&\Psi_{i,j}^{(n+1),(k+1)} = \\ &\Psi_{i,j}^{(n+1),k} + \omega\Big\{a_x\left(\Psi_{i+1,j}^{(n+1),k} + \Psi_{i-1,j}^{(n+1),(k+1)}\right) + a_y\left(\Psi_{i,j+1}^{(n+1),k} + \Psi_{i,j-1}^{(n+1),(k+1)}\right) + a_{xy} \\ &\left(\Psi_{i+1,j+1}^{(n+1),k} - \Psi_{i-1,j+1}^{(n+1),k} - \Psi_{i-1,j-1}^{(n+1),(k+1)} + \Psi_{i+1,j+1}^{(n+1),k}\right) + a_{TSx}\left(T_{i+1,j}^{(n+1)} - T_{i-1,j}^{(n+1)}\right) + a_{TSy}\left(T_{i,j+1}^{(n+1)} - T_{i,j-1}^{(n+1)}\right)\ \Big\}\end{aligned} \tag{3.22}$$

Where the parameters: $a_p, a_x, a_y, a_{xy}, a_{TSx}$ and a_{TSy} are given by :

$$a_p = -\frac{\left[2\left(1+V_a\cdot F(\phi)\cdot G\right)\left(\Delta X^2+\Delta Y^2\right)V_a + 2\left(V^2\Delta Y^2 + U^2\Delta X^2\right)F(\phi)\cdot G\right]}{V_a\Delta X^2\Delta Y^2}$$

$$a_x = \left[\frac{\left(1+V_a\cdot G\cdot F(\phi)\right)V_a + V^2GF(\phi)}{V_a\Delta X^2}\right]/a_p \ ,$$

$$a_y = \left[\frac{\left(1+V_a\cdot G\cdot F(\phi)\right)V_a + U^2GF(\phi)}{V_a\Delta Y^2}\right]/a_p$$

$$a_{xy} = \left[\frac{UVGF(\phi)}{2V_a\Delta X\Delta Y}\right]/a_p \ , \ a_{TSx} = \frac{R_T H(\phi)\cos\gamma}{2\Delta X a_p} \ , \ a_{TSy} = -\frac{R_T H(\phi)\sin\gamma}{2\Delta Y a_p} \tag{3.23}$$

With the same approache we obtain the general expression of the momentum equation (eq.2.31) for the seconde case of the following form

$$\begin{aligned}&\Psi_{i,j}^{(n+1),(k+1)} = \\ &\Psi_{i,j}^{(n+1),k} + \omega\Big\{a_{x1}\left(\Psi_{i+1,j}^{(n+1),k} + \Psi_{i-1,j}^{(n+1),(k+1)}\right) + a_{y1}\left(\Psi_{i,j+1}^{(n+1),k} + \Psi_{i,j-1}^{(n+1),(k+1)}\right) + a_{xy1} \\ &\left(\Psi_{i+1,j+1}^{(n+1),k} - \Psi_{i-1,j+1}^{(n+1),k} - \Psi_{i-1,j-1}^{(n+1),(k+1)} + \Psi_{i+1,j+1}^{(n+1),k}\right) + a_{TSx1}\left(T_{i+1,j}^{(n+1)} - T_{i-1,j}^{(n+1)}\right) + a_{TSy1}\left(T_{i,j+1}^{(n+1)} - T_{i,j-1}^{(n+1)}\right)\ \Big\}\end{aligned} \tag{3.24}$$

Where the parameters: $a_{p1}, a_{x1}, a_{y1}, a_{xy1}, a_{TSx1}$ and a_{TSy1} are given by :

$$a_{p1} = -\frac{\left[\begin{array}{l} 2\left(1+V_a \cdot F(\phi)\cdot G\right)\left(\Delta X^2+\Delta Y^2\right)V_a + 2\left(V^2\Delta Y^2 + U^2\Delta X^2\right)F(\phi)\cdot G + \\ 2C_1\left(\Delta X^2\cos^2\xi + \Delta Y^2\sin^2\xi\right)V_a \end{array}\right]}{V_a\Delta X^2\Delta Y^2}$$

$$a_{x1} = \left[\frac{\left(1+V_a\cdot G\cdot F(\phi)+C_1\sin^2\xi\right)V_a + V^2GF(\phi)}{V_a\Delta X^2}\right] / a_{p1} \ ,$$

$$a_{y1} = \left[\frac{\left(1+V_a\cdot G\cdot F(\phi)+\cos^2\xi\right)V_a + U^2GF(\phi)}{V_a\Delta Y^2}\right] / a_{p1}$$

$$a_{xy1} = \left[\frac{UVGF(\phi)}{2V_a\Delta X\Delta Y} + C_1\sin\xi\cos^2\xi\right] / a_{p1} \ , \ a_{TSx1} = \frac{R_T H(\phi)\cos\gamma}{2\Delta X a_{p1}} \ , \ a_{TSy1} = -\frac{R_T H(\phi)\sin\gamma}{2\Delta Y a_{p1}}$$

(3.25)

The parameter ω is the over-relaxation factor; its value is between 1 and 2, to accelerate convergence. Its optimal value ω_{opt} depends on the shape of the domain, the mesh and the type of boundary conditions.

For a rectangular domain with a uniform mesh, is given by:

$$\omega_{opt} = \frac{2}{\zeta^2}\left[1-\sqrt{1-\zeta^2}\right] \qquad (3.26)$$

where :

$$\zeta = \left[\frac{\cos\left(\pi / N_{x+1}\right)+\left(\Delta x^2/\Delta y^2\right)\cos\left(\pi/N_{y+1}\right)}{1+\left(\Delta x^2/\Delta y^2\right)}\right]$$

N_{x+1} and N_{y+1} denote the numbers of the nodes in the horizontal and vertical directions, respectively.

3.4 Velocity fields discretization

The components of the velocity field are obtained from the current function according to the relations (2.21). The discretization of these equations by a first order centered finite difference scheme gives:

$$U_{i,j}^{n+1} = \frac{\Psi_{i,j+1}^{n+1} - \Psi_{i,j-1}^{n+1}}{2\Delta Y} \qquad (3.27)$$

$$V_{i,j}^{n+1} = \frac{\Psi_{i,j+1}^{n+1} - \Psi_{i,j-1}^{n+1}}{2\Delta X} \tag{3.28}$$

3.5 Discretization of velocity boundary conditions

The velocity boundary conditions are discretized according to a finite differences scheme, decentered to the right and to the left of the third order:

$$\left.\begin{array}{lll} U_{1,j} = 0, \quad , & V_{i,1} = -\dfrac{18\Psi_{2,j} - 9\Psi_{3,j} + 2\Psi_{4,j}}{6\Delta X} & \text{à} \quad X = -\dfrac{1}{2} \\ U_{Nnx,j} = 0, & V_{i,Nny} = \dfrac{18\Psi_{Nnx-1,j} - 9\Psi_{Nnx-2,j} + 2\Psi_{Nnx-3,j}}{6\Delta X} & \text{à} \quad X = \dfrac{1}{2} \end{array}\right\} \tag{3.29}$$

$$\left.\begin{array}{lll} V_{i,1} = 0, & U_{1,j} = \dfrac{18\Psi_{i,2} - 9\Psi_{i,3} + 2\Psi_{i,4}}{6\Delta Y} & \text{à} \quad y = -\dfrac{1}{2} \\ V_{i,Nny} = 0, & U_{Ny+1,j} = -\dfrac{18\Psi_{i,Nny-1} - 9\Psi_{i,Nny-2} + 2\Psi_{i,Nny-3}}{6\Delta Y} & \text{à} \quad y = \dfrac{1}{2} \end{array}\right\} \tag{3.30}$$

3.6 Calculation algorithm

The main steps of our calculation algorithm are:

1. Mesh generation.
2. Initialization and reading of data.
3. Calculation of the over-relaxation factor.
4. Introduces of the initial conditions on the temperature, and on the current function, Ψ .
5. Initial velocity field assessment $U_{i,j}$ et $V_{i,j}$.
6. Start of the time loop.

6.1. Solving the energy equation (3.9) and (3.15) by the ADI method and calculating the temperature field $\theta_{i,j}$.

6.2. Resolution of the equation of motion (3.22) by the SOR method and calculation of the field of the current function $\Psi_{i,j}$.

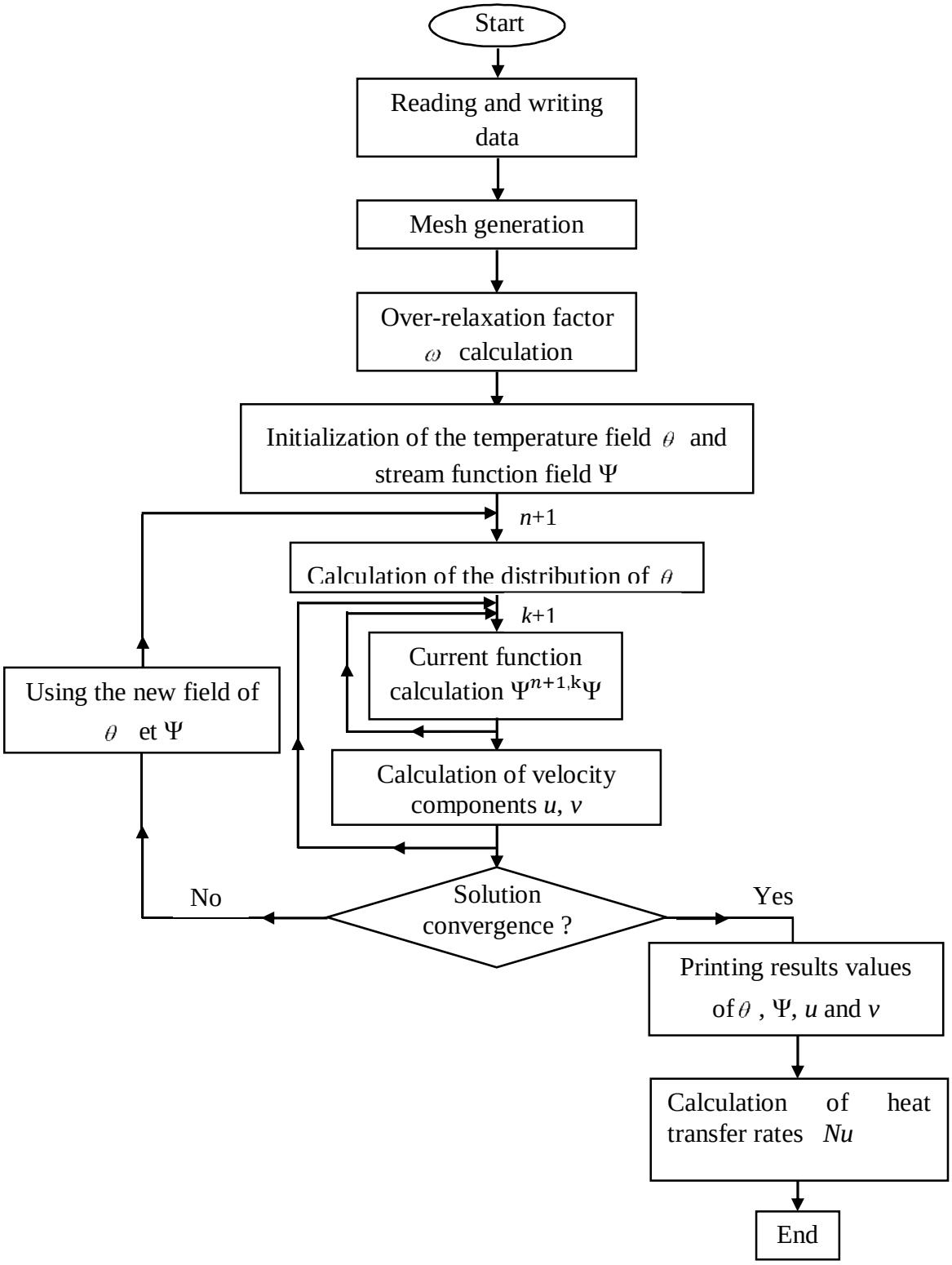
6.3. Velocity field calculation $U_{i,j}$ et $V_{i,j}$.

6.4. Repeat step (6.1) until the solution converges to a permanent or oscillating solution.

7. Printing the results.
8. End of program.

The convergence criterion when solving equation (3.20) is given by:

$$\frac{\sum_i \sum_j \left|\Psi_{i,j}^{k+1} - \Psi_{i,j}^{k}\right|}{\sum_i \sum_j \left|\Psi_{i,j}^{k}\right|} \leq 10^{-6} \qquad (3.31)$$



3.7 Conclusion

Through this chapter, we have presented the finite difference numerical method for solving the obtained non-linear differential equations system for the both cases, the discretized energy and momentum equations, in addition to boundary conditions. At the end, we have presented the algorithm used for implementing the Fortran code to resolve the discretized energy and momentum equations

CHAPTER IV
RESULTS AND DISCUSSION

CHAPTER IV

RESULTS AND DISCUSSION

This chapter is interested in the presentation of the numerical results for the both studied cases. In the first case, the results of the free convection of Cu-Water nanofluid saturated an inclined square Aluminium foam porous medium are presented and discussed for the following governing parameters Rayleigh number R_T, nanoparticles volume fraction ϕ, inertila effect parameter G, inclination angle of the cavity γ and the porosity of the porous medium and ε. In addition, for the seconde case the results of the natural convection of SWCNT-Water and Al_2O_3-Water saturated a tilted rectangular porous medium subjected an external magnetic filed have been presented and discussed for the following governing parameters Rayleigh number R_T, nanoparticles volume fraction ϕ, inertial effect parameter G, Hartmann number Ha, inclination angle of the cavity γ and the inclination angle of magnetic field ξ.

4.1. First application : Cu-Water nanofluid saturated Aluminium foam porous medium without magnetic field effect

The aim of the present work is to analyse the heat transfer performances of nanofluid (Cu-Water) saturated an inclined highly conductive porous medium (aluminium foam) by investigating the relationship among the Rayleigh number R_T, nanoparticles volume fraction ϕ, inertial effect parameter G, inclination angle γ, and the porosity of porous medium ε. The numerical results reported in this study cover the ranges $0 \le R_T \le 200$, $0 \le \phi \le 0.10$, $10^{-3} \le G \le 10$, $-90° \le \gamma \le 90°$ and $0.3 \le \varepsilon \le 0.8$.

The grid sizes are tested from 60×60 to 400×400. Table. 4.1 shows the effect of the mesh size on the average Nusselt number of both hot and cold walls and the maximum absolute value of the maximum absolute value of stream function. It is found that the 200×200 grid is sufficiently enough to resolve the equations system.

In order to prove the accuracy of the code, a comparison analysis has been performed by comparing the numerical results with previous works. First, the results are tested through the streamlines trajectories of **"Sheremet et al. (2015),"** see Figure. 4.1. This comparison shows that the streamlines are so consistent, and the difference between the $|\psi|_{max}$ values is due to the numerical method used and the different convergence criteria during the solving process.

Grid size	$\lvert\psi\rvert_{max}$	$\overline{Nu}_L$	$\overline{Nu}_R$	$\Delta = \frac{\lvert\Psi_{i,j} - \Psi_{400\times400}\rvert}{\lvert\Psi_{400\times400}\rvert}\times100\%$ $\lvert\psi\rvert_{max}$	$\Delta = \frac{\lvert\overline{Nu}_{L\,i,j} - \overline{Nu}_{L\,200,200}\rvert}{\overline{Nu}_{L\,200,200}}\times100\%$ $\overline{Nu}_L$
60x60	18.539	816 .66	816 .66	0.97	4.3
100x100	18.637	845.40	845.40	0.47	0.94
150x150	18.683	852.66	852.66	0.20	0.09
200x200	18.702	853.42	853.42	0.10	--
250x250	18.711	852.75	852.75	0.05	0.07
300x300	18.717	851.81	851,81	0.02	0.18
400x400	18.722	850. 30	850. 30	--	0.36

Table 4.1. Variations of the average Nusselt number of hot wall , cold wall and the maximum absolute value of stream function with different grid sizes (Cu water nanofluid-Aluminium foam as solid matrix of porous medium $R_T = 1000$, $\phi = 0.05$, $\varepsilon = 0.8$, $\gamma = 0°$, $G = 0$).

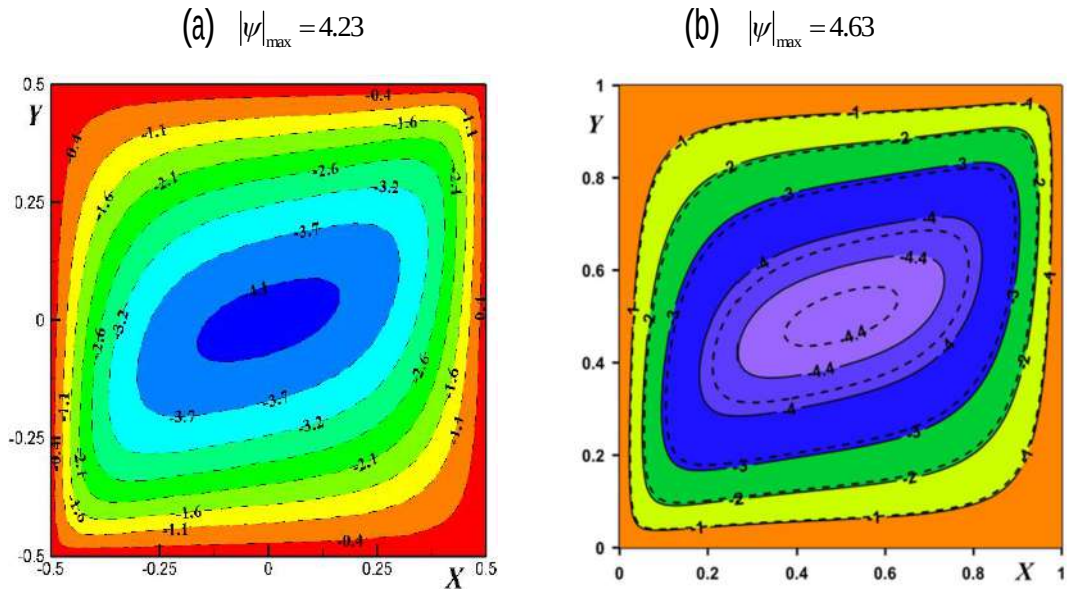


Figure.4.1. Comparison between the present results (a) and **"Sheremet et al. (2015),"** (b) at $\phi = 0.05$, $\varepsilon = 0.5$, $G = 0$, $R_T = 100$, $\gamma = 0°$ and the aluminium foam as the solid matrix of the porous medium.

The second test was done by examining the accuracy of present results via the maximum absolute value of stream function and the average Nusselt number of **"Nawaf and Pop (2005),"** see Table 4.2. The table clearly shows that the implemented code produces reasonably accepted results compared to **"Nawaf and Pop (2005)."** The completion of the above two tests gives

courage to further extend the present numerical code, which is reported in the forthcoming section.

Inertial effect parameter	Present results						"Nawaf et Pop (2005),"	
	100 x 100		200 x 200		300 x 300		42×42	
G	$\overline{Nu}_L$	$\lvert\psi\rvert_{max}$	$\overline{Nu}_L$	$\lvert\psi\rvert_{max}$	$\overline{Nu}_L$	$\lvert\psi\rvert_{max}$	$\overline{Nu}_L$	$\lvert\psi\rvert_{max}$
0	13.585	20.373	13.773	20.457	13.758	20.476	13.442	20.489
0.1	4.841	8.054	4.822	8.052	4.818	8.052	4.732	7.993
10	1.322	1.744	1.321	1.712	1.321	1.706	1.295	1.652

Table 4.2. Effect of the inertial effects parameter G on the average Nusselt number and the maximum absolute value of stream function for $R_T = 10^3$, $\phi = 0$ and $\gamma = 0°$

By taking the following key parameters $R_T = 200, \phi = 0.05$, $\varepsilon = 0.5$, $\gamma = 0°$ and the aluminium foam as the solid matrix of porous medium, the effect of inertial parameter G on the flow field (streamlines) and the thermal field (isotherms) of nanofluid is shown in Fig.4.2.

(a) $G=10^{-3}$ (b) $G=1$ (c) $G=10$

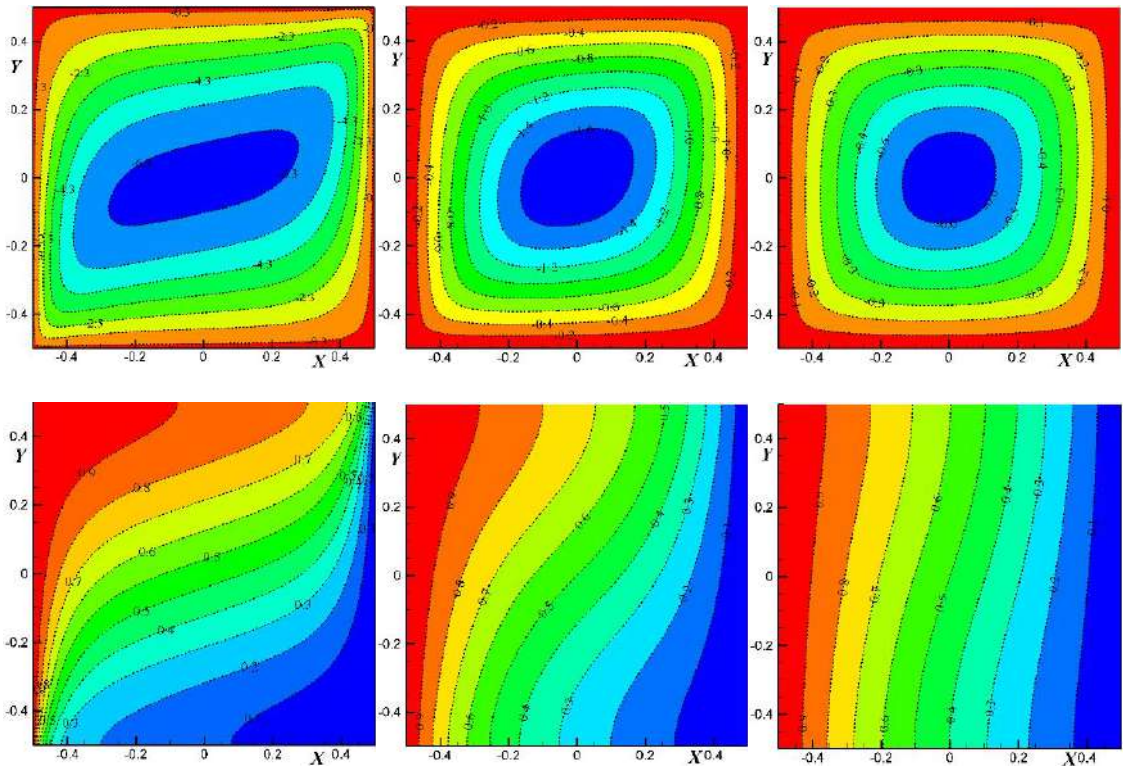


Figure 4.2. Streamlines (upper) and isotherms (lower) for $R_T = 200$, $\phi = 0.05$, $\varepsilon = 0.5$, $\gamma = 0°$

In addition, isotherms have a tendency to have parallel lines at the upper left and lower right corners, and the boundary layers become less significant. The heat transfer by conduction mode

is dominated for high values of inertial parameter, whereas the convection mode is dominated for low values ($\overline{Nu}_L^{\,G=10^{-3}} = 729.85 > \overline{Nu}_L^{\,G=1} = 230.25 > \overline{Nu}_L^{\,G=10} = 176.75$). These results are confirmed in Figure. 4.3 by taking a constant Rayleigh number.

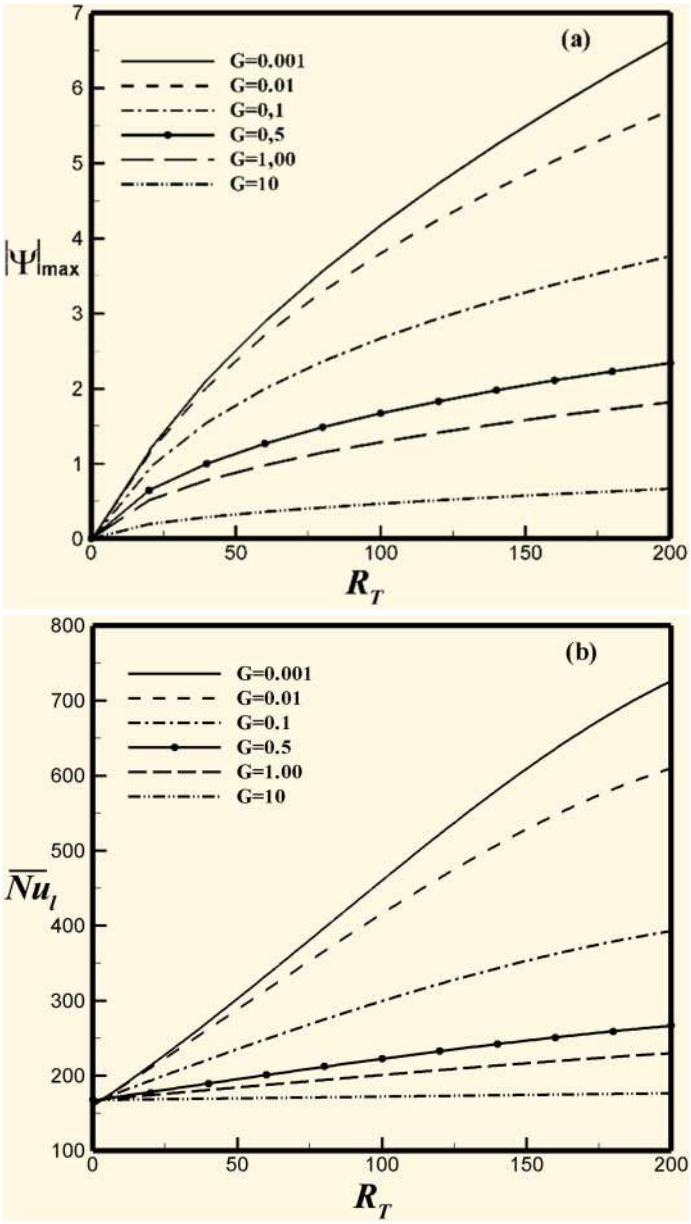


Figure.4.3. Variation of the maximum absolute stream function (a) and the average left Nusselt number (b) with the Rayleigh number for $\phi = 0.05$, $\varepsilon = 0.5$, $\gamma = 0°$ and different values of inertial effects parameter G.

Figure 4.3 displays the behaviour of the maximum absolute stream function, the average left Nusselt number with the Rayleigh number for different values of inertial effects parameter G at $\phi = 0.05$, $\varepsilon = 0.5$, $\gamma = 0°$ and the aluminium foam as the solid matrix of the porous

medium. The average Nusselt number is calculated along the left wall for different Rayleigh number and different non-Darcy term G (inertial effects parameter). It is clear that for a given Rayleigh number, the natural convection is inhibited with the increase of inertial parameter and reduces the average Nusselt number. Figure. 4.3 also demonstrates that the Rayleigh number has more effects on the average Nusselt number for low values of inertial effects parameter G compared to high values of this latter. No change is recorded in the average Nusselt number for the value of $G=1$ and 10 for all Rayleigh numbers (from 0 to 200), nor for the maximum absolute stream function, where the variation is insignificant. At those values of inertial effects parameter G ($G=1$ to 10), the heat transfer by conduction mode is dominated and the fluid is approximately stationary. In the absence of convection ($R_T=0$), the conduction mode is the only heat transfer mechanism, which is presented by the $|\psi|_{max}=0$ and $\overline{Nu}_L=167.79$ due to the high conductivity of porous matrix. By comparing this result with the work of **"Sheremet et al. (2015),"** we find in Figure. 4.3b for $R_T=100$, $G=0.001$, $\phi=0.05$, $\varepsilon=0.5$, $\gamma=0°$ and the aluminium foam as the solid matrix of the porous medium, that $\overline{Nu}_L\approx 480$, while in (Figure. 6a) of Sheremet work for $R_T=100$, $G=0$, $\phi=0.05$, $\varepsilon=0.5$ that $\overline{Nu}_L\approx 510$ the difference is due to the inertial effect parameter which is $G=0.001$ in our case.

The effect of nanoparticles volume fraction on the streamlines and isotherms is presented in Figure. 4.4. It has to be mentioned that nanoparticles volume fraction ϕ is a crucial parameter in the studies of heat transfer using nanofluid, and it is the main parameter, which is used to evaluate the heat transfer performances of nanofluid.

Figure.4.4 illustrates the variation of streamlines and isotherms for Cu- Water nanofluid under different values of ϕ for $R_T=200$, $G=0.5$, $\varepsilon=0.5$, $\gamma=0°$ and aluminium foam as the solid matrix of the porous medium.

It is shown that the increase of nanoparticles from 0% (pure water) to 10% does not lead to significant changes in the streamlines and isotherms of the nanofluid saturated porous medium. By checking the maximum absolute values of stream function and the average Nusselt number

we find: $|\psi|_{max}^{\phi=0\%} = 2.696 > |\psi|_{max}^{\phi=5\%} = 2.340 > |\psi|_{max}^{\phi=8\%} = 2.176 > |\psi|_{max}^{\phi=10\%} = 2.080$ and $\overline{Nu}_L{}^{\phi=0\%} = 294.21 > \overline{Nu}_L{}^{\phi=5\%} = 266.98 > \overline{Nu}_L{}^{\phi=8\%} = 255.23 > \overline{Nu}_L{}^{\phi=10\%} = 248.68$.

(a) ϕ=0.05 (b) ϕ=0.08 (c) ϕ=0.10

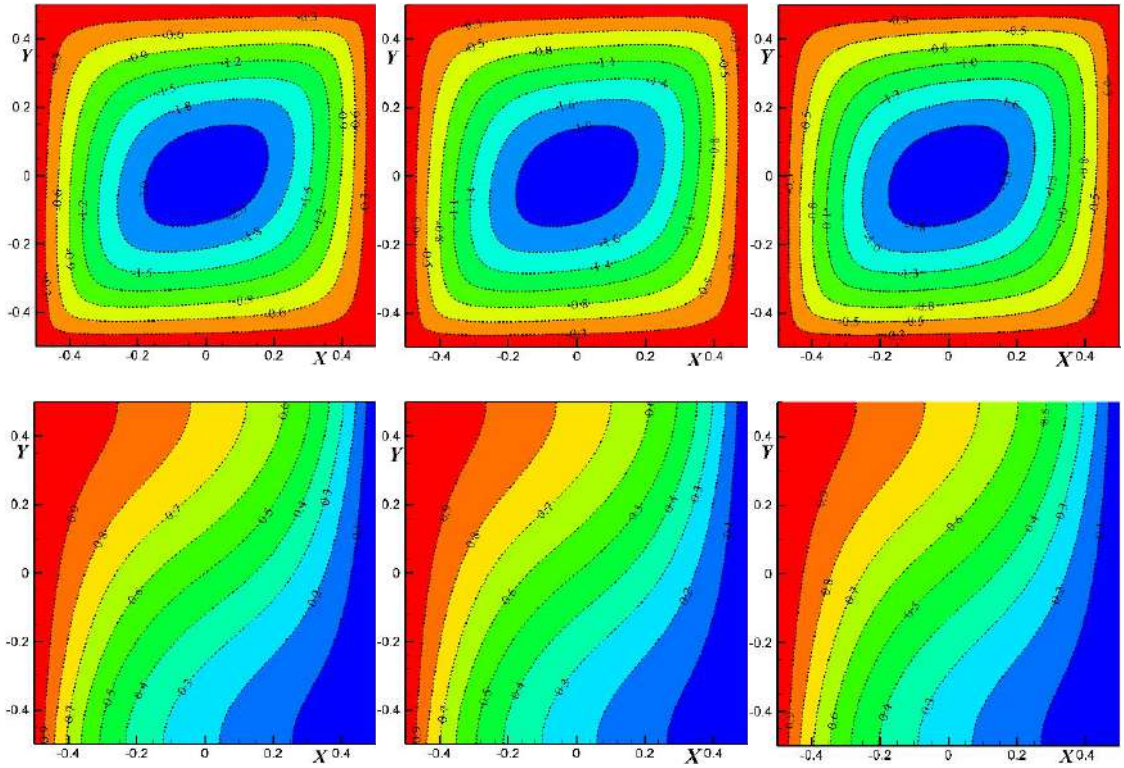


Figure.4.4. Streamlines (upper) and isotherms (lower) for $R_T = 200$, $G = 0.5$, $\varepsilon = 0.5$ and $\gamma = 0°$.

In order to emphasize on the effect of nanoparticles percentage on the heat transfer of the nanofluid saturated porous medium, the previous analysis was extended to show the variation of flow and thermal fields under the effect of Rayleigh number, which is presented in Figure. 4.5. The figure represents the behaviour of maximum absolute value of stream function and the average Nusselt number as a function of the Rayleigh number for different nanoparticles volume fractions. The results are reported for four nanoparticles percentages $\phi = 0$ (pure fluid), 0.05, 0.08 and 0.1. As seen for $R_T = 0$, the heat transfer mechanism is the conduction mode only via the high conductive porous medium ($|\psi|_{max} = 0$ and $\overline{Nu}_L = 167.79$).

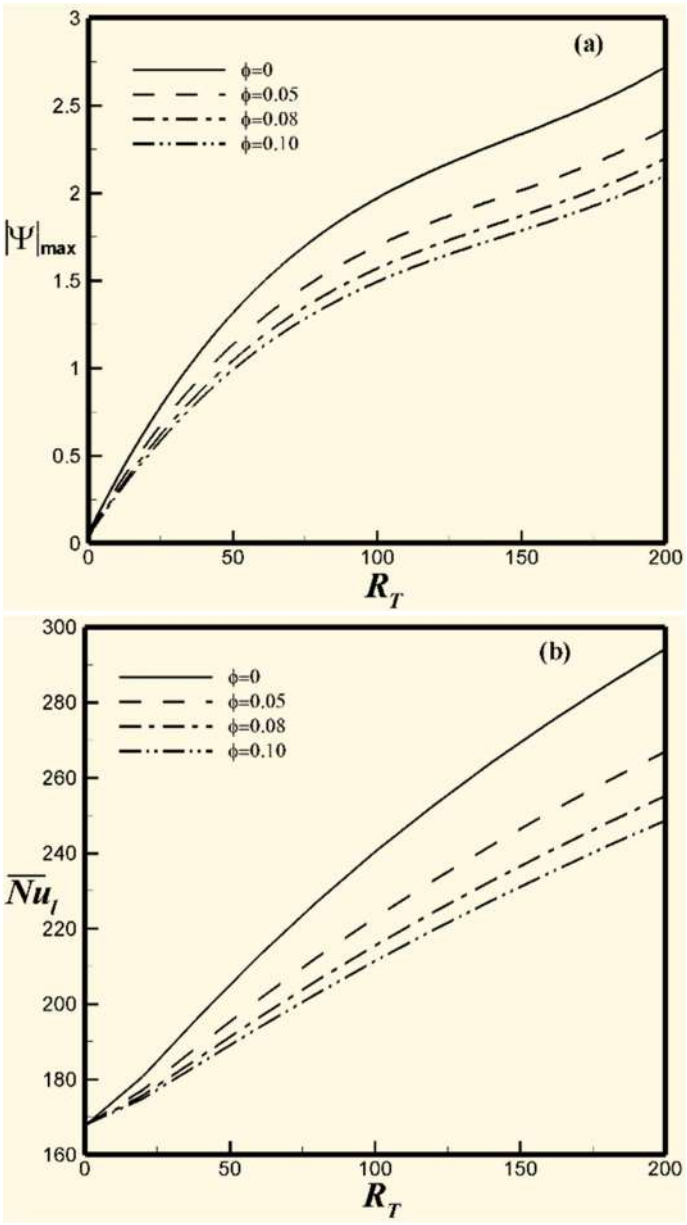


Figure. 4.5. Variation of the maximum absolute stream function (a) and the average left Nusselt number (b) for $G = 0.5$, $\varepsilon = 0.5$, $\gamma = 0°$ with the Rayleigh number, R_T, and different values of nanoparticles volume fraction, ϕ.

After that, the higher ϕ is, the lower are the maximum absolute value of stream function and the average Nusselt number values for a given Rayleigh number, meaning that the heat transfer efficiency decreases with the increase of nanoparticles percentage. In addition, it is clear that the decreasing rate increases with the increase of Rayleigh number.

The decrease of convection heat transfer with the increase of nanoparticles volume fraction is due to the enhancement of the thermal conductivity of nanofluid compared to the base fluid

because the presence of nanoparticles is associated with an increase in the nanofluid viscosity. The increase of the viscosity causes the nanofluid velocity to decrease and results in a decrease of convection heat transfer inside the cavity. Furthermore, the decrease in convection heat transfer due to the increase of nanofluid viscosity is more important compared to the heat transfer enhancement because of the presence of nanoparticles. It has to be mentioned that these results are in a good agreement with the work of **"Ghalambaz et al. (2015)."**

Figure 4.6 reveals the effect of the porous medium porosity on the flow and thermal fields of the Cu-Water nanofluid saturated the porous medium.

(a) ε = 0.3 (b) ε = 0.5 (c) ε = 0.8

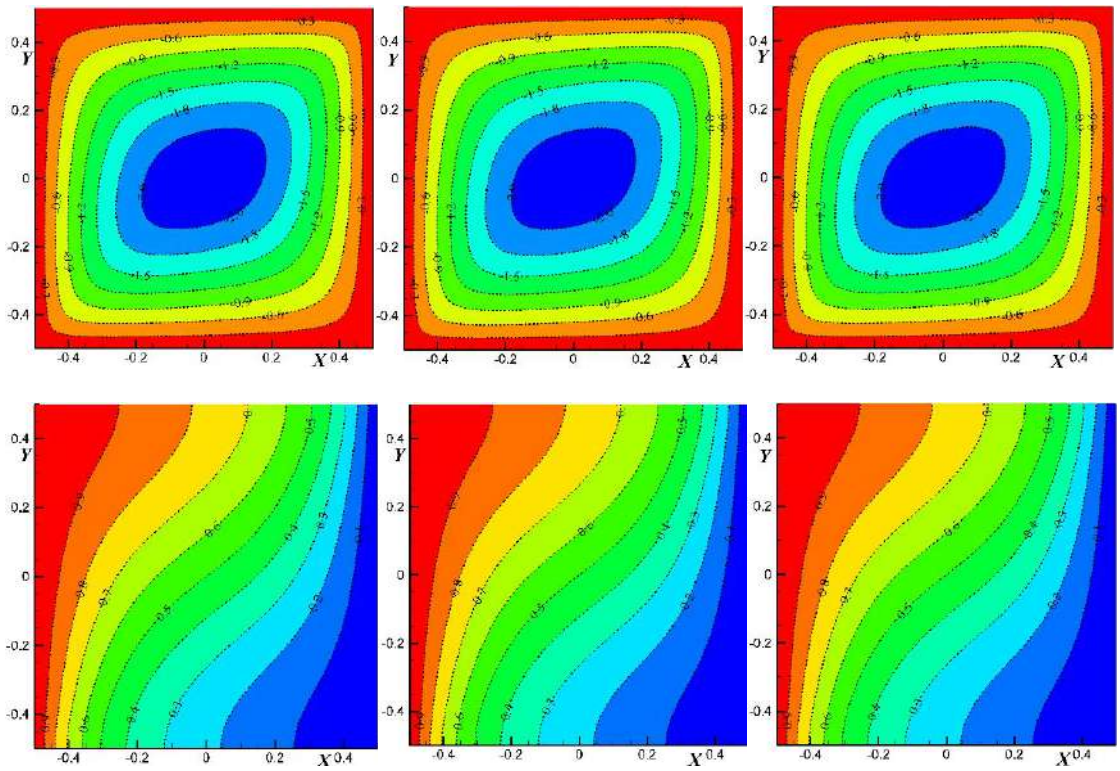


Figure. 4.6. Streamlines (upper) and isotherms (lower) for $R_T = 200, G = 0.5, \phi = 0.05$ and $\gamma = 0°$.

The streamlines and isotherms are presented for three values of porosity; $\varepsilon = 0.3$, 0.5 and 0.8 for $R_T = 200$, $G = 0.5$, $\phi = 0.05$ and $\gamma = 0°$.

As seen in this figure, no noticeable change is recorded among the three values of porosity on the streamlines and isotherms. This result is in accordance with that of **"Sheremet et al. (2015),"**

Figure.4. Even in their case, the inertial effect it is not taken into consideration $G = 0$ (Darcy flow).

But by comparing the maximum absolute values of stream function and the average Nusselt number values we find: $|\psi|_{max}^{\varepsilon=0.3} = 2.341 > |\psi|_{max}^{\varepsilon=0.5} = 2.340 > |\psi|_{max}^{\varepsilon=0.8} = 2.338$ and $\overline{Nu}_L{}^{\varepsilon=0.3} = 373.09 > \overline{Nu}_L{}^{\varepsilon=0.5} = 266.98 > \overline{Nu}_L{}^{\varepsilon=0.8} = 107.82$, meaning that there is a negligible change on the nanofluid flow inside the cavity, but there is a decrease on the efficiency of convection heat transfer with an increase on the porosity.

To shed light on this point, Figure. 4.7 demonstrates the effect of porosity on the maximum absolute values of stream function and the average Nusselt number with the variation of Rayleigh number.

As seen, there is an increase on the maximum absolute stream function and average Nusselt number with the increase of Rayleigh number. However, for a given Rayleigh number, no change in the nanofluid flow behaviour recorded with the variation of porosity (expressed by the maximum absolute stream function), taking into account the effect of inertia, where $G = 0.5$. In addition, despite the fact that there is no change in the fluid behaviour with increasing porosity at constant Rayleigh number, a significant decrease in the average Nusselt number is recorded. This can be explained by the fact that the strength of heat transfer between the left wall (hot) and right wall (cold) is dominated by the high thermal conductivity of porous matrix compared to the mechanism of convection heat transfer by the nanofluid (the thermal conductivity of Cu-Water nanofluid is lower than that of porous matrix).

The increase of porosity means an increase of the void space in the cavity, which is occupied by the nanofluid; and due to the high thermal conductivity difference between the porous matrix and the nanofluid, this exchange results in a decrease in the overall thermal conductivity of the cavity (nanofluid saturated the porous matrix).

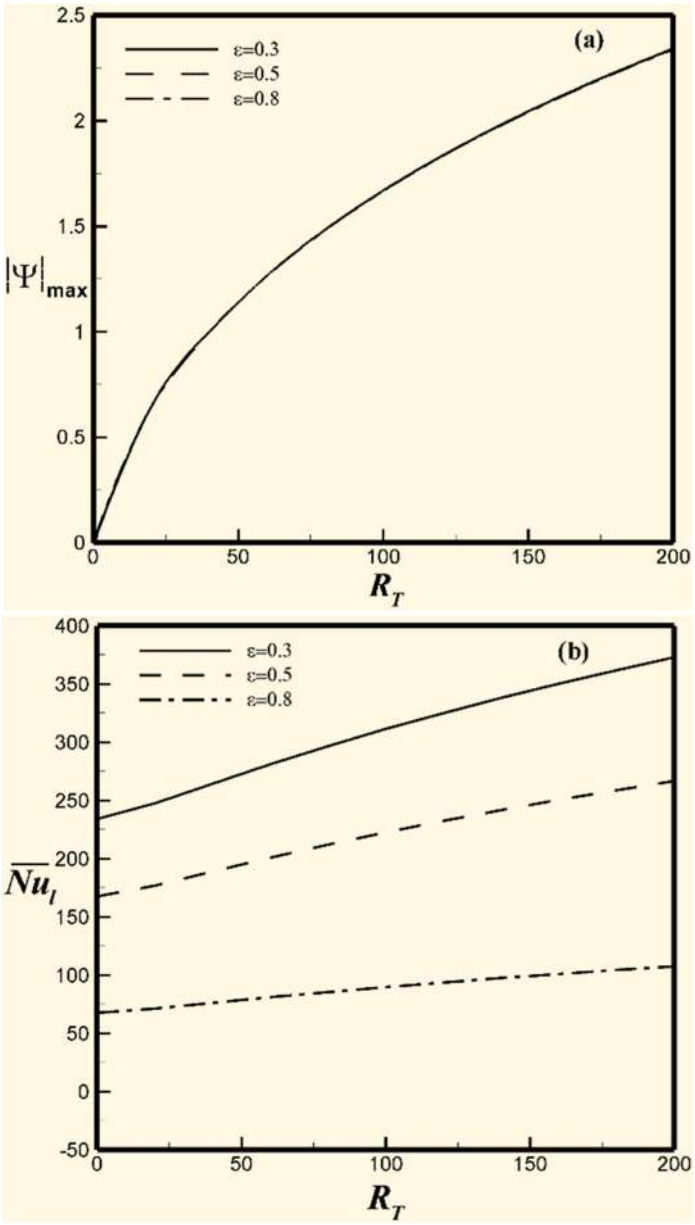


Figure. 4.7. Variation of the maximum absolute stream function (a) and the average left Nusselt number (b) with the Rayleigh number for $G = 0.5$, $\phi = 0.05$, $\gamma = 0°$ and different values of porosity ε.

Figure 4.8 illustrates the effect of inertial parameter G on the flow field and thermal field for three values of porosity $\varepsilon = 0.3$, 0.5 and 0.8. This figure demonstrates that the porosity does not have an effect on flow field, but it has a significant effect on thermal field, which comply with the results mentioned previously in Figure. 4.7. In addition, the maximum absolute stream function decreases sharply with the increase of inertial parameter G until about the value of

$G = 2$, After that the decreasing rate continues slowly to $G = 4$, where it becomes insignificant from $G = 4$ to 10. Furthermore, the increase of inertial parameter G from 0 to 1 reduces quickly the average Nusselt number, and the noticeable effect of the inertial effect on departure from the Darcien flow can be seen. At this interval from $G = 1$ to 10, the effect of G becomes negligible for the three values of porosity.

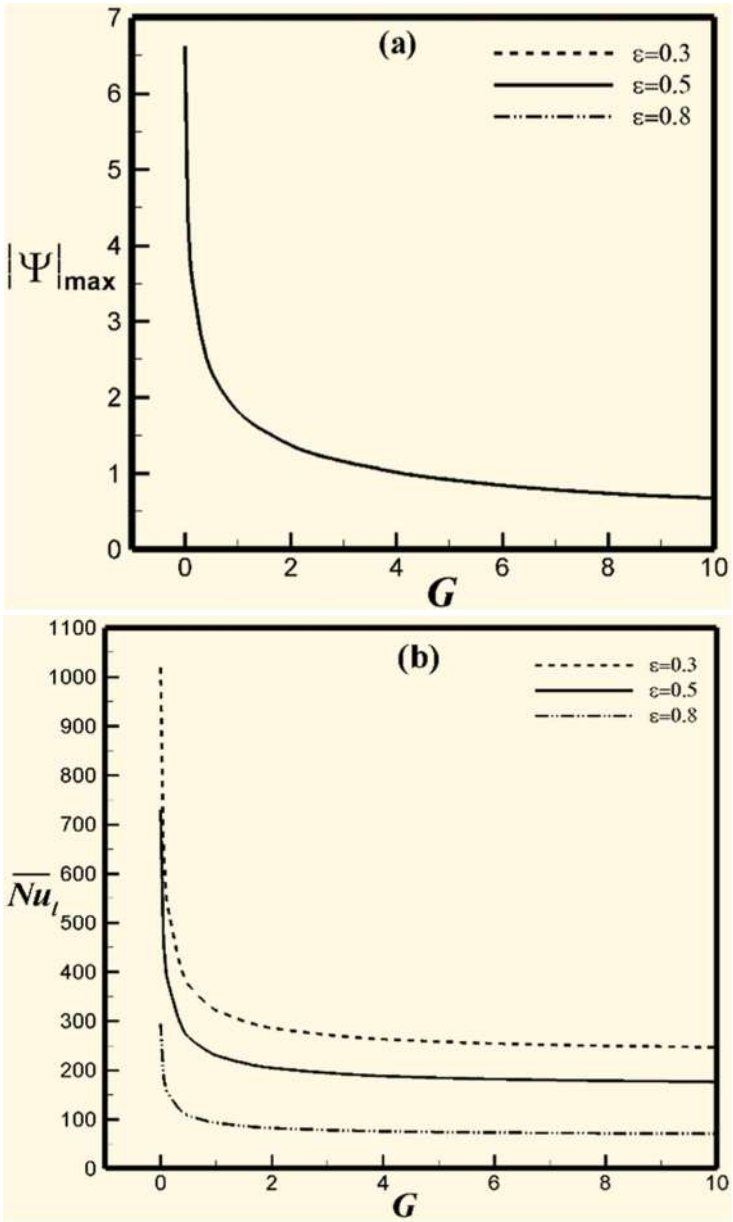


Figure.4.8. Dependence of the maximum absolute stream function (a) and the average left Nusselt number (b) on inertial effect parameter for $R_T = 200$, $\phi = 0.05$ and $\gamma = 0°$ and different porosity, ε.

For a constant value of inertial parameter G , the lower the porosity, the higher the Nusselt number, which is interpreted already by the strength of heat transfer dominated by the high thermal conductivity of porous matrix compared to the mechanism of convection heat transfer by the nanofluid.

The effect of inclination angle on the free convection heat transfer of nanofluid saturated porous medium is presented in Figure.4.9 in terms of streamlines and isotherms for the angles $\gamma = -45°$, $\gamma = 0°$ and $\gamma = 45°$ taking $R_T = 200$, $G = 0.5$, $\phi = 0.05$, $\varepsilon = 0.5$, the aluminium foam being the solid matrix of the porous medium. It is noticeable that a single circulation flow in the clockwise direction is formed inside the enclosure.

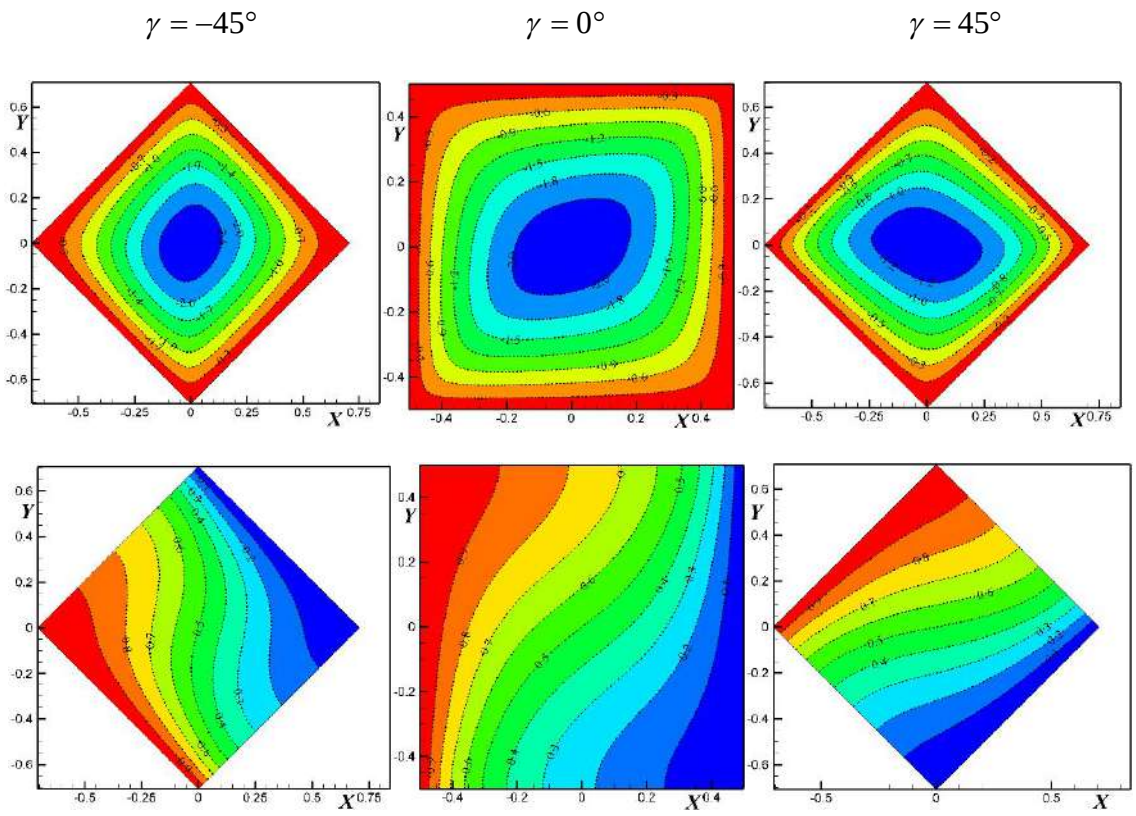


Figure.4.9. Streamlines (upper) and isotherms (lower) for $R_T = 200$, $G = 0.5$, $\phi = 0.05$, and $\varepsilon = 0.5$.

In addition, as the inclination angle shifts from -45° to 45°, the average Nusselt number decreases from 282.26 at -45° to a high value of 266.98 at 0°, and after that it decreases to

211.33 at 45°. This means that for the inclination angle of -45° a strong convection vortex is formed compared to the other angles.

To show more detail about the effect of inclination angle, Figure. 4.10 demonstrates the dependence of the flow and thermal fields on inclination angle γ for different inertial effect parameter G for $R_T = 200$, $\phi = 0.05$ and $\varepsilon = 0.5$.

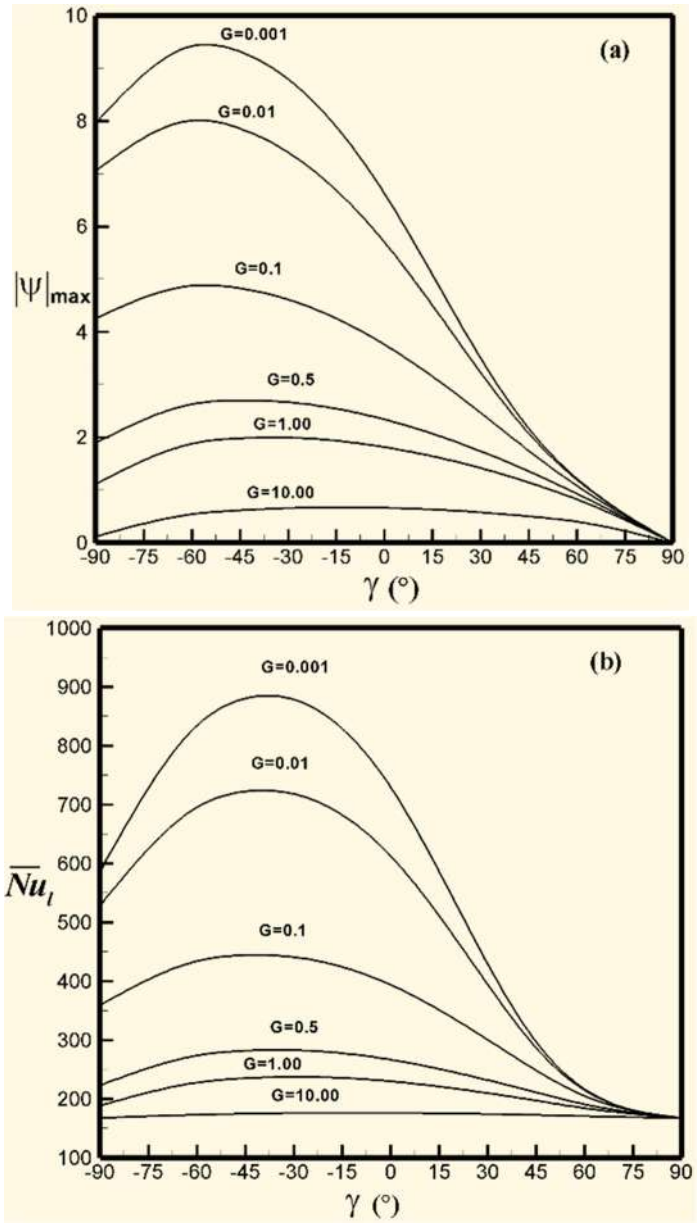


Figure.4.10. Dependence of the maximum absolute stream function (a) and the average left Nusselt number (b) on inclination angle γ for $R_T = 200$, $\phi = 0.05$, $\varepsilon = 0.5$ and different inertial effect parameter G .

As it can be seen, the inclination angle has a significant effect on the maximum absolute stream function and average Nusselt number for low values of inertial parameter ($G \leq 0.1$), and it has less impact for the inertial parameter of $G > 0.1$. In addition, for a given inertial parameter G , the increase of inclination angle increases both the maximum absolute value of stream function and the average Nusselt number to peak value. After that it decreases, except for the high values of G (about 10), where it has insignificant effect. Furthermore, the inclination of about -40° represents the angle for the peak values of average Nusselt number for a given inertial parameter G , which is the angle where the convection rate is maximum. With the increase of inclination angle beyond the peak angle, the average Nusselt number for different inertial parameter G values decreases for a single value $\overline{Nu}_L = 167.71$ at $\gamma = 90°$ where the cavity is heated from the top and the convection is vanished ($|\psi|_{max} = 0$), the heat transfer mechanism being the conduction mode.

The inclination angle effect on flow field and thermal field for a given nanoparticles volume percentage is presented in Figure. 4.11.

The graphs clearly illustrate that the inclination angle γ has a dominant effect on both the convection strength and the heat transfer rate. As the inclination angle γ increases from -90° to 90°, the average Nusselt number first increases to a peak value for a given nanoparticles volume fraction at $\gamma \approx 40°$ and after that it decreases to approximately to a fixed value which represents the pure conduction heat transfer mode. In addition, it is seen that as the nanoparticles volume fraction ϕ increases, the average Nusselt number decreases. What is noticeable is when the inclination angle approaches the value of $\gamma = 90°$, both the nanoparticles volume fraction ϕ and the average Nusselt number increase. To make this situation clear, Figure. 4.12 illustrates the average Nusselt number for $0 \leq R_T \leq 200$ and for nanoparticles volume fraction of $\phi = 0$, 0.05, 0.08 and 0.1 at the inclination angle of $\gamma = 90°$. This figure demonstrates that the Rayleigh number has no effect on the average Nusselt number due to the disappearing of convection at this angle, which represents the top heating of the cavity. In addition, the increase of nanoparticles volume fraction ϕ increases slightly the average Nusselt number and enhances the heat transfer. This is because of the enhancement of nanofluid thermal conductivity due to the increase of naopartciles volume fraction, which has an effect on the overall thermal conductivity of the cavity (nanofluid and porous matrix).

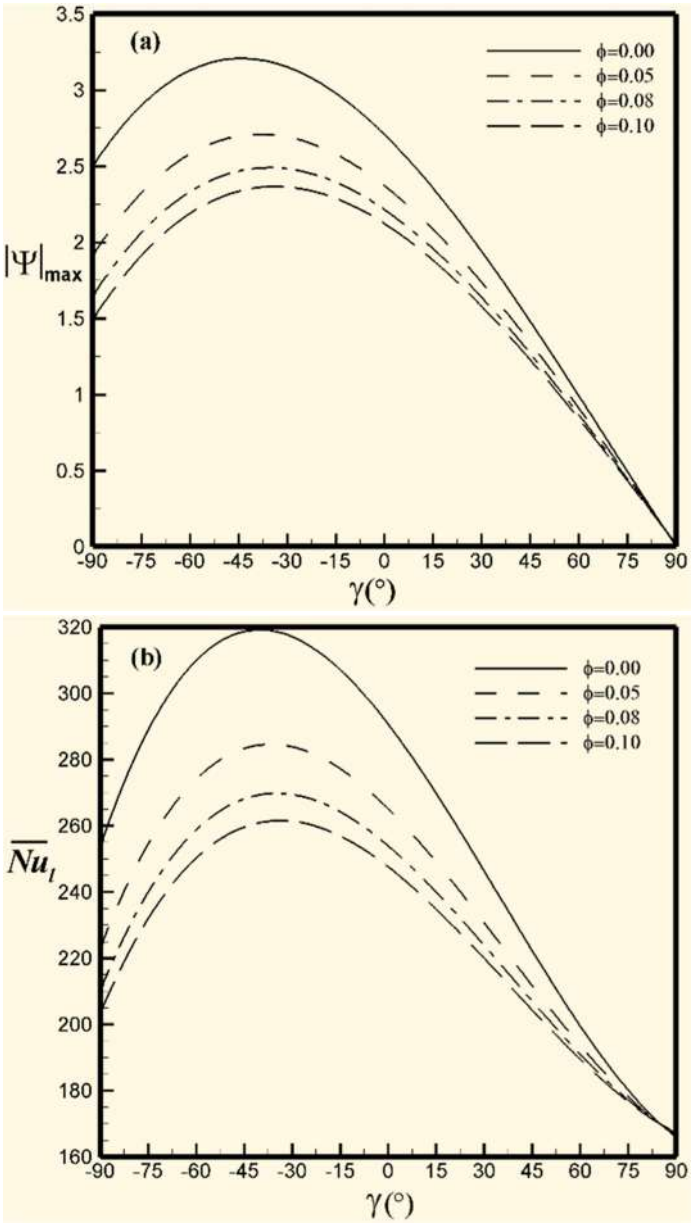


Figure.4.11. Dependence of the maximum absolute stream function (a) and the average left Nusselt number (b) on inclination angle γ for $R_T = 200$, $G = 0.5$, $\varepsilon = 0.5$ and different nanoparticles volume fraction ϕ.

Furthermore, with the disappearing of convection at this angle $\gamma = 90°$, the effect of dynamic viscosity vanishes, as previously seen concerning its effect on the heat transfer deterioration inside the enclosure with the increase of nanoparticles volume fraction ϕ.

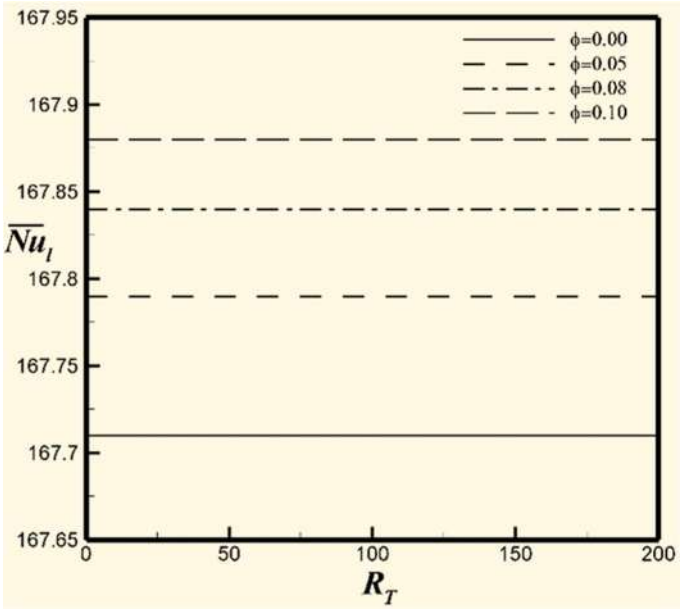


Figure 4.12. Variation of the average left Nusselt number with Rayleigh number for different values of nanoparticles volume fraction ϕ (G =0.5, ε =0.5, γ=90°).

Figure. 4.13 shows the effect of nanoparticles volume fraction on the maximum absolute value of stream function and average left Nusselt number for the porosity $\varepsilon = 0.3$, 0.5 and 0.8. As it can be noticed the increase of nanoparticles volume fraction ϕ decreases the convection strength (represented by the maximum absolute value of stream function) by the same rate for the three values of porosity $\varepsilon = 0.3$, 0.5 and 0.8, and for a given ϕ. The porosity does not have an effect on the convection rate. While for thermal field, for a given nanoparticles volume fraction ϕ, the higher ϕ is, the lower the average left Nusselt number becomes. In addition, for a given porosity, the increase of nanoparticles volume fraction decreases the average Nusselt number, and the reduction rate decreases with the increase of the porosity of porous medium. For example, it can be seen for $\varepsilon = 0.8$, that the nanoparticles volume fraction has approximately no effect on the average left Nusselt number. The reduction in the convection strength and the resulting heat transfer with the increase of nanoparticles volume fraction is caused by the increase of dynamic viscosity of nanofluid as a result of the presence of nanoparticles, which has a significant effect than the enhancement of the thermal conductivity. Also, the reduction in the heat transfer rate with the increase of porosity for a given nanoparticles volume fraction ϕ is due to the fact that the conduction mode is dominated for the heat transfer compared to the convection rate due the higth thermal conductivity of porous medium. The increase of the porosity of porous medium means an increase in void space, which

results in a decrease of the overall thermal conductivity, while the convection strength of nanofluid cannot overcome this reduction in the overall thermal conductivity of the enclosure.

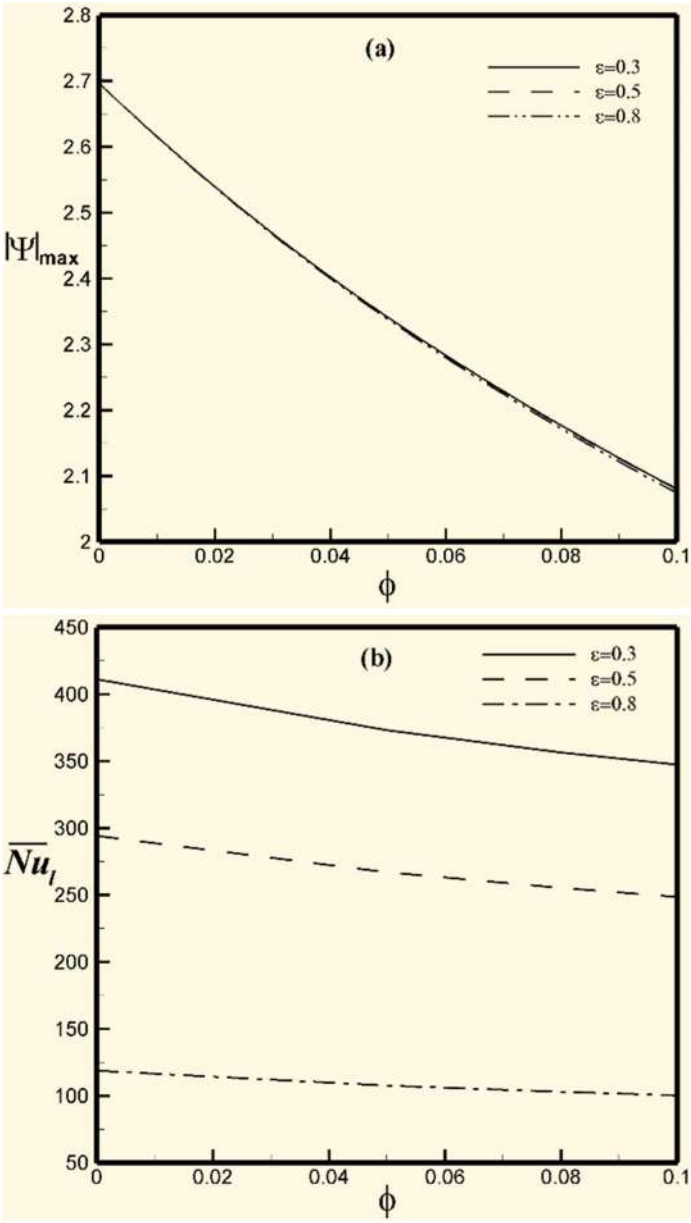


Figure.4.13. Dependence of the maximum absolute stream function (a) and the average left Nusselt number (b) on nanoparticles volume fraction for $R_T = 200$, $G = 0.5$, $\gamma = 0°$ and different porosity values ε.

Finally, Figure. 4.14 depicts nanoparticles volume fraction ϕ on the maximum absolute stream function and average Nusselt number for the given values of inertial parameter $G = 0.001$, 0.01, 0.1, 0.5, 1 and 10.

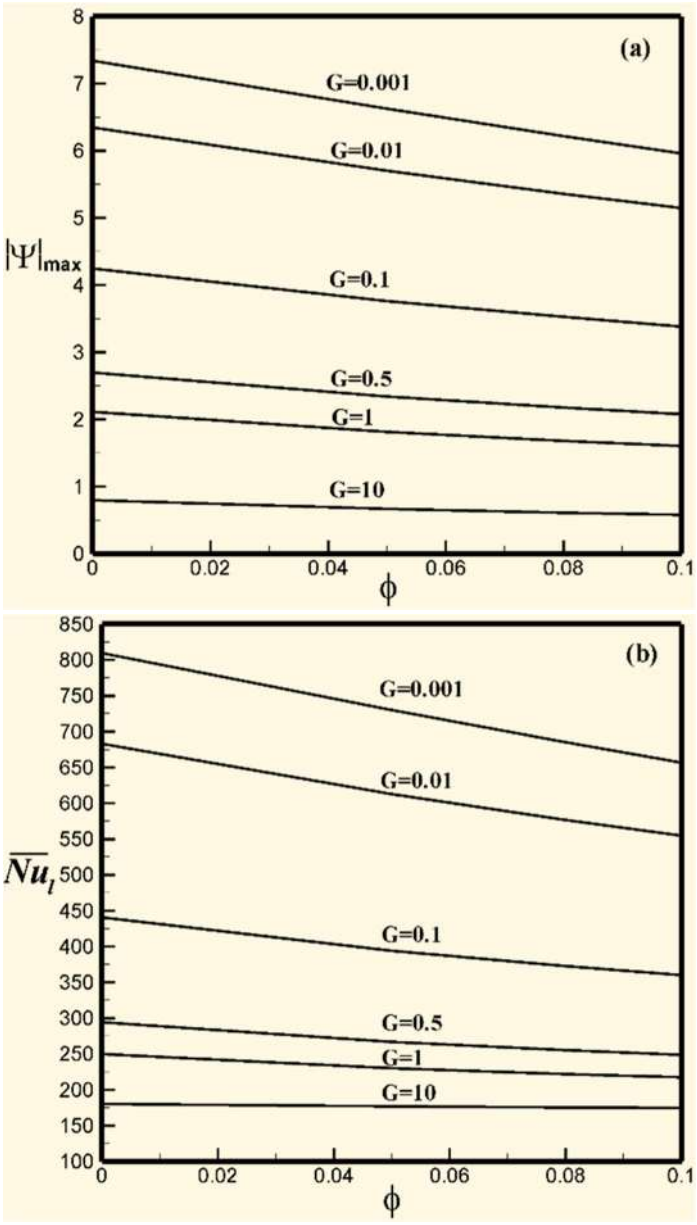


Figure.4.14. Dependence of the maximum absolute stream function (a) and the average left Nusselt number (b) on nanoparticles volume fraction for $R_T = 200$, $\varepsilon = 0.5$, $\gamma = 0°$ for different inertial parameter G .

It is shown that for the low values of inertial parameter G , the increase of nanoparticles volume fraction from 0 (pure fluid) to 10% decreases slightly both the maximum absolute stream function and average Nusselt number, while for high values, it has an insignificant effect. In

addition, the higher the inertial parameter is, the lower the flow and thermal fields strength become. For a given G , the increase of nanoparticles volume fraction weakens the flow and thermal rates due the increase of the dynamic viscosity that obstructs the flow and which results in a weak convection heat transfer (the enhancement of nanofluid thermal conductivity cannot overcome the effect of dynamic viscosity). Furthermore, for a high value of inertial parameter G from 1 to 10, the addition of more nanoparticles has no effect on both the flow and the thermal field, the fluid is at stagnation state, and the heat transfer is done by the conduction mode only (the porous medium matrix has a high thermal conductivity).

4.2 Second application : SWCNT-Water and Al_2O_3-Water nanofluid saturated porous medium with magnetic field effect

The grid sizes are tested from 60×60 to 400×400. Table 4.3 shows the effect of the mesh size on the average Nusselt number of the hot wall and the maximum absolute value of the stream function. It is found that the 200×200 grid is adequately enough to resolve the equations system, see Table 4.3.

Grid size	$\lvert\psi\rvert_{max}$	$\overline{Nu}_L$	$\Delta = \frac{\lvert\Psi_{i,j} - \Psi_{400\times400}\rvert}{\lvert\Psi_{400\times400}\rvert}\times100\%$ $\lvert\psi\rvert_{max}$	$\Delta = \frac{\lvert\overline{Nu}_{L\ i,j} - \overline{Nu}_{L\ 200,200}\rvert}{\overline{Nu}_{L\ 200,200}}\times100\%$ $\overline{Nu}_L$
60x60	2.7946	2.3594	--	--
100x100	2.7915	2.3592	0,11	0.008
150x150	2.7906	2.3592	0,14	0.008
200x200	2.7902	2.3592	0,15	0.008
250x250	2.7902	2.3592	0,15	0.008
300x300	2.7902	2.3592	0,15	0.008
400x400	2.7902	2.3592	0,15	0.008

Table 4.3. Variations of the average Nusselt number of hot wall and the maximum absolute value of stream function with different grid sizes ($R_T = 200$, $G = 0.5$, $\gamma = 0$, $\xi = 0$, $Ha = 0.5$, $\phi = 0.05$).

In order to ensure the accuracy of the obtained results, an analysis of three comparisons has been performed by comparing the numerical results with previous works. First, the results are tested by comparing the average Nusselt number with that given by different authors as shown in Table 4.4. The second test is done by examining the accuracy of present results via the

maximum absolute value of stream function and the average Nusselt number of **Nawaf and Pop (2005)**, see Table 4.5. The third test has been performed between the results of the present study and those reported by **Mahmud and Fraser (2004)**, which are presented in table 4.6 and Figure.4.15. The completion of the above three tests clearly show that the implemented code produces reasonably accepted and confident results and gives courage to further extend the present numerical code, which is reported in the forthcoming section.

Author	R_T		
	10	**10^2**	**10^3**
Walker and Homsy (1978)	-	3.097	12.96
Bejan (1979)	-	4.2	15.8
Beckermann et al. (1986)	-	3.113	-
Gross et al. (1986)	-	3.141	13.448
Moya et al. (1987)	1.065	2.801	-
Manole and Lage (1992)	-	3.118	13.637
Baytas and Pop (1999)	1.079	3.16	14,06
Present results	1.079	3.113	13.770

Table 4.4. Comparison of the average Nusselt number with previous numerical results for $G = 0$, $Ha = 0$, $\phi = 0$ and $\gamma = 0$.

Inertial effect parameter	Nawaf and Pop (2005)		Present results	
	42×42		200 x 200	
G	$\overline{Nu}_L$	$\lvert\psi\rvert_{max}$	$\overline{Nu}_L$	$\lvert\psi\rvert_{max}$
0	13.442	20.489	13.773	20.457
0.1	4.732	7.993	4.822	8.052
1	2.373	4.050	2.428	4.097
5	1.503	2.223	1.539	2.278
10	1.295	1.652	1.321	1.712

Table 4.5. Effect of the inertial effects parameter G on the average Nusselt number and the maximum absolute value of stream function for $R_T = 10^3$, $\phi = 0$, $Ha = 0$ and $\gamma = 0°$

		Mahmud and Fraser (2004)	Present results
R_T	Ha	Ψ_{max}	Ψ_{max}
	0	4.70727	4.70749
10^2	5	0.473645	0.473740
	10	0.123691	0.123702
	0	20.4897	20.4537
10^3	5	4.59179	4.59115
	10	1.2836	1.2837

Table 4.6. Comparison of the maximum value of stream function with the results of **Mahmud and Fraser (2004)** $\phi = 0$, $G = 0$, $\gamma = 180°$ $\xi = 90°$.

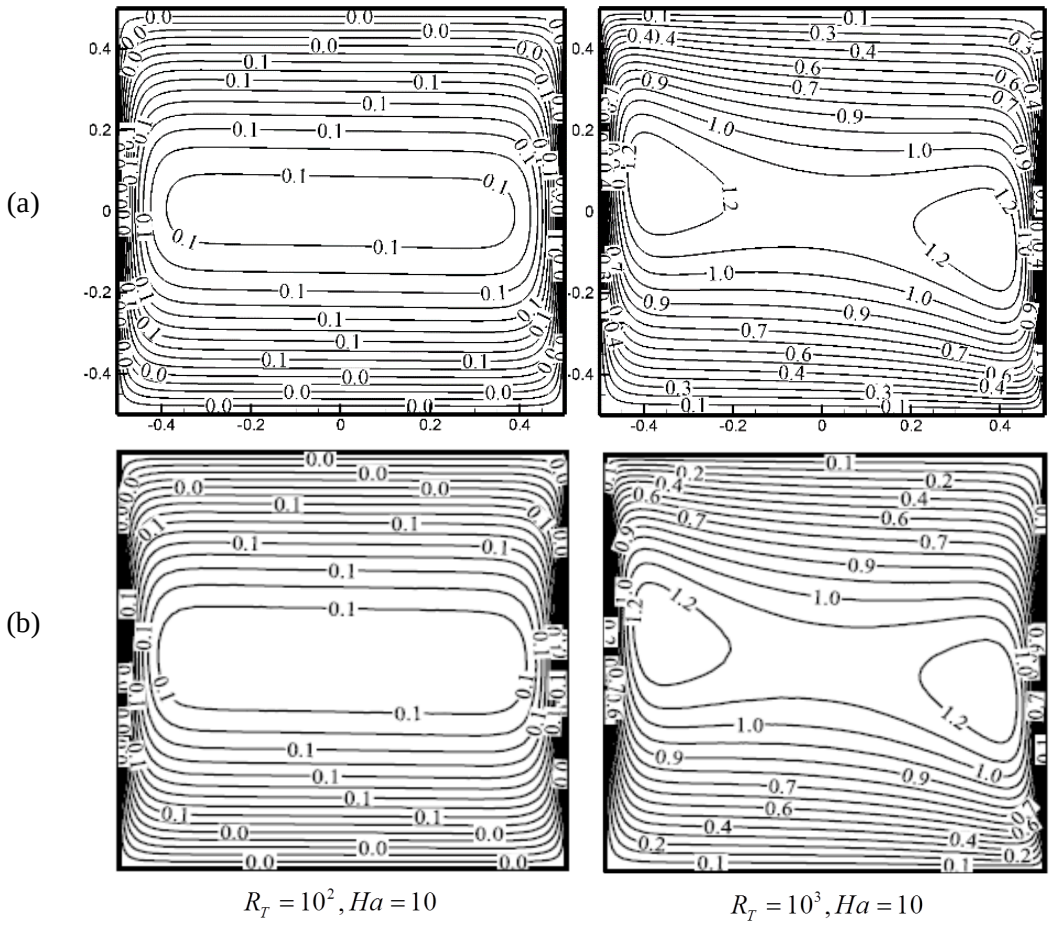


Figure. 4.15. Comparison between the present results (a) and **Mahmud and Fraser (2004)** (b) at $\phi = 0$, $G = 0$, $\gamma = 0°$ $\xi = -90°$.

The aim of the present work is to investigate the heat transfer performance of a nanofluid (SWCNT-water) in an inclined saturated porous medium under the effect of a magnetic field by investigating the relationship among the Rayleigh number R_T, nanoparticles volume fraction ϕ, inertial effect parameter G, inclination angle γ, Hartmann number Ha and the inclination angle of magnetic field ξ. The numerical results reported in this study cover the ranges $0 \le R_T \le 200$, $0 \le \phi \le 0.10$, $10^{-3} \le G \le 10$, $-90° \le \gamma \le 90°$, $0 \le Ha \le 10$ and $0 \le \xi \le 180$.

The effect of the presence of nanoparticles on the flow and thermal fields is shown in Figure.4.16 taking the three values: $\phi = 0$, $\phi = 0.05$ and $\phi = 0.10$ for the following parameters $R_T = 200, G = 0.5$, $Ha = 0.5$, $\gamma = 0°$ and $\xi = 0°$

Regardless of the volume fraction of nanoparticles, a single clockwise circulating cell is formed inside the cavity. With the increase of nanoparticles volume fraction, a weak change is noticed in the streamlines, and for the isotherms, they tend to have parallel lines at the lower right the upper left corners. By comparing the average Nusselt number for the three cases we find $\overline{Nu}_L{}^{\phi=0} = 1.739 < \overline{Nu}_L{}^{\phi=0.05} = 2.359 < \overline{Nu}_L{}^{\phi=0.10} = 3.177$, which means that there is an enhancement of heat transfer with the addition of nanoparticles.

The behaviour of maximum absolute stream function and the average Nusselt number with the Rayleigh number at different values of nanoparticles volume fraction at $G = 0$, $Ha = 0$, $\gamma = 0°$ and $\xi = 0°$ are presented in Figure.4.17 for the SWCNT and AL_2O_3 nanofluids.

This figure demonstrates that the convection mode for SWCNT becomes important with the increase of the Rayleigh number for all values of the nanoparticles volume fraction. In addition, it noticeable that for a Rayleigh number less than 100, the increase of nanoparticles volume fraction decreases the maximum absolute stream function and increases significantly the average Nusselt number.

The decrease of the maximum absolute stream function can be attributed to the dynamic viscosity increase due to the presence of nanoparticles, while the increase of Nusselt number attributed to the noticeable enhancement of thermal conductivity. It can be concluded that the conduction mode is more dominant compared to the free convection at the Rayleigh number less than 100.

$\phi = 0.00$ $\phi = 0.05$ $\phi = 0.10$

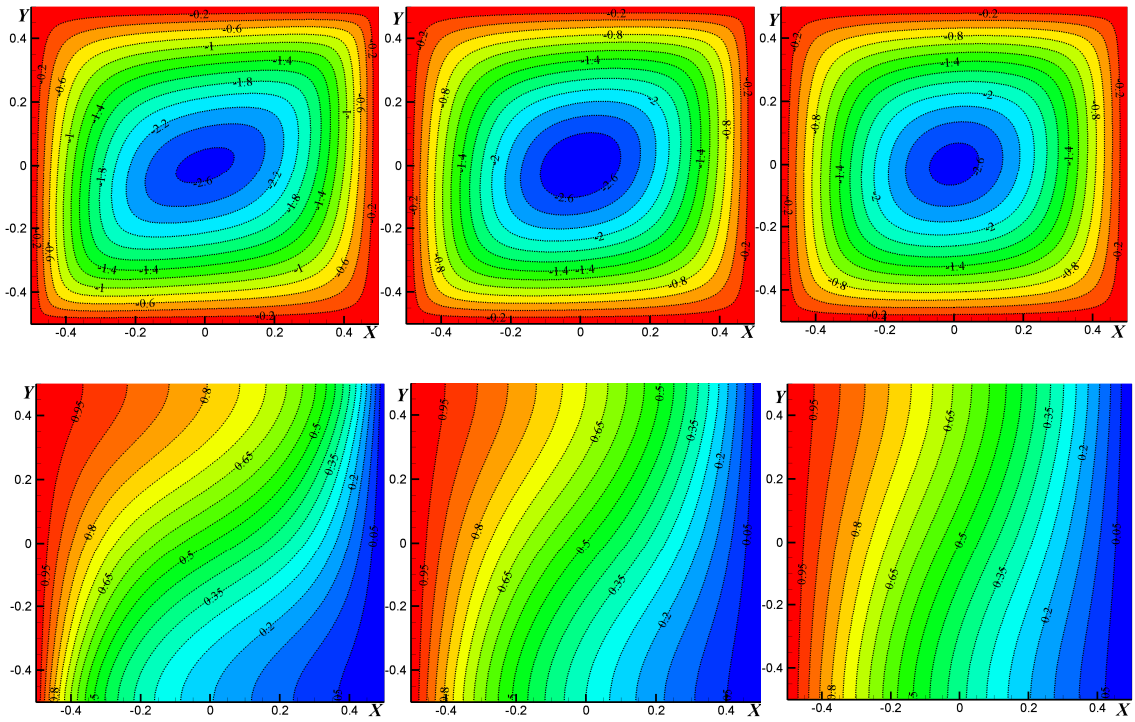


Figure. 4.16. Streamlines (upper) and isotherms (lower) for SWCNT at $R_T = 200$, $G = 0.5$ $Ha = 0.5$. $\gamma = 0^\circ$. $\xi = 0^\circ$.

For Rayleigh number more than 100, the convection mode become important, but the addition of more nanoparticles become less significant for the heat transfer enhancement by approaching the value 200 due to the increase of dynamic viscosity. This significant increase in dynamic viscosity for Carbon nanotubes has been recorded in the experimental work of **Harish et al. (2012) and Estellé et al. (2015).**

For the AL_2O_3 nanofluid, the fluid velocity and the convection rate increase by increasing the Rayleigh number. In addition, the increase of nanoparticles volume fraction increases the heat transfer for Rayleigh number less than 40, more than that the addition of more nanoparticles of AL_2O_3 nanofluid has a reverse effect on the heat transfer rate. This situation is due to the fact that for low Rayleigh number, by addition more AL_2O_3 nanoparticles, the effect of enhanced thermal conductivity overcomes the effect of the increased dynamic viscosity, but for high Rayleigh number, the increased dynamic viscosity effect overcomes the enhancement effect of the thermal conductivity which reduces the thermal convection rate. The reduction of

convection rate by increasing the nanoparticles concentration of AL2O3 has been noticed in several papers such as the work of **Mehryan et al. (2017)**.

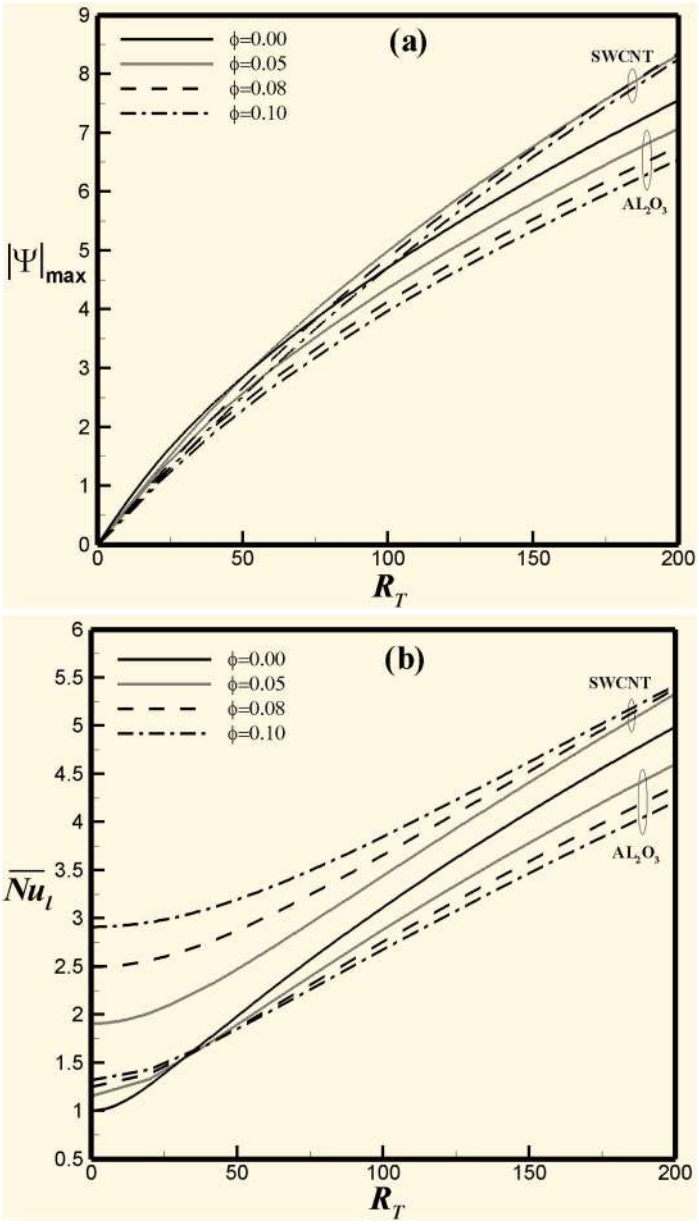


Figure. 4.17. Variation of the maximum absolute stream function (a) and the average left Nusselt number (b) with the Rayleigh number, R_T , and different values of nanoparticles volume fraction, ϕ at $G = 0$, $Ha = 0$, $\gamma = 0°$, $\xi = 0°$

The average Nusselt number ration $\overline{Nu}_L / \overline{Nu}_{L\,\phi=0.00}$ is plotted as a function of Rayleigh number for different nanoparticles volume fraction of SWCNT and AL_2O_3 in Figure 4.18. The results show for SWCNT water nanofluid that the enhancement of heat transfer by increasing the nanoparticles rate is higher for a low Rayleigh number where the conduction mode is dominant

and the enhancement in thermal conductivity of the nanofluid is significant. However, by increasing the Rayleigh number, the enhancement of heat transfer decreases to a fixed value, but is still above the value of 1.00 which represent the pure fluid case. The addition of more nanoparticles to the base fluid become insignificant for high Rayleigh number which explained by the important increase in the nanofluid dynamic viscosity due to the presence of nanoparticles. However, for the AL_2O_3 water nanofluid, the increase in Rayleigh number reduces the ration $\overline{Nu}_L / \overline{Nu}_{L\,\phi=0.00}$, which means that the enhancement in heat transfer rate due to the presence of nanofluid decreases with the increase of Rayleigh number, this decrease is attributed to the increase in dynamic viscosity because of the presence of nanoparticles. What is more is that for Rayleigh number at about 40, the heat transfer rate decreases below than that of base fluid. For the AL_2O_3 water naofluid, with the increase of Rayleigh number, the increase of dynamic viscosity due to the presence of nanoparticles overcomes the effect of increased thermal conductivity on the heat transfer inside the porous medium decreases.

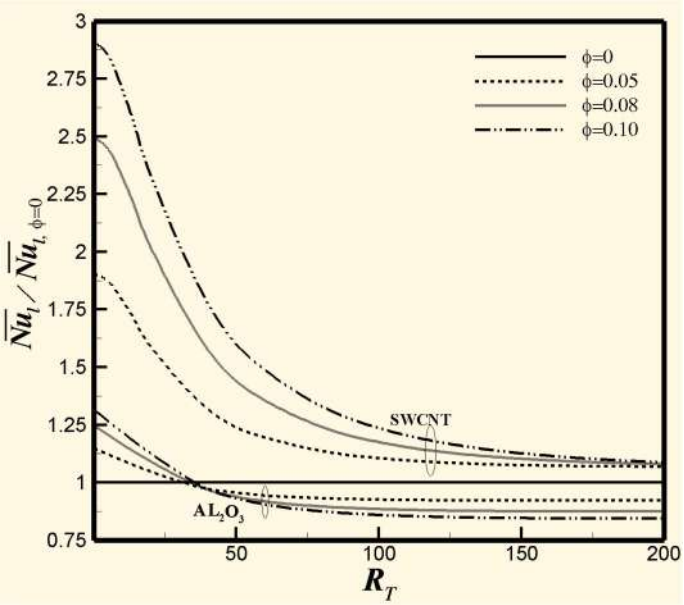


Figure. 4.18. Variation of average Nusselt number ration with Rayleigh number for different nanoparticles volume fraction at $G=0$, $Ha=0$, $\gamma=0°$, $\xi=0°$

Figures 4.19 and 4.20 present the dependency of the streamlines and isotherms on the inertial effect parameter G and Hartmann number Ha at $R_T=200$, $\phi=0.05$, $\gamma=0$ and $\xi=0$ respectively.

For the case of $G=0$ and $Ha=0$ a clockwise circulating cell is formed inside the cavity and a convection current is established. As the Hartmann number increases, the Lorentz force

increases and leads to a decrease in the flow strength. The Lorentz force, which is perpendicular to the buoyancy forces retards the motion of the nanofluid saturated the porous medium, and a significant percentage of the nanofluid inside the middle of the porous medium becomes stationary.

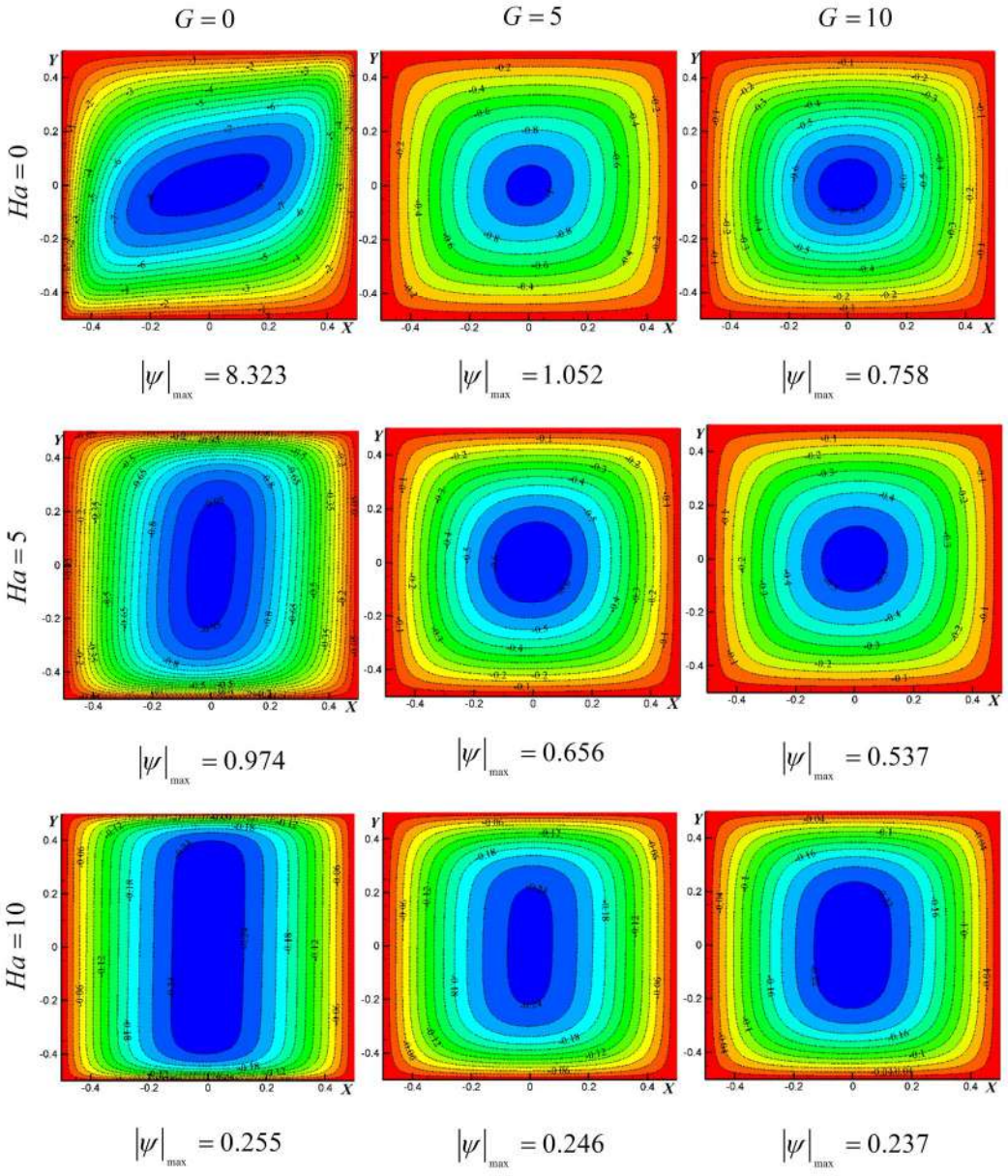


Figure.4.19. Streamlines for different values of G and Ha for SWCNT at $R_T = 200$, $\phi = 0.05$, $\gamma = 0$, $\xi = 0$

This it can be noticed by the decrease of the maximum absolute stream function $|\psi_{\max}|$, and it can be supported by the isothermes presented in Figure 4.20. As it can be seen that the

distortion of isothermal lines occurred in the case of absence of magnitude field and starts to vanish with the increase of Hartmann number.

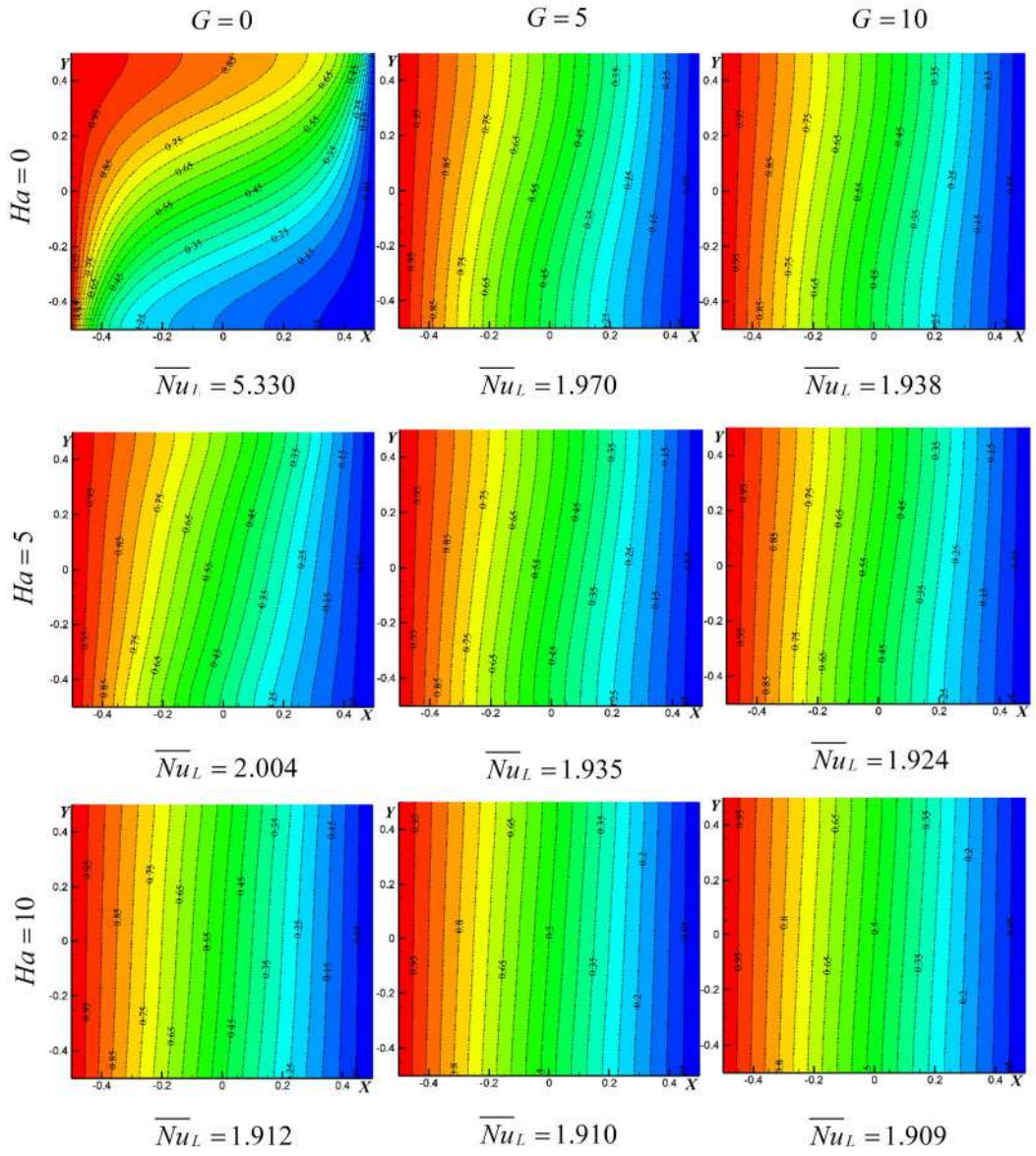


Figure. 4.20. Isotherms for different values of G and Ha for SWCNT at $R_T = 200$, $\phi = 0.05$, $\gamma = 0$, $\xi = 0$

The horizontal elongation of the isotherms decreases and they become parallel, which indicates that the convection strength decreases and the heat transfer mechanism becomes in a quasi-

conduction regime. As it can be noticed by the significant decrease recorded for the average Nusselt number for the increasing of Hartmann number from 0 to 10.

Over and above the effect of Hartmann number on the streamlines and isotherms, the effect of inertial effect parameter G is presented in Figures 4.19 and 4.20 For a fixed value of Hartmann number, the increase of inertial effect parameter leads to decrease in flow strength and the same time the heat transfer by convection mode weakens, which can be noticed by the decrease of the maximum absolute stream function. Furthermore, the increase of inertial effect parameter G causes to the boundary layers to become less significant, the distortion of isothermal lines disappear and they become parallel to the vertical wall. By checking the average Nusselt numbers, we can see that as the inertial effect parameter G increase, the heat transfer by conduction mode is dominated compared to the convection mode. The combination of inertial effect and the Lorentz force lead to a decrease of the convection strength, and the conduction mode become significant.

Figure 4.21 shows how the average Nusselt number and the maximum absolute stream function vary with SWCNT loading ϕ at different values of Hartmann number. For a given SWCNT volume fraction, the increase of Lorentz force by increasing the Hartmann number decrease the nanofluid flow strength and the heat transfer rate. Furthermore, the increase of nanotube loading does not have a significant effect on the nanofluid flow strength, but it has an important effect on heat transfer, due to the enhancement of the nanofluid thermal conductivity.

The increase of nanotube loading weakens the flow strength due the increase of the dynamic viscosity, which reduces the nanofluid velocity. In addition, high dynamic viscosity results in a weak convection strength, but in this case and due to the high thermal conductivity of the SWCNT, the enhancement in the thermal conductivity overcomes the effect of high dynamic viscosity on the heat transfer rate.

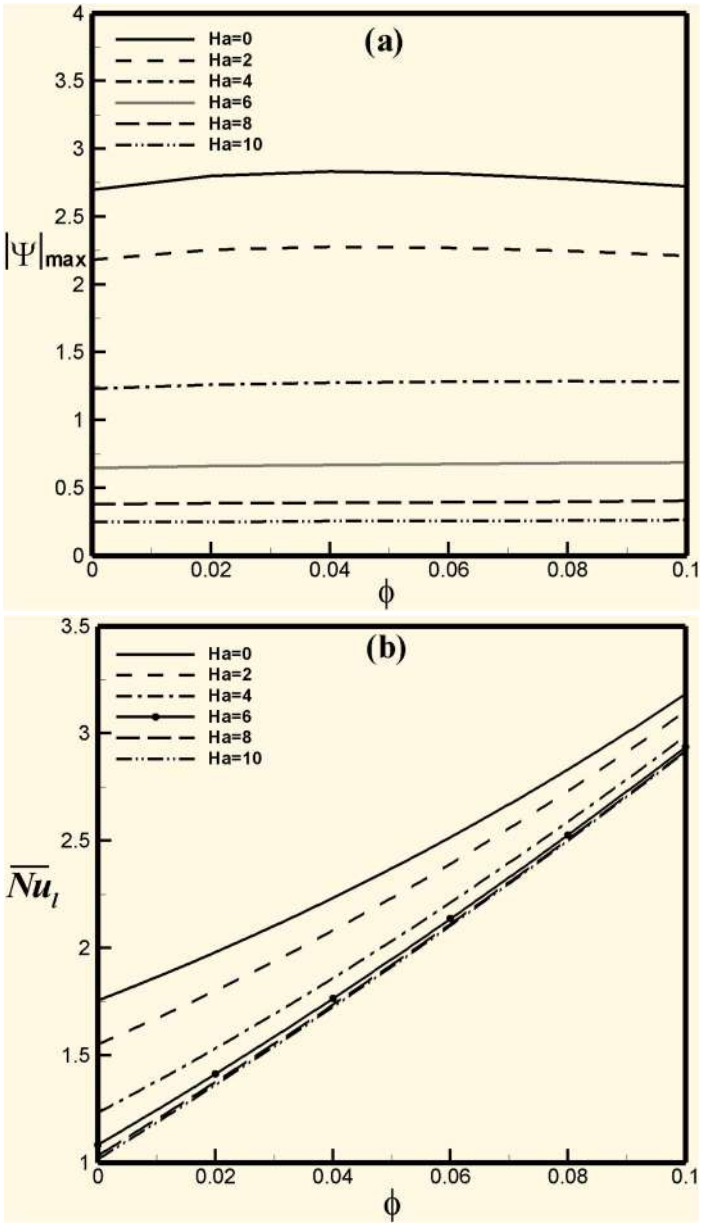


Figure. 4.21. Dependence of the maximum absolute stream function (a) and the average left Nusselt number (b) on nanoparticles volume fraction for SWCNT at $R_T = 200$, $G = 0.5$, $\gamma = 0$, $\xi = 0$ for different Hartmann number Ha.

Figure 4.22 depicts SWCNT loading ϕ on the nanofluid flow strength (a) and heat transfer rate (b) at different values of inertial effect parameter G . It is shown that the higher the inertial parameter is, the lower the flow and thermal fields strength become, the augmentation of inertial parameter slowdown the natural convection currents in the porous medium which reduces the average Nusselt number.

For the values of inertial parameter from 0.001to 0.1, the increase of SWCNT loading has a slight effect on nanofluid flow strength, while for high its effect is insignificant. In addition, For a given G , the increase of SWCNT loading, enhances the heat transfer rate due to the enhancement of the thermal conductivity of nanofluid saturated the porous medium. This enhancement is recorded for the range of G from 0.001to 0.1, but with the increase of G from 0.1 toward 10, the effect of loading the fluid by more nanotube become less significant.

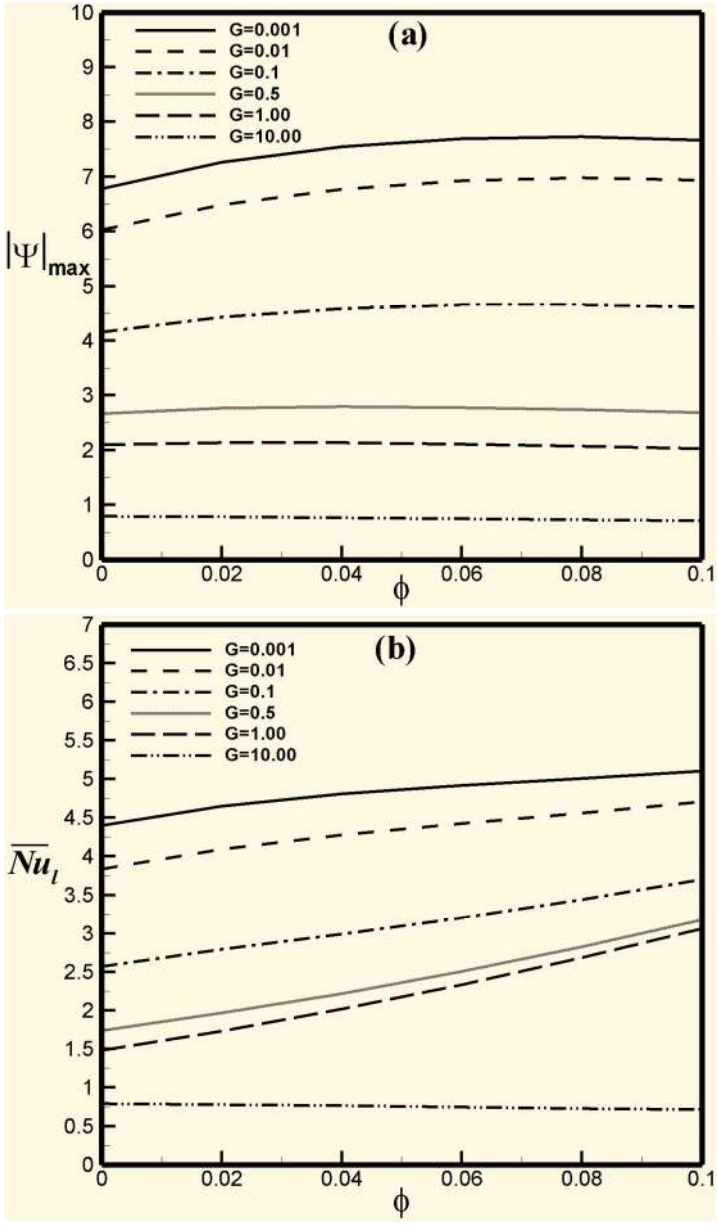


Figure. 4.22. Dependence of the maximum absolute stream function (a) and the average left Nusselt number (b) on nanoparticles volume fraction for SWCNT at $R_T = 200$, $Ha = 0.5$, $\gamma = 0$, $\xi = 0$ for different inertial effect parameter G .

Figure 4.23 illustrates the effect of inertial parameter G on the flow and thermal fields for different values of Hartmann number. It is clear that the increase of Hartmann number decreases the nanofluid flow and the heat transfer strength. As the inertial parameter increases, the decreasing rate of the nanofluid velocity and the convection heat transfer with the increasing of Lorentz force become less significant.

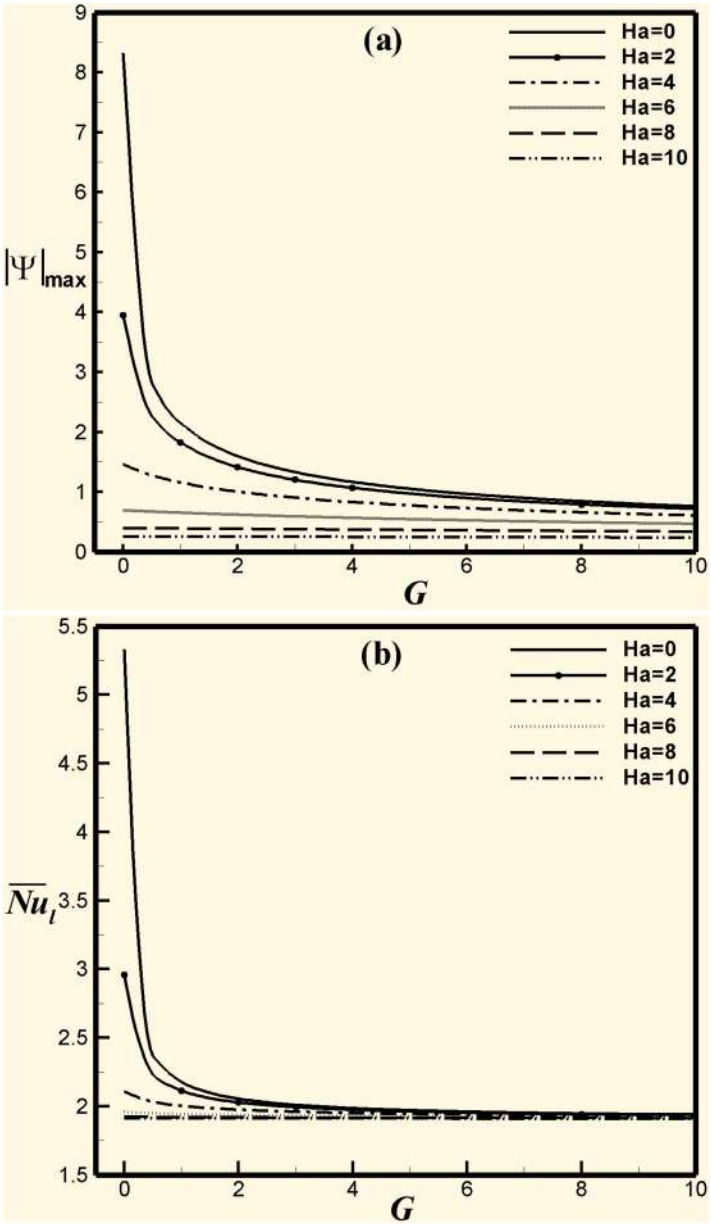


Figure. 4.23. Dependence of the maximum absolute stream function (a) and the average Nusselt number (b) on inertial effect parameter G for SWCNT at $R_T = 200$, $\phi = 0.05$, $\gamma = 0°$ and $\xi = 0°$ for different Hartmann number.

The nanofluid velocity decreases sharply with the increase of inertial parameter to about the value of $G = 2$ for Hartmann number from 0 to 2, after that the decreasing rate becomes insignificant, while for Hartmann number more than 2, the increasing of inertial parameter does not have a noticeable effect of fluid velocity. Furthermore, the increase of inertial parameter G from 0 to 1 reduces quickly the average Nusselt number for the Hartmann number from 0 to 2, and the noticeable effect of the inertial effect on departure from the Darcian flow can be seen.

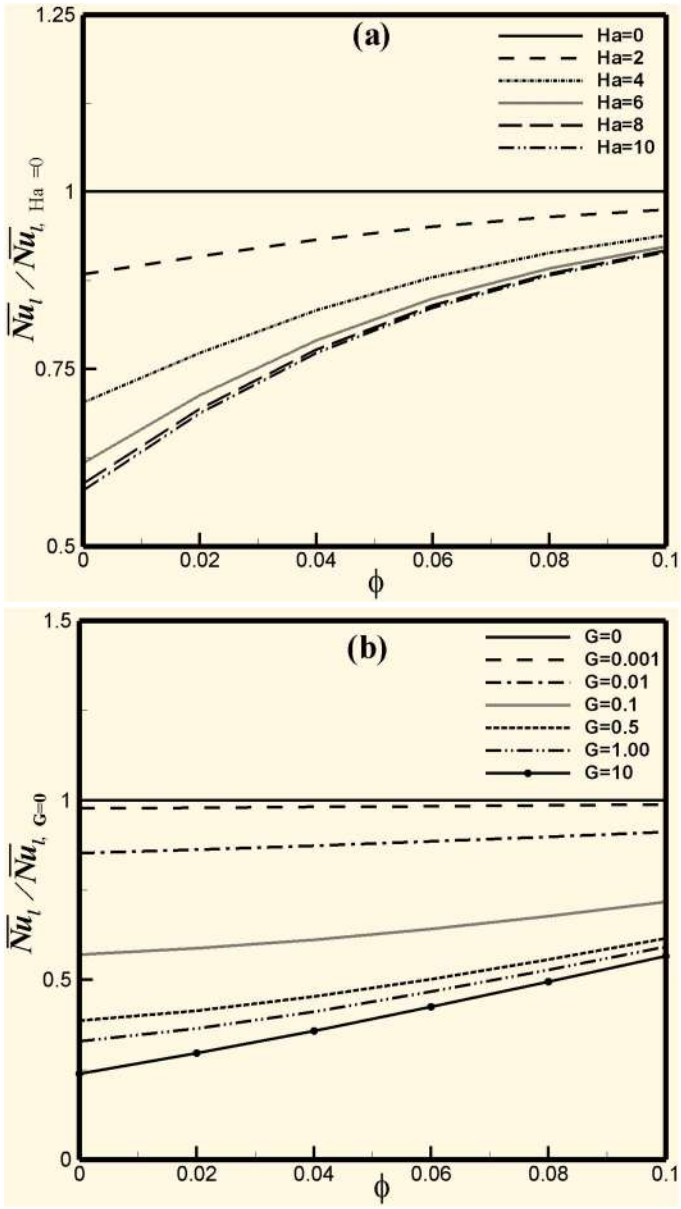


Figure.4.24. Variation of the average Nusselt number ration with SWCNT loading (a) for different Harman number for SWCNT at $R_T = 200$, $G = 0.5, \gamma = 0°, \xi = 0°$, (b) for different inertial effect parameter at $R_T = 200$, $Ha = 0.5, \gamma = 0°, \xi = 0°$.

In addition, For Hartmann number more than 2, the effect G becomes negligible for all values of Hartmann number. The increasing of both Harman number and inertial parameters results to the nanofluid becomes almost motionless, and the heat transfer by conduction mode is dominant compared to the convection mode.

In order to examine the effect of volume fraction of SWCNT in the heat transfer enhancement rate, the rations $\overline{Nu}_L / \overline{Nu}_{L\,Ha=0}$ and $\overline{Nu}_L / \overline{Nu}_{L\,G=0}$ have been plotted with respect to loading rate by SWCNT at various values of Hartmann number (Figure.4.24 (a)), and at various values of inertial effect number (Figure.4.24 (b)).

In Figure 4.24 (a), the average Nusselt number ratio at $Ha = 0$ is taken as a reference value and the inertial parameter at $G = 0.5$. The results show that for the increase of Harman number from $Ha = 0$ to $Ha = 10$, the rate of decrease in average Nusselt number ration decreases with the increase of nanotube volume fraction. This behaviour is due to the fact that even with the inhibition of nanofluid flow by the increasing of Lorentz force, the enhancement in the thermal conductivity gained by the addition of nanotubes has more effect on heat transfer, which is dominated by the conduction mechanism.

In Figure 4.24 (b), the average Nusselt number ratio at $G = 0$ is taken as a reference value and the Hartmann number $Ha = 0.5$. As the inertial parameter increases from $G = 0$ to $G = 10$, the results show the same behaviour as the precedent results of Figure.4.24 (a), except that the decreasing rate with the increase of nanotube volume fraction is lower. Furthermore, the loading by more nanotube has a noticeable effect on heat transfer enhancement for inertial parameter more than 0.5.

Figure 4.25 presents the average Nusselt number with respect to inertial effect parameter at various values of Hartmann number. The average Nusselt number ratio at $Ha = 0$ is taken as a reference value for $R_T = 200$ and $\phi = 0.05$. As it can be seen, the decreasing rate of the average Nusselt number ration with the increase of Hartmann number from $Ha = 0$ to $Ha = 10$ decreases with the increase of inertial parameter. For inertial parameter G more than 2, the decline in the Nusselt number ration is insignificant, which due to the fact that the nanofluid is at a stagnation state, the convection mode is inhibited and the heat transfer is in quasi-conduction mode.

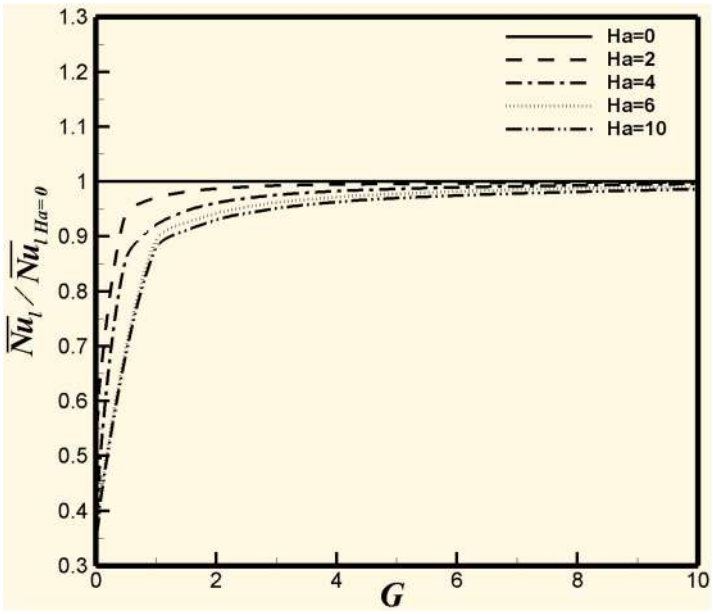


Figure.4.25. Variation of the average Nusselt number ration with inertial effect parameter for different Harman number for SWCNT at $R_T = 200$, $\phi = 0.05$, $\gamma = 0°$, $\xi = 0°$.

To investigate the effect of magnetic field inclination angle on the flow and thermal fields, Figure 4.26 demonstrates the variation maximum absolute volume fraction and average Nusselt number with the magnetic field inclination angle ξ.

The results are presented for four value of SWCNT loading percentage. The results illustrates that the inclination angle of the magnetic field has a weak effect on the fluid flow and insignificant effect on thermal field. In addition, the as the volume fraction of SWCNT increase, the effect of inclination angle of magnitude field decrease, which is due to the increase in the overall dynamic viscosity of nanofluid.

Figure 4.27 depicts the effect inclination angle of the cavity with the Hartmann number on the nanofluid flow and the heat transfer strength at $R_T = 200, G = 0.5$ $\phi = 0.5$ and $\xi = 45°$.

For the case of heating the cavity from bottom ($\gamma = -90°$), the increase of Hartmann number from $Ha = 0$ to $Ha = 2$ decreases the fluid flow and the heat transfer rate, after this interval, from $Ha = 2$ the fluid flow is in stagnation state and the convection is totally inhibited, and the heat transfer is done via the conduction mode. The inclination of the cavity $\gamma = -45°$ represents the angle where the maximum of fluid flow strength is recorded, for the fluid flow the Hartmann is from $Ha = 0$ to $Ha = 2$, where for the heat transfer strength is from $Ha = 0$ to $Ha = 1$. After those ranges of Hartmann number, the maximum of fluid flow strength and the heat transfer rate is become for the inclination of $\gamma = 0°$ where the cavity is

heated from the vertical left wall. For high values of Hartmann number, from $Ha = 8$ to $Ha = 10$ the inclination of the cavity becomes insignificant for the convection rate.

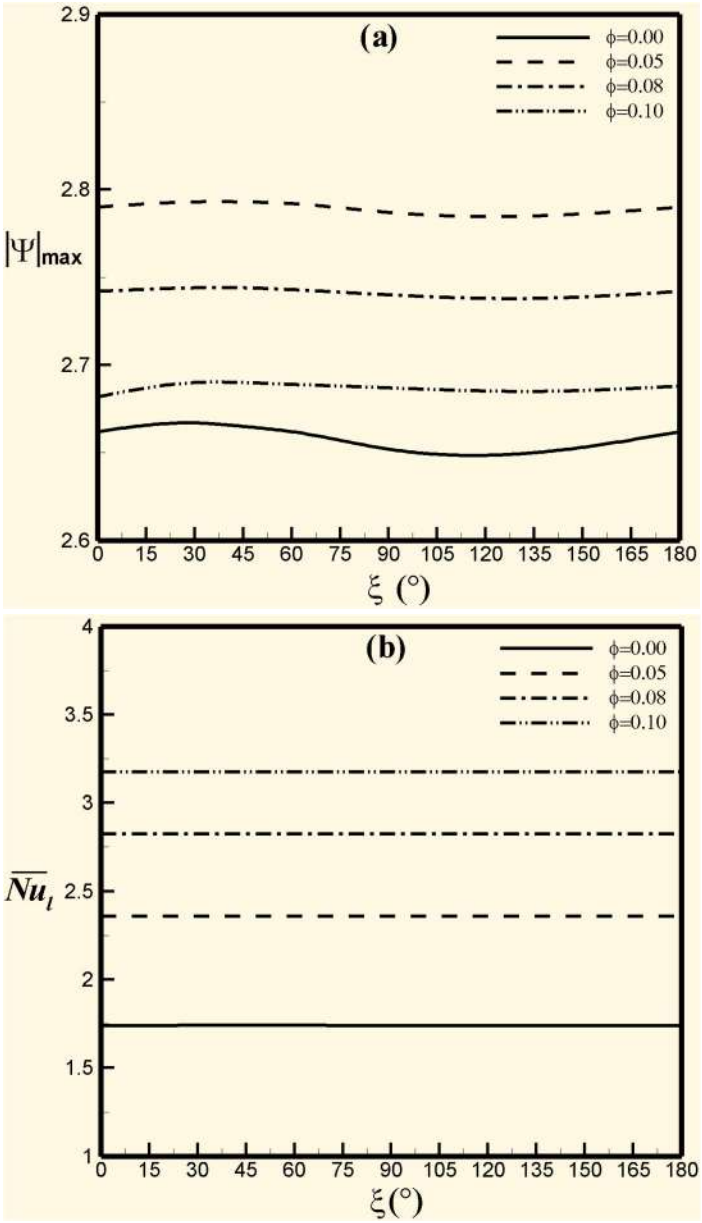


Figure. 4.26. Dependence of the maximum absolute stream function (a) and the average Nusselt number (b) on magnetic field inclination angle for SWCNT at $R_T = 200, G = 0.5$ $Ha = 0.5$ and $\gamma = 0°$ for different nanoparticles volume fraction.

The effect of Hartmann number, the inclination angle of magnetic field with respect to the cavity inclination for $R_T = 200, G = 0.5$ $\phi = 0.05$ is demonstrated in Figure. 4.28. As mentioned in the previous sections, the increase of Hartmann number reduces both the fluid

flow strength and the heat transfer rate regardless the inclination angles of the cavity and the magnetic field.

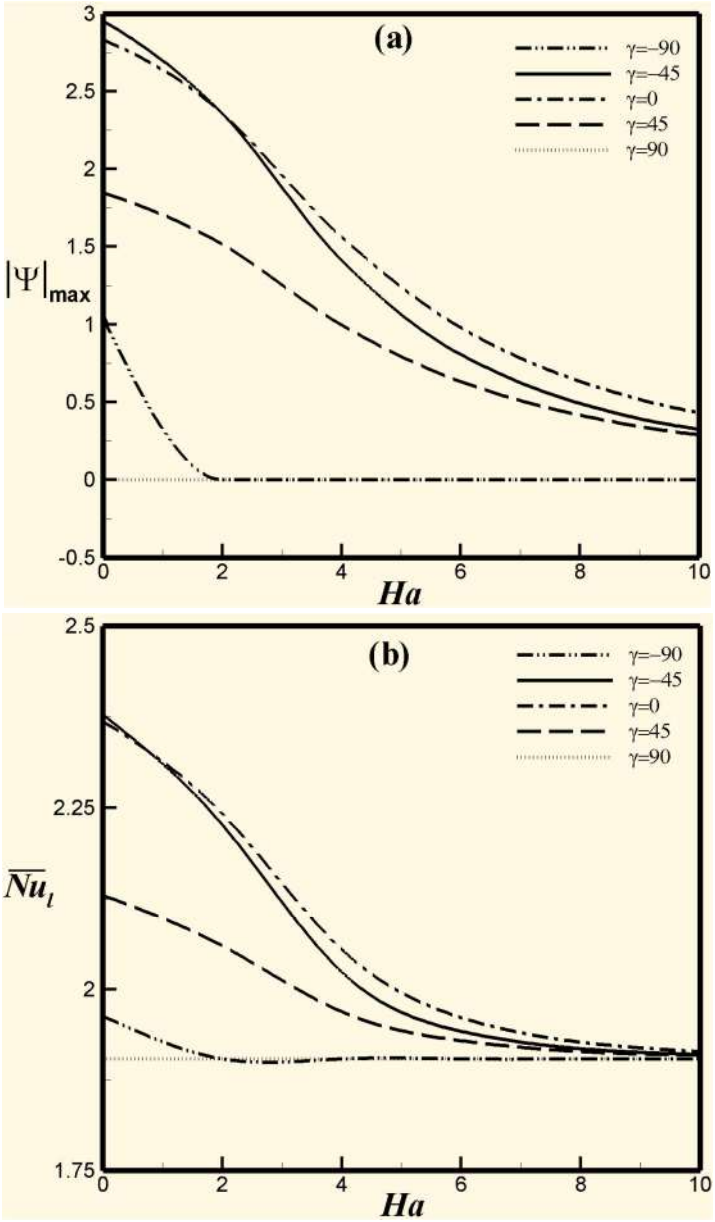


Figure. 4.27. Dependence of the maximum absolute stream function (a) and the average Nusselt number (b) on Hartmann number for SWCNT at $R_T = 200, G = 0.5$ $\phi = 0.05$ and $\xi = 45°$ for different inclination angles of the cavity.

In the absence of magnetic field ($Ha = 0$), the maximum fluid flow strength and convection rate is recorded, and the peak value is for the magnetic field inclination of between $\gamma = -15°$ and $\gamma = -30°$. For the Hartmann number $Ha = 5$ the inclination angle $\xi = 45°$ of the magnetic field is where the high fluid flow strength and heat transfer rate is recorded regardless

the inclination angle of the enclosure. In the case of the Hartmann number $Ha = 10$, there is a slight effect of the inclinations angles of the enclosure and the magnetic field on the fluid flow strength, and no effect on the heat transfer rate.

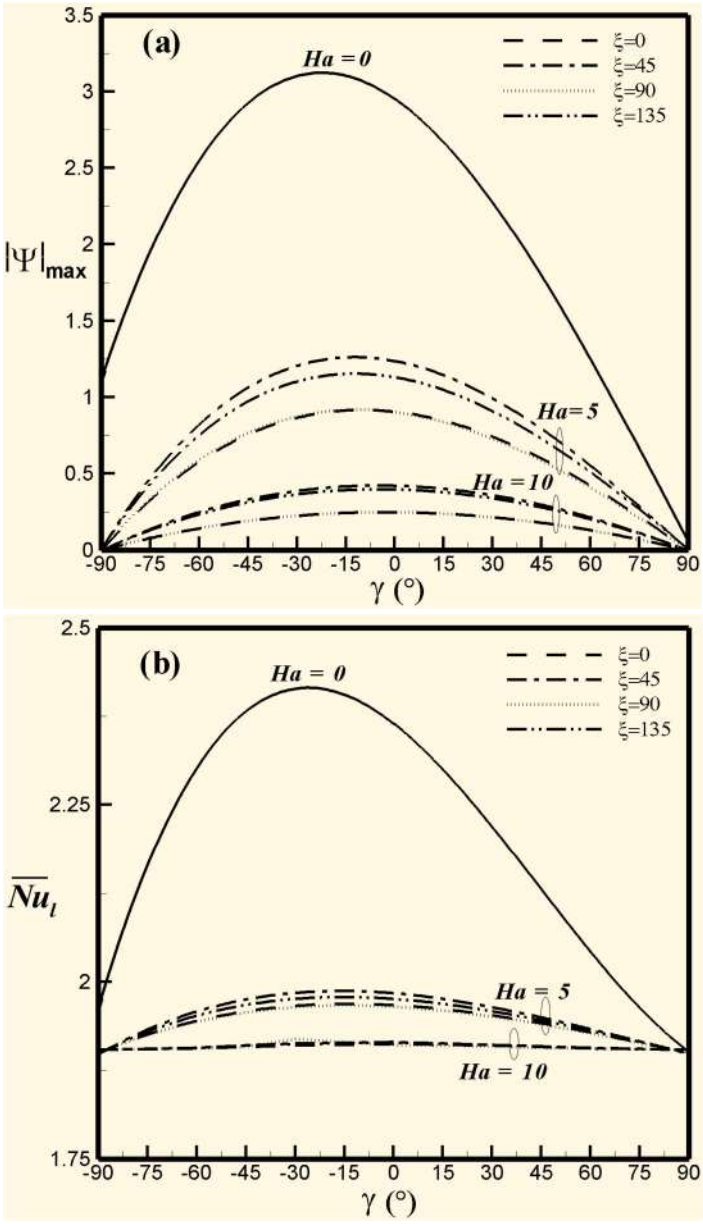


Figure.4.28. Variation of the maximum absolute stream function (a) and the average Nusselt number (b) with the inclination of the cavity γ for different Hartmann numbers Ha and magnetic field inclination angle ξ for SWCNT at $R_T = 200, G = 0.5$ $\phi = 0.05$.

Finally, the effect of Rayleigh number on the nanofluid flow strength and the heat transfer rate is illustrated in Figure 4.29 for different Hartmann number Ha and magnetic field inclination

angle ξ for $G = 0.5 \quad \phi = 0.05, \gamma = 0$. With the absence of magnetic field, the Rayleigh number has a strong effect on the strength of fluid flow and convection, the increase of Rayleigh number increases both the maximum absolute stream function and the average Nusselt number.

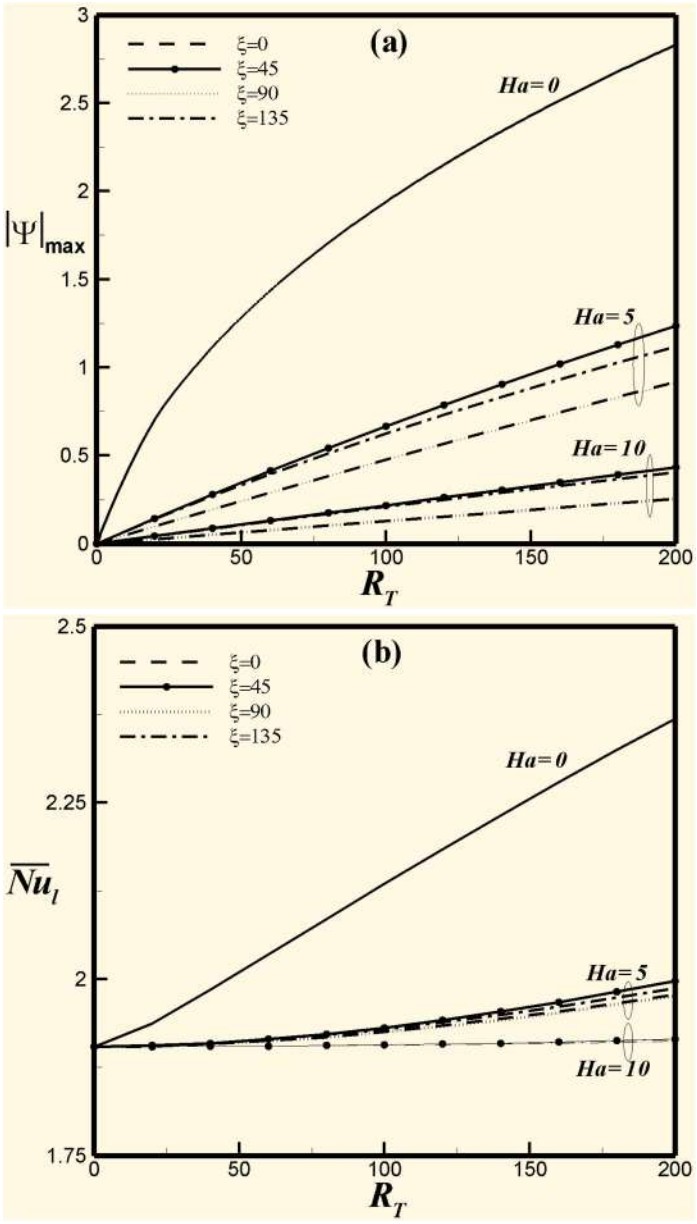


Figure. 4.29. Variation of the maximum absolute stream function (a) and the average Nusselt number (b) with the Rayleigh number R_T for different Hartmann numbers Ha and magnetic field inclination angle ξ for SWCNT at $G = 0.5 \quad \phi = 0.05, \gamma = 0$.

By introducing the effect of magnetic field, for a given Rayleigh number, the fluid flow strength and the heat transfer rate decrease with the increase of Hartmann number. In addition, the

magnetic field inclination angle of $\xi = 45°$ denotes the highest value for the strength of the fluid flow and the heat transfer rate for a given Rayleigh number and Hartmann number. Furthermore, for Hartmann number $Ha = 10$, the heat transfer by convection mode is totally inhibited for any given value of Rayleigh number and inclination angle of magnetic field.

4.3 Conclusion

In this section, the obtained results of the both studied cases which have been obtained by an implemented Fortran computer code, have been presented and discussed. The Finit difference method has been used the results have been validated with other results found in the literature. A good match was obtained. The effects inertia and magneyic field, the dependency of the fluid flow and the heat transfer rate on Raleigh number (R_T); nanotubes volume fraction (ϕ); Hartmann number (Ha); inertial effect parameter (G);inclination angle of the cavity (γ) and inclination angle of the magnetic field (ξ) are discussed in detail.

CHAPTER V

CONCLUSION AND RECOMMENDATIONS

CHAPITER V

CONCLUSION AND RECOMMENDATIONS

5.1. Conclusion

In this doctoral thesis, we studied numerically the heat transfer by natural convection induced by temperature gradient of nanofluid saturated porous medium. The enclosure studied is a two dimensional inclined square subjected to two different temperatures T_h and T_f ,while the other two walls are adiabatic. The Dupuit-Darcy model, which includes the effect of inertia for low or large Reynolds flows, and the Boussinesq approximation were used to model natural convection inside the porous medium. Two applications have been performed in this study, the first one is about the free convection of Cu-Water nanofluid saturated an Aluminium foam porous medium, while the second application is about the free convection of SWCNT-Water and Al2O3-Water saturated a tilted rectangular porous medium subjected an external magnetic field . The governing equations have been solved together with boundary conditions using the finite difference method with uniform grid size mesh by an implemented FORTRAN code.

The influence of each of the parameters of the problem was discussed in this thesis. These parameters are the Rayleigh number R_T , the nanoparticles volume fraction ϕ , the inertial effect parameter G , the Hartman number Ha , the porosity of the porous medium ε , the inclination angle of the cavity γ and the inclination angle of magnetic field ξ . The calculation codes were validated based on the results available in the literature.

The main conclusions found in this study are summarized below:

5.1.1: Cu-Water nanofluid saturated Aluminium foam porous medium:

- The increase of Rayleigh number has a significant effect on the nanofluid flow and heat transfer strength.

- The inertia has a significant adverse effect impact on the convective heat transfer of the nanofluid the porous medium, the flow convection decreases with the increase of the inertial effect parameter. In addition, the heat transfer by conduction mode is

dominated for high values of inertial effect parameter, where for low values the convection mode is dominated. The effect of Rayleigh number on the average Nusselt number is more significant for low values of inertial effect parameter compared to its higher values.

- The efficiency of convection heat transfer decreases with the increase of nanoparticles volume fraction. This is due to the increase in the nanofluid effective viscosity, which causes the nanofluid velocity to decrease and results in a decrease of convection heat transfer inside the cavity.

- The increased nanoparticles volume fraction into the base fluid decreased the rate of heat transfer by convection in the enclosure due to the increased dynamic viscosity of the nanofluid which overcomes the effect of the enhanced thermal conductivity.

- The average Nusselt number decreases with the increase of the porosity due to the high difference between the porous matrix material thermal conductivity and that of nanofluid. The heat transfer in the cavity is dominated by the high thermal conductivity of porous matrix compared to the mechanism of convection heat transfer by the nanofluid.

- The inclination angle has a considerable effect on the convection strength of nanofluid saturated the porous medium for low values of inertial parameter. As the inertial parameter G increases the inclination angle effect decreases. Furthermore, the inclination angle of about -40° represents the better angle for maximum convection rate of the nanofluid saturated the porous medium for a given inertial parameter or nanoparticles volume fraction. A slight heat transfer enhancement with the increase on nanoparticles volume fraction is noted while the cavity is heated from the top.

- **5.1.2: SWCNT-Water nanofluid saturated porous medium and influenced by external magnetic field:**

- The increase of Rayleigh number has a significant effect on the nanofluid flow and heat transfer strength.

- The convection strength increases with the increase of SWCNT concentration, but with the increase of Rayleigh number the enhancement of convection heat transfer become insignificant due to the increase in dynamic viscosity.

- The increase of magnetic field strength and the inertial effect parameter decreases significantly the strength of fluid flow and convection and the heat transfer mechanise convert from convection mode toward the conduction mode.

- Even with the inhibition of the fluid flow inside the enclosure by increasing the Hartmann number or the inertial effect parameter, the loading of the fluid by SWCNT enhance the heat transfer due to the significant enhancement of the thermal conductivity of the nanofluid.

- For Hartmann number more than $Ha = 2$, the fluid flow is almost inhibited and the heat transfer mechanism is by conduction mode.

- The inclination angle $\xi = 45°$ of the magnetic field represents the best for fluid flow strength and heat transfer rate regardless the Hartmann and Rayleigh numbers.

- **5.2. Recommandations**

It would be a significant scientific contribution to be able to couple numerical research with experimental research, especially in developing correlations for well predicting the thermophysical properties of nanofluids.

It is desirable to consider studies of heat transfer in the presence of nanofluids in which the following effects could be considered:

- Effect of the shape and size of the nanoparticles.

- Turbulent regime and Double phase flow.

REFERENCES

Alam,T, and Kim M,H., A Comprehensive Review on Single-Phase Heat Transfer Enhancement Techniques in Heat Exchangers Applications, Renewable and Sustainable Energy Review., vol. 81, pp. 813-839, 2018.

Alawi, O. A., N.A.C. Sidik, H.W. Xian, T. H. Kean, S.N. Kazi., Thermal Conductivity and Viscosity Models of Metallic Oxides Nanofluids, Int. J. Heat and Mass Transfer., vol. 116, pp. 1314-1325, 2018.

Alfven H. Existence of electromagnetic-hydrodynamic waves. Nature 1942;150:405.

Ali .N, Teixeira. J.A, Addali .A , A Review on Nanofluids: Fabrication, Stability, and Thermophysical Properties, Journal of Nanomaterials, Volume 2018, Article ID 6978130, pp 1-33,2018

Alkasassbeh, M.M., Zurni, O., Mebarek-Oudina, F., Raza, J. and Chamkha, A.J., Heat Transfer Study of Convective fin with Temperature-Dependent Internal Heat Generation by Hybrid Block Method, Heat Transfer-Asian Res, Wiley Periodicals, Inc., vol. 48, pp. 1225-1244, 2019.

Alloui, Z., Rebhi, R., Mamou, M. and Vasseur, P., Effect of Quadratic Drag on Natural Convection in a Tilted Porous Layer with Uniform Heat Flux From the Side; International Journal of Heat and Mass Transfer., vol. 115, pp. 314-325, 2017.

Alsabery, A.I., Engin Gedik., Chamkha, A.J. and Hashim, I., Impacts of Heated Rotating Inner Cylinder and Two-Phase Nanofluid Model on Entropy Generation and Mixed Convection in a Square Cavity, Heat and Mass Transfer., vol. 56, pp. 3221-3238-, 2019.

Alsabery, A.I., Ismael, M, A., Chamkha, A.J. and Hashim, I., Effect of Nonhomogeneous Nanofluid Model on Transient Natural Convection in a non-Darcy Porous Cavity Containing an Inner Solid Body; International Communications in Heat and Mass Transfer; vol. 110, pp. 104442, 2020.

Armaghani. T, Chamkha. A.J, Rashad.A.M, Mansour. M.A, Inclined magneto: convection, internal heat, and entropy generation of nanofluid in an I-shaped cavity saturated with porous media, Journal of Thermal Analysis and Calorimetry, 1-13. 2020

Asharafizadeh, S.A. and Zhongchao. Tan., Mass and Energy Balances, Basic Principles for Calculation, Design and Optimization of Macro\Nano Systems, Springer, 2018.

Baytas. A.C, Pop. I, Free convection in oblique enclosures filled with a porous medium. Int. J. Heat Mass Transf. 42, 1047–1057, 1999

Bear J. Dynamics of Fluids in Porous Media. Elsevier, (1972).

Beckermann. C, Viskanta. R, Ramadhyani. S, A numerical study of non-Darcian natural convection in a vertical enclosure filled with a porous medium. Numer. Heat Transfer 10, 446–469,1986

Beckerman. C and Viskanta R, Double-diffusive convection during dendritic solidification of binary mixture. Physico Chem. Hydrodyn., Vol. 10, pp. 195-213, (1988).

Bejan, A, On the boundary layer regime in a vertical enclosure filled with a porous medium. Lett. Heat Mass Transf. 6, 82–91,1979

Bories S. A. Fragment de description de la physique des transferts thermiques dans le sous- sol. Vol. 3. La Houille Blanche, (1985).

Bühler. L, Mistrangelo. C, Najuch.T, Magnetohydrodynamic flows in model porous structures, Fusion Engineering and Design, 98-99, 1239-124. 2015

Buonomo, , B., H, Celik, C., Ercole, D., Manca, O. and Mo bedi, M., Numerical study on Latent Thermal Energy Storage Systems with Aluminium Foam in Local Thermal Equilibrium; Applied Thermal Engineering., vol. 159, pp. 113980, 2019.

Bianco, V., Manca, O., Nardini, S. and Vafai, K., Heat Transfer Enhancement with Nanofluids, Taylor Francis Group, LLC., 2015.

Bourantas, G.C., Skouras, E.D., Loukopoulos, V.C. and Burganos, V.N., Heat Tansfer and Natural Convection of Nanofluids in Porous Media, Eur J Mech B Fluids., vol. 43, pp. 45-56, 2014.

Brinkman H. C. A calculation for the viscous force exerted by a flowing fluid on a dense swarm of particules. Appl. Sci. Res., Vol A1, pp. 27-34, (1947).

Chamkha. A.J, Jena.S.K, Mahapatra. S.K, MHD Convection of Nanofluids: A Review, Journal of Nanofluids 4 (3), 271-292. 2015

Choi, S.U.S., Enhancing Thermal Conductivity of Fluids with Nanoparticles, in The Proceedings of the 1995 ASME International Mechanical Engineering, Congress and Exposition, San Francisco, USA, ASME, FED, 231/MD, vol. 66, 99, 1995.

Chand, R., Nanofluid Technologies and Thermal Convection Techniques, IGI Global., 2017.

Choi, S.U.S., George, Zhang,., Yu, W., Lockwood, F.E. and Grulke, E.A., Anomalously Thermal Conductivity Enhancement in Nanotube Suspensions, Appl Phys Lett., vol. 79, pp. 2252-2254, 2001.

Collins R. E. Flow of fluids through porous materials. New York, Reinhold Publishing Corp., 270 p, (1961).

Darcy H. P. C. Les fontaines publiques de la ville de Dijon (Victor Dalmont, Paris, 1856).

Dybbs A and Edwards R. V. A new look at porous media fluid mechanics Darcy to turbulent. Fundamentals of Transport Phenomena in Porous Media Martinus Nishoff, Dordrecht, pages 199-256, (1984).

Dupuit J. E. J. Études théoriques et pratiques sur le mouvement des eaux dans les canaux découverts et à travers les terrains perméables (Victor Datmont, Paris, 1863).

Emami, R.Y., Siavashi, M. and Shahriari Moghaddam, G., The effect of Inclination Angle and Hot Wall Configuration on Cu-Water Nanofluid Natural Convection Inside a Porous Square Cavity, Advanced Powder Technology, vol. 29, pp. 439-848, 2018.

Ergum, S., Fluid Flow Through Packed Columns, Chem Eng Prog., vol. 48, pp. 89-94, 1952.

Estellé. P, Halelfadl. S, Maré. T, Thermal conductivity of CNT water based nanofluids: Experimental trends and models overview , Journal of Thermal Engineering 1 (2), 381-390, 2015

Forchheimer P. Wasser bewe gung durch Boden. VDIZ. 45, 1782-1788, (1901).

Ghadimi. A, Saidur.R, Metselaar.H.S.C, A review of nanofluid stability properties and characterization in stationary conditions, Int. J. Heat Mass Transf. 54 (2011) 4051–4068. doi:10.1016/j.ijheatmasstransfer.2011.04.014.

Ganji, D.D. and Malvandi, A., Heat Transfer Enhancement Using Nanofluid Flow in Microchannels, Elsevier, 2016.

Ghalambaz, M., Mikhail., Sheremet, A. and Pop, I., Free Convection in a Parallelogrammic Porous Cavity Filled with a Nanofluid Using Tiwari and Das' Nanofluid Model, PLOS ONE., vol. 10, e0126486, 2015.

Ghalambaz, M., Sheremet, M. A., Mehryan, S. A. M., Kashkooli, F. M. and Pop, I., Local Thermal non-Equilibrium Analysis of Conjugate Free Convection within a Porous Enclosure Occupied with Ag–MgO Hybrid Nanofluid, Journal of Thermal Analysis and Calorimetry., vol.135, pp. 1381-1398, 2018.

Ghalambaz, M., Chamkha, A.J. and Wen, D., Natural Convective Flow and hHeat transfer of Nano-Encapsulated Phase Change Materials (NEPCMs) in a cavity, International Journal of Heat and Mass Transfer., vol. 138, pp. 738-749, 2019.

Ghalambaz, M., Mehryan, S.A.M., Izadpanahi, E., Chamkha, A.J. and Wen, D., MHD Natural Convection of Cu–Al2O3 Water hybrid Nanofluids in a Cavity Equally Divided Into Two Parts by a Vertical Flexible Partition Membrane, Journal of Thermal Analysis and Calorimetry., vol.138, pp. 1723-1743, 2019.

Ghalambaz, M., Doostani, A., Izadpanahi, E. and Chamkha, A.J., Conjugate Natural Convection Flow of Ag–MgO/Water Hybrid Nanofluid in a Square Cavity, Journal of Thermal Analysis and Calorimetry., vol. 139, pp. 2321-2336 , 2019.

Garandet. J.P, Albussoiere. T, Moreau. R, Buoyancy driven convection in a rectangular enclosure with a transverse magnetic field, Int. J. Heat Mass Transfer 35, 741–748. 1992

Gross. R, Bear. M.R, Hickox. C.E, The application of flux-corrected transport (FCT) to high Rayleigh number natural convection in a porous medium. In: Proceedings 7th Int. Heat Transfer Conference, San Francisco, 1986

Gupta, M., Singh, V., Rajesh, Kumar. and Said, Z., A Review on Thermophysical Properties of Nanofluids and Heat Transfer Applications, Renewable and Sustainable Energy Reviews., vol. 74, 638-670, 2017.

Haddad, Z., Oztop, H.F., Abu-Nada,E. and Mataoui, A., A Review on Natural Convective Heat Transfer of Nanofluids, Renewable and Sustainable Energy Reviews., vol. 16, pp. 5363-5378, 2012.

Harish. S, Ishikawa. K, Einarsson. E, Aikawa. S, Inoue. T, Zhao. P, Watanabe. M, Chiashi. S, Shiomi. J, Maruyama. S, Temperature dependent thermal conductivity increase of aqueous nanofluid with single walled carbon nanotube inclusion, Materials Express 2 (3), 213-223, doi:10.1166/mex.2012.1074, 2012

Hayat.T, Haider.F, Muhammad. T, Alsaedi. A, Three-dimensional rotating flow of carbon nanotubes with Darcy-Forchheimer porous medium. PLoS ONE 12(7): e0179576. https://doi.org/10.1371/journal.pone.0179576, 2017

Hoseinzadeh, S., Heyns, P.S., Chamkha, A.J. and Shirkhani, A., Thermal Analysis of Porous Fins Enclosure with the Comparison of Analytical and Numerical Methods, Journal of Thermal Analysis and Calorimetry., vol. 138, pp. 727-735, 2019.

Hossin, M.A., Rees, D.A.S., Non-Darcy Convection Along a Horizontal Heated Surface, Transport in Porous Media., vol. 29, pp. 309-321, 1997.

Ishak, M.S., Alsabery, A.I., Chamkha, A.J. and Hashim. I., Effect of Finite Wall Thickness on Entropy Generation and Natural Convection in a Nanofluid-Filled Partially Heated Square Cavity, International Journal of Numerical Methods for Heat & Fluid Flow., 2019.

Jabbari, F., Rajabpour, A. and Saedodin S., Thermal Conductivity and Viscosity of Nanofluids : A Review of Recent Molecular Dynamic Studies, Chemical Engineering Science., vol. 174, pp. 67-81, 2017.

Javaherdeh. K, Najjarnezami. A, Lattice Boltzmann simulation of MHD natural convection in a cavity with porous media and sinusoidal temperature distribution, Applied Mathematics and Mechanics volume 39, 1187-1200, 2018

Kasaeian, A., Daneshazarian, R., Mahian, O., Kolsi, L., Chamkha, A.J., Wongwises, S. and Pop, I., Nanofluid Flow and Heat Transfer in Porous Media: A Review of the Latest Developments, Int. J. Heat and Mass Transfer., vol. 107, pp. 778-791, 2017.

Khan, M. M,K,, Chowdhury, A.A. and Hassan, N.M.S., Application of Thermo-fluid Processes in Enery Systems, Key Issues and Recent Developments for a Sustainable Future, Springer, 2018.

Khan. W. A, Khan. Z. H, Rahi. M, Fluid flow and heat transfer of carbon nanotubes along a flat plate with Navier slip boundary, Springer, DOI 10.1007/s13204-013-0242-9, 2013Kozeny J. Flow in porous media. S. B. Akad. Wiss, 2a: 126, (1927).

Lage, J.L; The Fundamental Theory of Flow Through Permeable Media From Darcy to Turbulence, Transport Phenomena in Porous Media., Ingham, D.B. and Pop, I., eds., Elsevier Science, Oxford, pp. 1-30; 1998.

Lage, J.L. and Antohe, B.V., Darcy's Experiments and the Deviation to Nonlinear Flow Regime, Journal of Fluids Engineering., ASME, vol. 122, pp. 619-625, 2000.

Mahdi, R.A., Mohammed, H.A., Munisamy, K.M. and Saeid, N.H., Review of Convection Heat Transfer and Fluid Flow in Porous Media with Nanofluid, Renewable and Sustainable Energy Reviews., vol. 41, pp. 715-734, 2015.

Mahian, O., Kolsi, L., M. Amani et al., Recent Advances in Modeling and Simulation of Nanofluid, Flows-Part I: Fundamental and theory, Physics Reports., vol. 790, pp. 1-48, 2018.

Mahmud. S, Fraser. R. A, Magnetohydrodynamic free convection and entropy generation in a square porous cavity, International Journal of Heat and Mass Transfer 47 (14-16), 3245-3256.2004

Manole. D.M, Lage. J.L, Numerical benchmark results for natural convection in a porous medium cavity. Heat Mass Transf. Porous Media 105, 44–59, 1992

Mansour. M.A, Chamkha .A.J, Mohamed. R.A, Abd El-Aziz.M.M, Ahmed. S.E, MHD natural convection in an inclined cavity filled with a fluid saturated porous medium with heat source in the solid phase, Nonlinear Analysis: Modelling and Control 15 (1), 55-70. 2010

Masuda. H, Ebata. A, Teramae. K. Hishinuma. N. Alteration of Thermal Conductivity and Viscosity of Liquid by Dispersing Ultra-Fine Particles. Dispersion of Al2O3, SiO2 and TiO2 Ultra-Fine Particles, Netsu Bussei. 7 (1993) 227–233. doi:10.2963/jjtp.7.227.

Maxwell. J, A Treatise on Electricity and Magnetism, second ed., Oxford University Press, Cambridge, UK, 1904.

Mebarek-Oudina, F. and Bessaïh, R., Numerical Simulation of Natural Convection Heat Transfer of Copper-Water Nanofluid in a Vertical Cylindrical Annulus with Heat Sources, Thermophysics and Aeromechanics., vol. 26, pp. 325-334, 2019.

Mehryan, S.A.M., Izadi, M., Zafar, Namazian. and Chamkha, A.J., Naatural Convection of Multi-Walled Carbon Nanotube-Fe3O4/Water Magnetic Hybrid Nanofluid Flowing in Porous Medium Considering the Impacts of Magnetic Field-Deependent Viscosity, Journal Thermal Analysis Calorimetry, vol. 138, pp. 1541-1555, 2019.

Mehryan, S.A.M., Izadpanahi, E., Ghalambaz, M. and Chamkha, A.J., Mixed Convection Flow Caused by an Oscillating Cylinder in a Square Cavity Filled with Cu–Al_2O_3/Water Hybrid Nanofluid, Journal of Thermal Analysis and Calorimetry., vol. 137, pp. 965-982, 2019.

Mehryan. S.A.M, Kashkooli. F.M, Ghalambaz. M, Chamkha. A.J, Free convection of hybrid Al2O3-Cu water nanofluid in a differentially heated porous cavity, Advanced Powder Technology 28 (9), 2295-2305, 2017.

M'hamed .B, Sidik. N.A.C, Yazid. M.N.A.W.M, Mamat. R, Najafi .G, Kefayati. G.H.R, A review on why researchers apply external magnetic field on nanofluids, International Communications in Heat and Mass Transfer 78, 60-67, 2016.

Minea, A.A., Advances in New Heat Transfer Fluids, Taylor Francis Group, LLC, 2017.

Mikkola, V., Puupponen, S., Granbohm, H., Saari, K., Ala-Nissila, T. and Seppälä, A., Influence of Particle Properties on Convective Heat Transfer of Nanofluids, Int. J Ther Sci., vol. 124, pp. 187-195, 2018.

Moreau, R. Magnetohydrodynamics. Kluwer. 1990

Moya. S.L, Ramos. E, Sen, M, Numerical study of natural convection in a tilted rectangular porous material. Int. J. Heat Mass Transf. 30, 630–645,1987

Nawaf, H.S. and I. Pop, Non-Darcy Natural Convection in a Square Cavity Filled with a Porous Medium, Fluid Dynamics Research., vol. 36, pp. 35-43, 2005.

Neal.G and Nader.W, Practical significance of Brinkman's extension of Darcy's law : coupled parallel flows within a channel and bounding porous medium. The Canadian J. Chem. Eng., Vol. 52, pp. 475-478, (1974).

Nield, D. A. and Kuznetsov, A.V., An Historical and Topical Note on Convection in Porous Media., Journal of Heat Transfer, ASME, vol. 135, 2013.

Nield, D.A. and Bejan, A., Convection in Porous Media, fifth ed., Springer, 2017.

Nithyadevi. N, Rajarathinam .M, Effect of inclination angle and magnetic field on convection heat transfer for nanofluid in a porous cavity , Journal of Applied Fluid Mechanics 9 (5), 2347-2358. 2016.

Nkurikiyimfura. I, Wang .Y, Pan. Z, Heat transfer enhancement by magnetic nanofluids-a review, Renewable and Sustainable Energy Reviews 21, 548-561.2013

Poulikakos, D. and Bejan, A., The Departure From Darcy Flow in Natural Convection in a Vertical Porous Layer, Physics of fluids., vol. 28, pp. 3477-3484, 1985.

Rashad. A.M, Rashidi .M.M, Lorenzini. G, Ahmed. S.E, Aly A.M, Magnetic field and internal heat generation effects on the free convection in a rectangular cavity filled with a porous medium saturated with Cu–water nanofluid, International Journal of Heat and Mass Transfer 104, 878-889. 2017

Rashidi, S., Esfahani, J.A., Rashidi, A., A Review on the Applications of Porous Materials in Solar Energy Systems, Renewable and Sustainable Energy Review., vol. 73, pp. 1198-1210, 2017.

Raja, M., Vijayan, R., Dineshkumar, P. and Venkatesan M., Review on Nanofluids Characterization, Heat Transfer Characteristics and Applications, Renewable and Sustainable Energy Reviews., vol. 64, pp. 163-173, 2016.

Ranga Babu, J.A., Kumar,K, K. and Rao,S, S., State-of-Art Review on Hybrid Nanofluids, Renewable and Sustainable Energy Reviews., vol. 77, pp. 551-565, 2017.

Raza, J., Mebarek-Oudina, F. and Chamkha, A.J., Magnetohydrodynamic Flow of Molybdenum Disulfide Nanofluid in a Channel with Shape Effects, Multidiscipline Modeling in Materials and Structures., Vol. 15, pp. 737-757, 2019.

Rebhi, R., Mamou, M. and Alliche, M., Form Drag Effect and Hopf Bifurcation in Dupuit-Darcy Thermal Convection in a Shallow Well-Packed Porous Enclosure, Phys Fluids., vol. 26, 074104, 2014 .

Rebhi, R., Mamou, M., Vasseur P. and Alliche, M., Form Drag Effect on the Onset of non-Linear Convection and Hopf Bifurcation in Binary Fluid Saturating a Tall Porous Cavity, Int. J. Heat Mass Transfer., vol. 100, pp. 178-190, 2016.

Rebhi, R., Mamou, M. and Vasseur, P., Bistability and Hysteresis Induced by Form Drag in Nonlinear Subcritical and Supercritical Double-Diusive Lapwood Convection in Shallow Porous Enclosures, J. Fluid Mech., vol. 812, pp. 463-500, 2017.

Rebhi, R., Hadidi. N , Mamou. M, Khechiba, K. Bennacer. R., The Onset of Unsteady Double-Diffusive Convection in a Vertical Porous Cavity Under a Magnetic Field and Submitted to Uniform Fluxes of Heat and Mass.; Special Topics & Reviews in Porous Media - An International Journal, 11(3):259–285, 2020.

Rebhi, R., Hadidi. N , K. Bennacer. R., Non-Darcian Effect on Double-Diffusive Natural Convection Inside an Inclined Square Dupuit-Darcy Porous Cavity Under a Magnetic Field; Thermal Science, Vol. 25, No. 1A, pp. 121-132, 2021.

Rees, D.A.S. and Hossain, M.A., Combined Effect of Inertia and a Spanwise pressure Gradient on free Convection from a vertical surface in porous media, Numerical Heat Transfer., vol. 36, pp. 725-736, 1999.

Riley, D.S. and Rees, D.A.S., Non-Darcy Natural Convection From Arbitrarily Inclined Heated Surface in Saturated Porous Media, J. Mech Appl Math., vol. 38, pp. 277-295, 1985.

Roubort, J., Nanofluids Industrial Cooling, North America: ANL Michellin, 2009.

Sarkar, J., A Critical Review on Convective Heat Transfer Correlations of Nanofluids, Renewable and Sustainable Energy Reviews., vol. 15, pp. 3271-3277, 2011.

Shah. Z, Babazadeh.H, Kumam.P, Shafee.A, Thounthong.P, Numerical simulation of magnetohydrodynamic nanofluids under the influence of shape factor and thermal transport in a porous media using CVFEM, Front. Phys. 7: 164. doi: 10.3389/fphy. 2019

Shankar. B.M, Kumar.J, Shivakumara. I.S, Magnetohydrodynamic stability of natural convection in a vertical porous slab, Journal of Magnetism and Magnetic Materials, 421, 152–164.2017

Sheikholeslami, M., Applications of Nanofluid Transportation and Heat Transfer Simulation, Advances in Chemical and Materials Engineering (ACME)., Book Series, IGB Global, 2019.

Sheikholeslami, M. and Ganji, D.D., Applications of Nanofluid for Heat Transfer Enhancement, Elsevier, 2017.

Sheikholeslami .M, Ellahi. R, Fetecau. C, CuO–Water Nanofluid Magnetohydrodynamic Natural Convection inside a Sinusoidal Annulus in Presence of Melting Heat Transfer, Mathematical Problems in Engineering, Hindawi. 2017

Sheikholeslami. M, Numerical investigation for CuO-H_2O nanofluid flow in a porous channel with magnetic field using mesoscopic method, Journal of Molecular Liquids, 249, 739-746. 2018

Sheikholeslami. M, Shehzad. S.A, Magnetohydrodynamic nanofluid convective flow in a porous enclosure by means of LBM, International Journal of Heat and Mass Transfer, 113, 796-805. 2017

Sheikholeslami, M., Rokni, H., B. (2017) : Simulation of nanofluid heat transfer in presence of magnetic field: A review, International Journal of Heat and Mass Transfer, vol. 115, pp. 1203 - 1233.

Sheremet, M.A. and Pop, I., Free Convection in a Porous Horizontal Cylindrical Annulus with a Nanofluid Using Buongiorno's Model, Computers and Fluids., vol. 118, pp. 182-190, 2015.

Sheremet, M.A., Grosan, T. and Pop, I., Free Convection in a Square Cavity Filled with a Porous Medium Saturated by Nanofluid Using Tiwari and Das'Nanofluid Model, Transp Porous Med., vol. 106, pp. 595-610, 2015.

Sheremet, M.A., Dinarvand, S. and Pop, I., Effect of Thermal Stratification on Free Convection in a Square Porous Cavity Filled with a Nanofluid Using Tiwari and Das'nanofluid Model, Physica E., vol. 69, pp. 332-341, 2015.

Sheremet, M.A., Pop, I. and Nazar, R., Natural Convection in a Square Cavity Filled with a Porous Medium Saturated with a Nanofluid Using the Thermal Non-equilibrium Model with a Tiwari and Das nanofluid model, Int. J. Mechanical Sciences., vol. 100, pp. 312-321, 2015.

Sivaraj. C, Sheremet.M.A, MHD natural convection in an inclined square porous cavity with a heat conducting solid block , Journal of Magnetism and Magnetic Materials 426, 351-360. 2017

Sureshkumar. S , Muthukumar .S, Muthtamilselvan. M , Deog-Hee Doh, Gyeong-Rae Cho, Eswari Prem, MHD convection of nanofluid in porous medium influenced by slanted

Lorentz force, The European Physical Journal Special Topics volume 229, pages331–346. 2020

Tiwari, R.K. and Das, M.K., Heat Transfer Augmentation in a Two-Sided Lid-Driven Differentially Heated Square Cavity Utilizing Nanofluids, Int. J. Heat and Mass Transfer., vol. 50, pp. 2002-2018, 2007.

Vadasz, P., Emerging Topics in Heat and Mass Transfer in Porous Media, New York: Springer, 2008.

Vafai, K., Handbook of Porous Media, third ed., New York: Taylor and Francis, 2015.

Vanaki, Sh.M., Ganesan, P. and Mohammed, H.A., Numerical Study of Convective Heat Transfer of Nanofluids, Renewable and Renewable and Sustainable Energy Reviews., vol. 54, pp. 1212-1239, 2016.

Walker. K.L, Homsy. G.M, Convection in a porous cavity. J. Fluid Mech. 87, 338–363, 1978

Wang .Y, Ali .N, Hayat .T, Peristaltic motion of a magnetohydrodynamic generalized second-order fluid in an asymmetric channel, Numerical Methods for Partial Differential Equations 27 (2), 415-435,2011

Wang.Z.H, Meng. X, Ni.M.J, Liquid metal buoyancy driven convection heat transfer in a rectangular enclosure in the presence of a transverse magnetic field, International Journal of Heat and Mass Transfer, 113, 514–523. 2017

Ward J. C. Turbulence flow in porous media, Proceedings of A. S. C. E. Journal of Hydraulics Division, 90, n° Hy. 5, September (1964).

Xu, H.J., Xing, Z.B., Wang, F.Q., Cheng, Z.M., Review on Heat Conduction, Heat Convection, Thermal Radiation and Phase Change Heat Transfer of Nanofluids in Porous Media, Fundamentals and Applications, Chemical Engineering Science., vol. 23, pp. 462-483, 2019.

Xue. Q.Z, Model for thermal conductivity of carbon nanotubebased composites. Phys B Condens Matter 368:302–307, 2005

Yang, L. and Du, K., A Comprehensive Review on Heat Transfer Characteristics of TiO2 Nanofluids, Int. Heat and Mass Transfer., vol. 108, pp. 11-31, 2017.

Zahmatkesh.I, Shandiz. M.R.H, Optimum constituents for MHD heat transfer of nanofluids within porous cavities, Journal of Thermal Analysis and Calorimetry 138, 1669-1681. 2019.

All the results presented in the first application have been the subject of an international publication in the journal Special Topics & Reviews in Porous Media — An International Journal entitled "Inerial and Porosity Effects on Dupuit-Darcy Natural Convection of Cu-Water Nanofluid Saturated High Thermal Conductive Porous Medium".

Special Topics & Reviews in Porous Media — An International Journal, 11(5):453–475 (2020)

INERTIAL AND POROSITY EFFECTS ON DUPUIT–DARCY NATURAL CONVECTION OF CU–WATER NANOFLUID SATURATED HIGH THERMAL CONDUCTIVE POROUS MEDIUM

D. Alilat,[1] M. Alliche,[1] R. Rebhi,[1,] & M.N. Borjini[2]*

[1]*University of Medea, Faculty of Technology, Department of Mechanical Engineering, Medea 26000, Algeria*

[2]*Université de Monastir, Ecole Nationale d'Ingénieurs de Monastir, Laboratoire de Métrologie et des Systems Énergétiques, 5019 Monastir, Tunisia*

*Address all correspondence to: R. Rebhi, University of Medea, Faculty of Technology, Department of Mechanical Engineering, Medea 26000, Algeria, E-mail: rebhi.redha@gmail.com

Original Manuscript Submitted: 1/27/2020; Final Draft Received: 3/21/2020

The natural convection in an inclined square porous enclosure saturated by Cu-water nanofluid is numerically studied. Aluminium foam is the porous matrix material. The vertical walls are assumed to be isothermal and differentially heated, while the horizontal ones are adiabatic. The Darcy–Dupuit model, which includes the inertial effects parameter, describes the flow in the porous medium. A finite difference method is used to solve the governing dimensionless partial differential equations along with the corresponding boundary conditions. The governing parameters for the problem are the Rayleigh number (Ra_T), inertial parameter (G), nanoparticles volume fraction (ϕ), porosity of porous medium (ε), and the inclination of the cavity (γ). A good agreement between the obtained results and previous publications reveals that the increasing of inertial effect parameter reduces the intensity of convection, and the conduction mode is dominated for the high value of inertial effect parameter. Furthermore, the increasing of nanoparticles volume fraction has a negative effect on convection intensity due to the increases of dynamic viscosity. The increase of porous medium porosity has a reverse effect on the convection rate. For high porosity, the heat transfer in the cavity is dominated by the high thermal conductivity of porous matrix compared to the nanofluid convection inside the cavity. The angle of around 40° represents a better cavity inclination for maximum convection.

KEY WORDS: *free convection, nanofluid, porous media, inertial effect parameter, Dupuit–Darcy model*

1. INTRODUCTION

Reducing energy consumption has become a main interest for engineers and researchers worldwide for future energy security and diversity by securing environmental energy sources. In order to minimize energy consumption, efficient and compact thermal products with improved design must be developed. The thermal control, material and energy saving in such a process can be achieved by enhancing the heat transfer rate using one of the two main techniques, passive or active technology (Ganji and Malvandi, 2016; Alam and Kim, 2018; Khan et al., 2018). The enhancement of heat transfer by natural convection has received increasing interest as an important heat transfer phenomenon because of its numerous advantages such the absence of need for external power for inducing the convective heat transfer. No electronic regulation and supply is required, and the absence of mechanical repair for the powering systems reduces costs and time (Ghalambaz et al., 2015). Researchers are always looking for new numerical methods to solve the natural convection and the design of efficient equipment (Alkasassbeh et al., 2019).

The convective heat transfer with porous media is gaining interest due to its large use in many engineering applications such as heat exchangers, ground water, and oil flow. Articles are being published at the rate of one a day

2151–4798/20/$35.00 © 2020 by Begell House, Inc. www.begellhouse.com

All the results presented in the seconde application have been the subject of an international publication in the journal International Journal of Fluid Mechanics Research entitled "Inertial Effects on the Hydromagnetic Natural convection of SWCNT-Water Nanofluid Saturated Inclined Ractangular Porous Medium".

International Journal of Fluid Mechanics Research, 47(5):461–483 (2020)

INERTIAL EFFECTS ON THE HYDROMAGNETIC NATURAL CONVECTION OF SWCNT-WATER NANOFLUID-SATURATED INCLINED RECTANGULAR POROUS MEDIUM

D. Alilat,[1,2] M. Alliche,[1] R. Rebhi,[1,] & Ali J. Chamkha[3]*

[1]*University of Medea, Faculty of Technology, Department of Mechanical Engineering, Medea 26000, Algeria*

[2]*Algerian Petroleum Institute, Sonatrach Company, Boumerdes 35000, Algeria*

[3]*Kuwait College of Science and Technology, 7th Ring Road, Doha District, Kuwait*

*Address all correspondence to: R. Rebhi, University of Medea, Faculty of Technology, Department of Mechanical Engineering, Medea 26000, Algeria, E-mail: rebhi.redha@gmail.com

Original Manuscript Submitted: 6/11/2020; Final Draft Received: 9/6/2020

The problem of magnetohydrodynamic (MHD) natural convection of a single-wall carbon nanotube (SWCNT)-water nanofluid in a tilted square cavity filled with a saturated porous medium and subjected to an inclined magnetic field is numerically studied. The Dupuit–Darcy model is adopted to describe the flow inside the porous medium for analyzing the departure from the linear Darcy situation. The enclosure is bounded by differentially heated vertical walls, and the horizontal ones are kept adiabatic. The dependency of the fluid flow and the heat transfer rate on the Rayleigh number (Ra_T), nanotubes volume fraction (ϕ), Hartmann number (Ha), inertial effect parameter (G), inclination angle of the cavity (γ), and the inclination angle of the magnetic field (ξ) is analyzed. The obtained partial differential equations (PDEs) governing the problem have been solved by the finite difference method along with their corresponding boundary conditions. It is found that increasing the SWCNT concentration significantly enhances the convection intensity until a threshold value of the Rayleigh number due to the increase of dynamic viscosity is reached. The increase of the inertial effect parameter or the Hartmann number reduces the fluid flow and the convection strength, and the conduction mode is dominated for high values of both parameters. Furthermore, the heating of the cavity through the left vertical walls produces a better fluid flow and convection strength for a Hartmann number greater than 2. The inclination angle $\xi = 45°$ of the magnetic field represents the best for the fluid flow strength and the heat transfer rate, regardless of the Hartmann and Rayleigh numbers.

KEY WORDS: *free convection, SWCNT-water nanofluid, porous media, magnetic field, inertial effect parameter, Dupuit–Darcy model*

1. INTRODUCTION

In recent years, the study of heat transfer in porous media has been an ongoing research field. This interest is due to the frequent use of research in many engineering and environmental applications like heat exchangers, ground water and oil flow, cooling electronic devices, nuclear reactor systems, and thermal insulation. In the process of designing a fusion reactor, the natural convection heat transfer, electrically conducting fluids, and liquid metals are essential problems because of the strong magnetic field and high temperature difference. Magnetic fields are used for the technologies of drying and lubrication, food cleaning, float glass, hydrodynamic behavior control during the processes of float glass production, solidification, and crystal growth. Moreover, magnetic field applications of nanofluid flows are gaining interest due to their large use in many technological applications such as nuclear reactor

2152–5102/20/$35.00 © 2020 by Begell House, Inc. www.begellhouse.com